

ERDC/CRREL LR-04-25

Cold Regions Research
and Engineering Laboratory



**US Army Corps
of Engineers®**
Engineer Research and
Development Center

USING HIGH SPATIAL RESOLUTION DIGITAL IMAGERY

Michael V. Campbell, Robert L. Fischer, and Timothy
Pangburn

July 2004

DISCLAIMER: The contents of this report are not to be used for advertising, publication, or promotional purposes. Citation of trade names does not constitute an official endorsement or approval of the use of such commercial products. All product names and trademarks cited are the property of their respective owners. The findings of this report are not to be construed as an official Department of the Army position unless so designated by other authorized documents.

USING HIGH SPATIAL RESOLUTION DIGITAL IMAGERY

Michael V. Campbell,* Robert L. Fischer,* and Timothy Pangburn†

**Topographic Engineering Center
7701 Telegraph Road
Bldg. 2592
Alexandria, Virginia 22315*

*†Cold Regions Research and Engineering Laboratory
72 Lyme Road
Hanover, NH 03755*

TABLE OF CONTENTS

LIST OF FIGURES AND TABLES	vi
EXECUTIVE SUMMARY	xii
 Report 1 - Land Cover Classification of Reference Wetlands Using High Spatial Resolution Digital Airborne Multispectral Imagery In Support of Poplar Island Restoration	
1.0 INTRODUCTION	2
1.1 Objective	2
1.2 Poplar Island Restoration Effort	3
1.3 Reference Wetlands.....	3
2.0 METHODS	4
2.1 Instrumentation	4
2.2 Mission Planning	9
2.3 Image Acquisition	9
2.4 Image Post-Processing.....	11
2.5 Image Classification.....	17
2.6 NDVI Mask.....	18
2.7 Unsupervised Clustering.....	20
2.8 Minimum Mapping Unit.....	20
3.0 RESULTS.....	23
3.1 Image Quality.....	23
3.2 Land Cover Classification.....	26
<i>Spillway #6</i>	26
<i>Knapps Narrows</i>	26
<i>Cabin Cover</i>	28
<i>Harbor Cove</i>	28
<i>Marsh Creek Sites (South, East, North)</i>	28
<i>Muddy Creek</i>	28
<i>Piney Creek</i>	28
<i>Hell Hook Marsh</i>	28
3.3 Land Cover Area Estimates	38
3.4 Output Images and Shapefiles	38
3.4.1 <i>Raw CAMIS Frames</i>	38
3.4.2 <i>Post-Processed CAMIS Frames</i>	38
3.4.3 <i>Ge-Registered Mosaics</i>	38
3.4.4 <i>NDVI Images</i>	43

3.4.5 Class Maps	43
3.4.6 Shape Files	43
4.0 CONCLUSIONS AND RECOMMENDATIONS.....	43
5.0 COST.....	44

Report 2 – Enhanced Levee Inspections Using High Spatial Resolution Digital Airborne Multispectral Imagery

1.0 INTRODUCTION	46
1.1 Objective	46
2.0 METHODS	46
2.1 Project Site	46
2.2 Instrumentation	46
2.3 Mission Planning and Image Acquisition.....	49
2.4 Image Post-Processing.....	49
3.0 RESULTS	52
4.0 UTILITY FOR ARCVIEW APPLICATIONS.....	58
5.0 COST.....	59
6.0 IMAGE DATA	60
7.0 CONCLUSION AND RECCOMENDATIONS	61

Report 3: Application of High Resolution Airborne and Satellite Multispectral Imagery for Invasive Species Mapping at Lake Okeechobee, Florida

1.0 INTRODUCTION.....	63
1.1 Objective.....	64
2.0 METHODS & RESULTS	64
2.1 Image Acquisition and Post-Processing.....	64
2.2 Field Data Collecion.....	66

2.3 Image Analysis.....	66
2.3.1 <i>CAMIS Imagery</i>	75
2.3.1.1 Signature Collection.....	75
2.3.1.2 Signature Separability	76
2.3.1.3 Minimum Mapping Unit.....	80
2.3.1.4 Accuracy Assessment	80
2.3.2 <i>IKONOS Imagery</i>	82
2.3.2.1 Histogram Matching	82
2.3.2.2 Unsupervised Classification.....	82
2.3.2.3 Minimum Mapping Unit.....	83
2.3.2.4 Accuracy Assessment	83
2.3.2.5 Final Product.....	86
3.0 COST.....	86
4.0 CONCLUSIONS AND RECCOMENDATIONS	88

**Report 4: Detailed Wetland Vegetation Mapping Over Blackwater Wildlife Refuge
using High Resolution Digital Airborne Hyperspectral Imagery**

1.0 INTRODUCTION.....	90
1.1 Objective.....	91
2.0 BACKGROUND	91
3.0 METHODS	94
3.1 Image Acquisition	94
3.2 Post-Processing.....	94
3.2.1 <i>Geometric Correction</i>	98
3.2.2 <i>Radiometric Correction</i>	100
3.2.2.1 Histogram Evaluation and Adjustment	100
3.2.2.2 Specular Reflectance or Water Glint.....	108
3.2.2.3 Reduction in Data Dimensionality	109
3.2.2.4 Cross-Track Illumination Correction	113
3.2.2.5 Histogram Equalization.....	114
3.2.3 <i>Mosaicking</i>	116
3.3 Field Data Collection	116
3.4 Signature Extraction.....	122
3.4.1 <i>30 June Mosaic</i>	128

3.4.2 7 June Mosaic	128
3.5 Image Subsetting.....	128
3.6 Signature Separability Analyses	128
3.6 Image Classification.....	132
3.6.1 Spectral Angle Mapper	132
3.6.2 Maximum Likelihood Classifier	135
4.0 RESULTS.....	135
4.1 Minimum Mapping Unit Filter	135
4.2 Accuracy Assessment.....	136
5.0 CONCLUSIONS	141
6.0 RECCOMENDATIONS.....	142
7.0 DATA.....	143
Appendix A.....	144

LIST OF FIGURES AND TABLES

Figures: Report 1

1	Location of reference wetlands on Tilghman Island and Poplar Island.....	5
2	Location of reference wetlands near Kent Narrows	6
3	Location of Hell Hook Marsh.....	7
4	CAMIS Model 4768P with four Sony XC8500 progressive scan cameras mounted on a sited solid base	8
5	Location and orientation of flightlines covering sites on Tilghman and Poplar Islands.....	10
6	Location and orientation of flightlines covering Kent Narrows and Piney Creek sites.....	10
7	Location and orientation of flightlines covering Hell Hook Marsh site	11
8	Raw false color CAMIS frame (top) and band registered false color CAMIS frame (bottom) Knapps Narrows, frame # 106	12
9	Band registered true color CAMIS frame (top) and radiometrically corrected true color CAMIS frame (below), Hell Hook Marsh, flightline 2, frame #108.....	13
10	True color, three-frame mosaic of Piney Creek (PIN) wetland	15
11	Knapps Narrows mosaic before and after geometric registration to DOQQ. The non-registered mosaic (left) is depicted using true-color (bands 3, 2, & 1); the geo-registered mosaic (right) is depicted using false-color (bands 4, 3, & 2)	16
12	Piney Creek (PIN) mosaic before (left) and after (right) geometric registration to digital 7.5' topographic quadrangle	16
13	Knapps Narrows and PIN mosaics after subsetting (or clipping)	17
14	NDVI image (left), NDVI histogram (upper right), and primary NVDI masks.....	19
15	Primary image segments after NDVI masking	21
16	Results of unsupervised classification of each primary segment.....	21
17	Class map of Knapps Narrows—full resolution	22
18	Class map of Knapps Narrows after application of Minimum Mapping Unit filter (MMU = 9 pixels)	24
19	Mosaic of Hell Hook Marsh showing significant holidays between flightlines	25
20	False color (left) and true color (right) mosaics for Spillway 6 site, within Poplar Island restoration/construction area	27

21	False color composite for Cabin Cove.....	29
22	Class map for Cabin Cove after application of Minimum Mapping Unit filter (MMU = 9 pixels)	30
23	False color composite for Harbor Cover.....	31
24	False color composite for Marsh Creek South.....	32
25	Class map for Marsh Creek South after application of Minimum Mapping Unit filter (MMU = 9 pixels).....	32
26	False color composite for Marsh Creek East	33
27	Class map for Marsh Creek East after application of Minimum Mapping Unit filter (MMU = 9 pixels).....	33
28	False color composite for Marsh Creek North.....	34
29	Class map for Marsh Creek North after application of Minimum Mapping Unit Filter (MMU = 9 pixels).....	35
30	False color composite for Muddy Creek.....	35
31	Class map for Muddy Creek after application of Minimum Mapping Unit filter (MMU = 9 pixels)	35
32	False color composite for Piney Creek.....	36
33	Class map for Piney Creek after application of Minimum Mapping Unit filter (MMU = 9 pixels)	36
34	Class map for Hell Hook Marsh after application of Minimum Mapping Unit filter (MMU = 25 pixels).....	37

Tables: Report 1

1	Areal extent of land cover classes for Knapps Narrows.....	39
2	Areal extent of land cover classes for Cabin Cove.....	39
3	Areal extent of land cover classes for Marsh Creek South.....	40
4	Areal extent of land cover classes for Marsh Creek East	40
5	Areal extent of land cover classes for Marsh Creek North.....	41
6	Areal extent of land cover classes for Muddy Creek	41
7	Areal extent of land cover classes for Piney Creek	42
8	Areal extent of land cover classes for Hell Hook Marsh	42

Figures: Report 2

1	ArcView project provided by Rock Island District depicting project area.....	47
2	Detail of project site.....	48
3	The CAMIS model 4768P airborne digital multispectral scanner.....	50
4	Orientation of the nine flightlines required to acquire a complete CAMIS image set over the Sny levee.....	51
5	Examples of: (a) poor geometric registration, and (b) good geometric registration.....	53
6	4 September 2001 geo-registered, false-color mosaic.....	54
7	4 September 2001 geo-registered, true-color mosaic.....	55
8	17 July 2002 geo-registered, false-color mosaic.....	56
9	17 July 2002 geo-registered, true-color mosaic.....	57

Figures: Report 3

1	(a) Overview of western shore of Lake Okeechobee and the IKONOS image area. (b) Location and orientation of CAMIS flightlines.....	65
2	True-color composite of Fisheating Bay and Monkey Box acquired 31 January 2001.....	67
3	False-color composite of Fisheating Bay and Monkey Box acquired 31 January 2001.....	68
4	True-color composite of Fisheating Bay, Monkey Box, and Moonshine Bay acquired 9 December 2001.....	69
5	False-color composite of Fisheating Bay, Monkey Box, and Moonshine Bay acquired 9 December 2001.....	70
6	Examples of extensive distribution of healthy water hyacinth and herbicide treated water hyacinth within Fisheating Bay.....	71
7	IKONOS image of western Lake Okeechobee, acquired July 2002; false-color composite.....	72
8	IKONOS image of western Lake Okeechobee, acquired July 2002; true-color composite.....	73
9	Location of field plots established during 9 December 2001 CAMIS image acquisition.....	74
10	Training signatures extracted from CAMIS mosaics. Vegetation types with high spectral response (i.e., brighter pixels).....	79

11	Training signatures extracted from CAMIS mosaics. Vegetation types with lower spectral response (i.e., darker pixels).....	79
12	Supervised classification results of CAMIS mosaics after application of the 144 pixel minimum mapping unit filter.....	81
13	Unsupervised classification results of IKONOS image after application of the 9 pixel minimum mapping unit filter.....	84
14	The final three class thematic product depicting the distribution of the invasive species of interest to the District.....	87

Tables: Report 3

1	Vegetation descriptions of training sites	77
2	Training statistics for each of the defined classes.....	81
3	Description of vegetation classes developed from the segmented unsupervised classification of the IKONOS multispectral image	85

Figures: Report 4

1	Configuration of the direct-vision, dispersing prism-grating-prism (PGP) spectrograph used in the AISA sensor.....	93
2	Location and orientation of AISA flightlines over Blackwater Wildlife Refuge.....	96
3	Examples of the geometric quality of the AISA imagery.....	99
4	True color mosaic of uncorrected lines BLINE7E and BLINE8W.....	101
5	False color mosaic of uncorrected lines BLINE7E and BLINE8W.....	101
6	Flightlines BLINE7E and BLINE8W and their associated mean reflectance spectra including the background pixels.....	103
7	Flightlines BLINE7E and BLINE8W and their associated mean reflectance spectra without the background pixels.....	105
8	Examples of histograms for 6 of 38 AISA bands.....	107
9	Example of NDVI image. Graphs of floating point NDVI values and NDVI values after scaling to 8-bit data.....	110

10	Flightlines BLINE7E and BLINE8W and their associated mean reflectance spectra after (1) removal of water pixels and (2) reduction in data dimensionality.....	111
11	Histogram equalization results between BLINE7E and BLINE8W.....	115
12	Southern Mosaic – flightlines BLINE7E through BLINE20E.....	117
13	Final mosaic for flightlines 1 through 5 acquired on 30 June 2000.....	118
14	Final mosaic for flightlines 1 through 6 acquired on 30 June 2000.....	119
15	Location of training sites within western part of northern mosaic.....	121
16	Location of training sites adjacent to Shorters Warf Road.....	123
17	ArcView shapefile polygons used to collect training spectra for classification of forest types.....	127
18	Southern Mosaic – flightlines BLINE7E through BLINE20E.....	129
19	(a) Spectral plots of low reflectance signatures used to classify the southern mosaic.....	133
19	(b) Spectral plots of high reflectance signatures used to classify the southern mosaic.....	134
20	Final vegetation class map for southern mosaic (7 June 2000).....	137
21	Final vegetation class map for northern mosaic (30 June 2000).....	138

Tables: Report 4

1	Subset of flightline header data provided in *.dcs files.....	97
2	Minimum and maximum reflectance values for flightlines BLINE7E and BLINE8W including background (i.e., zero) pixels.....	102
3	Minimum and maximum reflectance values for flightlines BLINE7E and BLINE8W excluding the background (i.e., zero) pixels.....	104
4	Minimum and maximum reflectance values for flightlines BLINE7E and BLINE8W excluding the background (i.e., zero) pixels and the water pixels.....	112
5	Location and description of field plots: Fall 2001 and Summer 2002.....	120

6	Location and description of 1-m2 quadrats.	124
7	Description of training classes for southern mosaic.	130
8	Description of training classes for northern mosaic.	131
9	Class names and areas of final 26 classes in southern mosaic.....	139
10	Class names and areas of final 19 classes in northern mosaic.....	140

EXECUTIVE SUMMARY

This multi-report document is presented as the culmination of nearly three years worth of applied research. The project was funded by the USACE Headquarters Geospatial Technology Research and Development Program. The overall objective of this multi-year investigation was to assess the utility of high spatial resolution digital imagery to Corps civil works operations. The sources of remotely sensed data used in this research effort include:

- digital airborne multispectral imaging technology
- digital airborne hyperspectral imaging technology, and
- digital satellite multispectral imaging technology.

System selection was based on the anticipated benefit(s) derived from the acquisition and processing of the unique high spatial resolution images, from each remotely sensed data source, at each independent study site.

The project developed and implemented four applications to evaluate the use of high resolution digital remotely sensed data in standard Corps operations. This document is divided into four individual reports. The following paragraphs provide a brief summary of each project.

Detailed Wetlands Mapping using Airborne Multispectral Imagery (Baltimore District):

The goal of the Poplar Island Restoration Project is to rebuild a naturally eroded group of islands within the upper Chesapeake Bay. The District engineers, hydrologists, and biologist are tasked with constructing a variety of functioning estuarine wetland systems. Existing wetland sites, distributed nearby the construction site on the Eastern Shore of Maryland, were selected for characterization and monitoring. These functioning sites were designated as reference wetlands and would guide the construction activities on Poplar Island. High spatial resolution digital airborne multispectral imagery were acquired over eight reference wetlands in February of 2001. The images were post-processed into geometrically and radiometrically corrected mosaics. An unsupervised classification approach was employed to delineate 16 land cover classes. These 16 classes provided adequate information to map three primary classes, including: persistent water channels and guts, tidal zones (e.g., mudflats) and areas supporting wetland/upland vegetation. The output products included vector formatted ArcView shapefiles for each site.

Enhance Levee Inspections (Rock Island District):

The Corps inspects thousands of miles of flood control structures each year. The Rock Island District has implemented an ArcView-based application, complete with real-time GPS navigation, to improve levee inspections. One-meter spatial resolution airborne multispectral imagery was acquired over the Sny levee. An evaluation of the complete mosaics determined that even higher resolution data (i.e., smaller pixels) would be necessary to provide the detail needed to delineate anomalies on the structure.

Invasive Species Mapping (Jacksonville District):

The Aquatic Plant Control Operations Support Center is responsible for managing exotic invasive species within a large wetlands complex distributed throughout the western portion of Lake Okeechobee, Florida. The objective of this research effort was to delineate areas supporting water hyacinth and water lettuce using high resolution multispectral imagery from both an airborne system and from a commercial satellite sensor. The airborne image products suggested that the spectral signatures of many of the marsh plant communities were very similar. The satellite imagery provided a much more cost-effective solution for creating a class map depicting the distribution of invasive species.

Wetlands Mapping with Airborne Hyperspectral Imagery (Baltimore District):

The Blackwater Wildlife Refuge, located on the Eastern Shore of Maryland (Cambridge, MD), supports a variety of wetland restoration initiatives. In conjunction with the Fish and Wildlife Service, high resolution airborne digital hyperspectral imagery was acquired over an area covering ~ 70,000 acres. A detailed vegetation map was produced using a limited amount of ground truth samples. The accuracy of the final vegetation classification was relatively low. Many of the classification errors were attributed to the poor radiometric properties of the hyperspectral image mosaic.

The project descriptions provided in each report describe image acquisition, image post-processing, and overall final product quality/accuracy. Each report is structured to include an introduction with background information for each application, followed by a methods section. Results, including both interim and final products, are presented using text and graphics. The concluding section in each report provides cost information comparing the benefits of the applied sensor to other sources of remotely sensed data.

The intended audience for this document includes natural resource managers, biologists, ecologists, GIS specialists, and others that are already using or are potentially planning to use high spatial resolution digital remotely sensed imagery for current or future projects. The primary points of contact for questions and comments concerning this document are Michael V. Campbell (703-428-6802 ext. 2367) and Robert L. Fischer (703-428-7140) of the Topographic, Imagery and Geospatial Research Division, US Army Topographic Engineering Center, Engineer Research and Development Center located in Alexandria, Virginia.

The image and map products, including both raster and vector formatted data, are not provided with this report. The total volume of geospatial data would exceed several gigabytes. The authors can provide the reader access to all of the imagery and final maps. Please note that some type of image processing software, such as ERDAS Imagine or RSI ENVI, is best used to display and manipulate multispectral and hyperspectral images. However, standard GIS software, such as ArcView, can display the remotely sensed data.

ACKNOWLEDGEMENTS

The following individuals are recognized for their participation in the development and implementation of this applied research effort. Scott Johnson, Baltimore District, supported the Poplar Island image acquisition and processing. Kevin Luebke, Baltimore District, provided both program and technical support for the Blackwater Wildlife Refuge vegetation mapping effort. Roger Stone and John Morton, US Fish and Wildlife Service, were instrumental in the completion of the Blackwater project. Kevin Carlock, Rock Island District, provided technical support throughout the Sny Levee mapping effort, including the current ArcView data layers. Jon Lane, Jacksonville District, provided extensive programmatic and technical leadership, including participation in the planning and implementation of field data collection activities, for the invasive species mapping initiative at Lake Okeechobee. Topographic Engineering Center (TEC) research staff that contributed to the overall project included: Ponder Henley, Jeff Ruby, Charlie Kershner, Aubrielle Smith and Charlie Shuey. The authors are grateful to the individuals that provided thorough technical review and editing of this document, especially Brian Graff (TEC) and Lorin Amidon (Cold Regions Research and Engineering Laboratory [CRREL]).

REPORT 1

Land Cover Classification of Reference Wetlands Using High Spatial Resolution Digital Airborne Multispectral Imagery

In Support of Poplar Island Restoration

1.0 INTRODUCTION

The newest digital airborne remote sensing systems combine the multispectral capabilities of commercial satellite sensors with the temporal and spatial flexibility of traditional aerial photographic systems. The high spatial resolution imagery provided by these systems greatly enhances environmental monitoring strategies. Sub-meter pixel resolutions increase the detail of surface features. However, too much data can degrade the accuracy and the utility of the final map product. Therefore, the effective use of high-resolution digital airborne imagery requires improved processing techniques that ensure accurate representation of the land cover classes of interest. The development of post-processing algorithms to remove radiometric and geometric distortions, which are typically present in all airborne images, is essential.

The Topographic Engineering Center (TEC), one of four U.S. Army Corps of Engineers (COE) research facilities within the Engineer Research and Development Center (ERDC), has been developing digital multispectral airborne remote sensing capabilities since 1994. The first system used was the Digital Multispectral Video System (DMSV). Developed by SpecTerra Systems (Canberra, Australia), DMSV imagery was shown to be successful in a variety of environmental applications, including oil spill detection, acid mine drainage characterization, and wetlands evaluation.

In 1998, TEC purchased the Computerized Airborne Multicamera Imaging System (CAMIS) from Flight Landata, Inc. (Lawrence, MA). This system used an enhanced lens design and an improved user interface resulting in more efficient data acquisition and improved image quality. The CAMIS system has acquired imagery for invasive plant species mapping, enhanced vegetation feature extraction, and ecosystem/ecotone characterization.

TEC research scientists have developed improved post-processing routines addressing radiometric distortions, which are typically present in all airborne images. Land cover category maps developed from such processed airborne imagery will provide critical input to the construction of wetland and upland plant communities within Poplar Island, MD.

1.1 Objective

The objective of this pilot project was to assess the utility of high spatial resolution airborne multispectral digital imagery in delineating three primary land cover types within selected estuarine wetlands. The three land cover categories include:

1. Persistent water bodies (open water, channels, guts, ponds, and potholes),
2. Intertidal mudflats (both vegetated and non-vegetated), and
3. Wetland and upland plant communities.

1.2 Poplar Island Restoration Effort

The following excerpt, extracted from Baltimore District's website, describes the ongoing Poplar Island restoration effort.

The group of islands known as Poplar Island are located in the upper middle Chesapeake Bay approximately 34 nautical miles southeast of the Port of Baltimore and 1 mile northwest of Tilghman Island, Talbot County, MD. The project to reconstruct Poplar Island to its approximate size in 1847 using uncontaminated dredged material from the Baltimore Harbor and Channels Federal navigation project has been developed through the cooperative efforts of many state and Federal agencies, as well as private organizations. Island restoration would create 1,110 acres of wildlife habitat by placing, shaping, and planting approximately 38 million cubic yards of dredged material. The habitat created would include approximately 555 acres each of intertidal wetland and upland habitat. The project design includes development of 50 percent wetland and 50 percent upland habitat. Of the wetlands, 80 percent will be developed as low marsh and 20 percent as high marsh. Small upland islands, ponds, and dendritic guts or channels will be created to increase habitat diversity within the marsh areas. It is expected that habitat diversity will be increased in the upland areas by constructing small ponds and providing both forested and relatively open scrub/shrub areas.

The detailed and long-term nature of this ongoing wetland restoration program provides an excellent test site for evaluating the utility of high resolution mapping techniques. As stated above, the project design includes the construction of various hydrologic features ("ponds, dendritic guts or channels"). The relative proportion (i.e., surface area) and configuration of these water bodies within the proposed wetland and upland plant communities are critical design parameters. District staff concluded that the natural conditions present in existing intertidal wetlands near the project site would supply estimates of the hydrologic characteristics, such as land-to-water ratios and channel dendricity, required throughout the construction site. COE personnel initially identified nearby estuarine wetlands as reference sites to aid in the design and installation of proposed constructed wetlands on Poplar Island. A preliminary cooperative effort between the Baltimore District and the National Marine Fisheries Service (NMFS) was underway to characterize the reference wetlands when TEC proposed the incorporation of high-resolution airborne multispectral imagery. CAMIS image acquisition was planned for as early as October 2000. However, poor weather and aircraft scheduling problems delayed acquisition until February 2001.

1.3 Reference Wetlands

The following sections describe the Poplar Island reference wetland sites.

Knapps Narrows, Cabin Cove, and Harbor Cove

These three sites are located on the western shores of Tilghman Island. The COE Baltimore District monitors these areas (Figure 1).

Spillway 6

This small site lies within the Poplar Island restoration area (Figure 1).

Marsh Creek: South (MCS), North (MCN), East (MCE); and Muddy Creek (MUD)

These four sites are located just east of the Kent Narrows Bridge (Route 50). The Marsh Creek wetland is south of the highway and the Muddy Creek wetland is north of the highway. These areas are currently under evaluation by NMFS (Figure 2).

Piney Creek (PIN)

This wetland lies west of the Kent Narrow Bridge and north of Route 50 (Figure 2). NMFS also monitors this site.

Hell Hook Marsh (HELL)

This large tidal wetland, adjacent to Honga Bay, is located roughly 10 miles south-southeast of Cambridge, MD (Figure 3).

2.0 METHODS

2.1 Instrumentation

A flight mission plan was developed and implemented to acquire the high-resolution imagery using the CAMIS model 4768P (Figure 4). Unlike other currently available airborne digital camera systems, which employ a single CCD technology, the CAMIS optical head consists of four Sony XC8500 progressive scan cameras mounted on a sited solid base (Figure 4). Each camera is sensitive in the range of 350–1100 nm. Bandpass interference filters determine the wavelength interval recorded by each camera. The standard wavelength configuration was used for this mission: 25 nm bandpass filters centered at 450 nm (blue), 550 nm (green), 650 nm (red), and 800 nm (near infrared). The CCD dimensions in each camera are 768 x 576 square pixels with 8-bit radiometric resolution. An aircraft altitude of 6115 ft (1865 m) above ground level (agl) produces a nominal spatial resolution of 1 m per pixel.

The CAMIS processing unit consists of a 233 MHz Pentium processor with 64 MB of RAM, 23 GB hard drive, and a Matrox Genesis Image Processing Card with 24 MB onboard memory. A Motorola Oncore GT GPS receiver obtains absolute code phase positions for the center pixel of each image. The system was mounted and flown onboard a Cessna 172 Skyhawk. The pilot navigated to each site and along each flightline using an onboard moving map with code phase global positioning system (GPS).



Figure 1. Location of reference wetlands on Tilghman Island and Poplar Island.

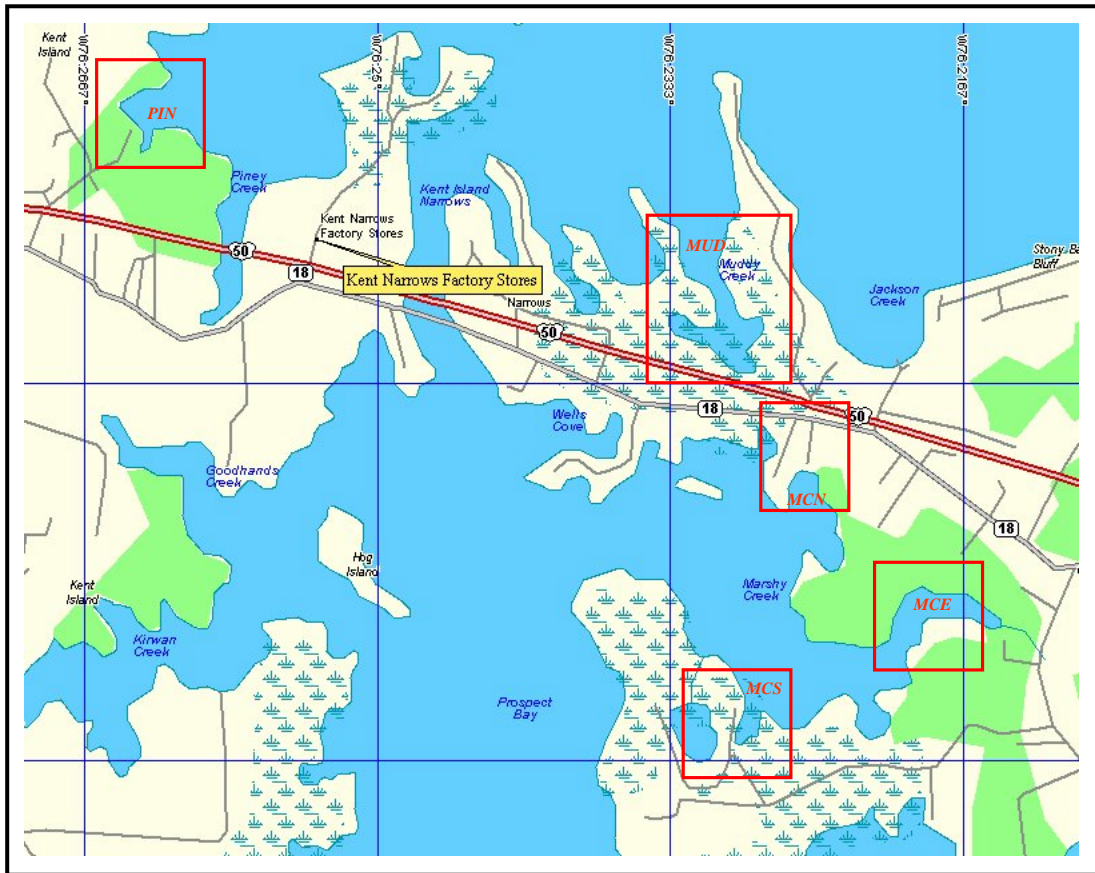


Figure 2. Location of reference wetlands near Kent Narrows.



Figure 3. Location of Hell Hook Marsh.

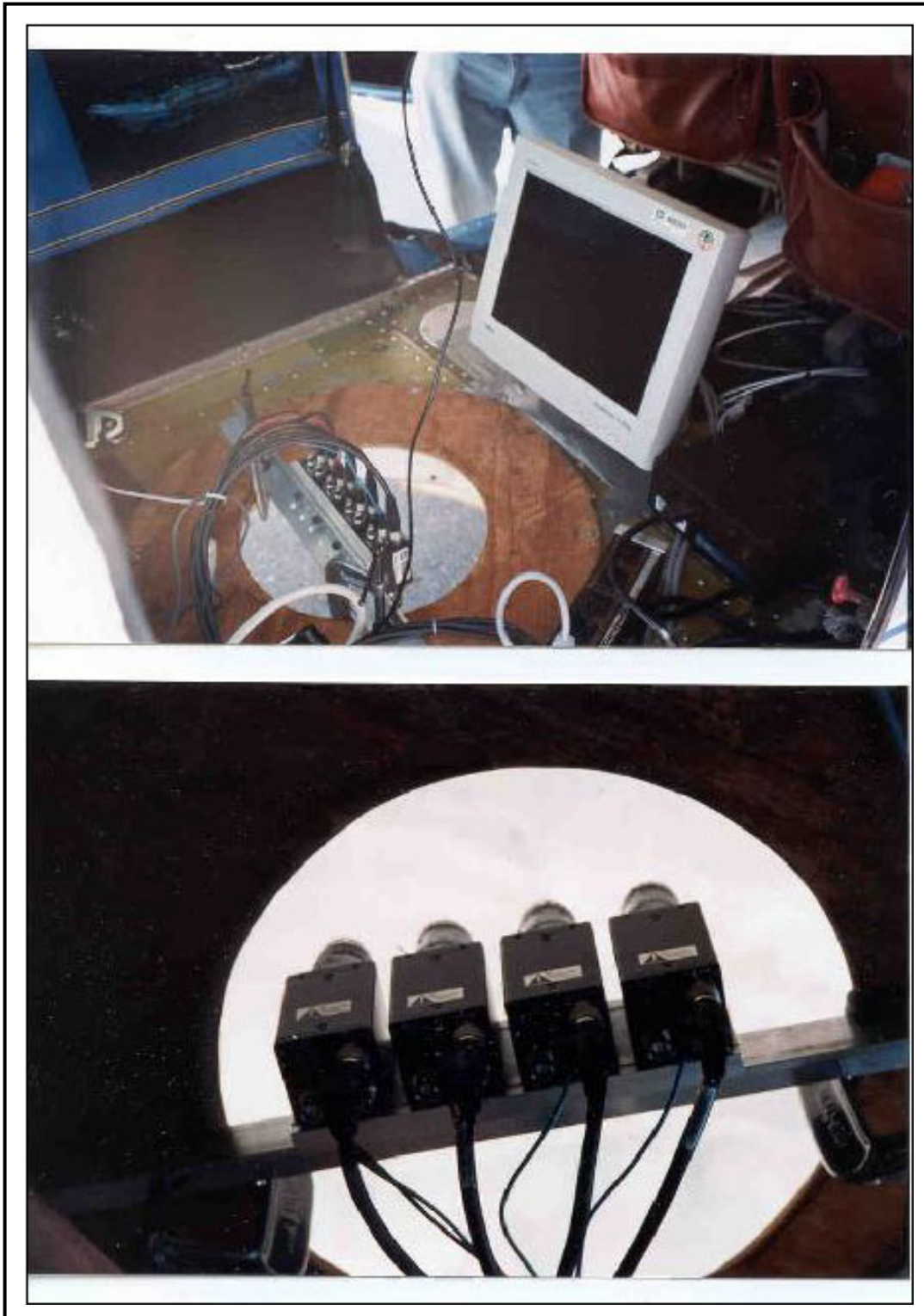


Figure 4. CAMIS Model 4768P with four Sony XC8500 progressive scan cameras mounted on a sided solid base.

2.2 Mission Planning

Geographic coordinates defining the extent of each individual reference wetland were provided by Will Nuckols, of Gahagan & Bryant Associates, Inc., and by NMFS personnel. A series of flightlines were developed that encompassed the extent of each set of coordinates. Since the CAMIS system acquires images as discrete four-band digital frames, flightline calculations are identical to those used for standard aerial photographic missions. For the Tilghman Island (Knapps Narrows, Cabin Cove, and Harbor Cove) and Poplar Island (Spillway 6) sites, a single flightline captured each wetland. The Piney Creek site also needed only a single flightline. Three overlapping flightlines were used to capture the four Kent Narrows sites (Marsh Creek North, South, and East, and Muddy Creek). For Hell Hook Marsh, six overlapping flightlines captured a large portion of the center of the swamp. In all cases, the aircraft would acquire the images using a south-to-north flightpath. Data capture would occur within +/- 1.5 hours of solar noon to ensure optimal solar illumination and to minimize shadows.

2.3 Image Acquisition

The aircraft arrived over the site at approximately 1100 hours on 11 February 2001. Conditions were sunny with light winds, providing adequate solar illumination and acceptable aircraft attitude during image acquisition. Solar noon was at ~1130 hours. Data capture commenced at 1103 hours and ceased at 1240 hours. During initial project planning, the research staff decided that image acquisition should coincide with low tide conditions.

Tidal charts predicted low tide at 1333 hours on 11 February. While this time is approximately 2 hours after local solar noon, the imagery would capture the wetland hydrologic conditions relatively close to low tide.

The completed mission produced 277 individual frames acquired over 12 flightlines. Figure 5 shows the approximate location and orientation of the flightlines over the Tilghman Island and Poplar Island sites. Inaccurate flightline coordinates for the Harbor Cove flightpath prevented a precise acquisition for this site. After several attempts to visually locate this site, a shortened flightpath appeared to successfully cover the area of interest (Figure 5). Figure 6 depicts the flightlines covering the four Kent Narrows wetlands and the Piney Creek site. Image acquisition was limited to the center four flightlines for Hell Hook Marsh (Figure 7). Including the flight to and from Manassas Municipal Airport (Manassas, VA), total airtime was approximately 3 hours.

The desired nominal spatial resolution was one m² per pixel. This required on aircraft altitude of approximately 6115 ft (1865 m) agl. However, air traffic control at the Baltimore Washington International Airport (BWI) restricted the aircraft to a ceiling altitude of 5500 ft (1677.5 m). The airspace above 6000 ft (1830 m) is reserved for incoming commercial aircraft. This lower altitude increased the nominal spatial resolution (i.e., decreased the pixel size) to ~0.75 m² per pixel (0.87 x 0.87 m pixel dimensions).

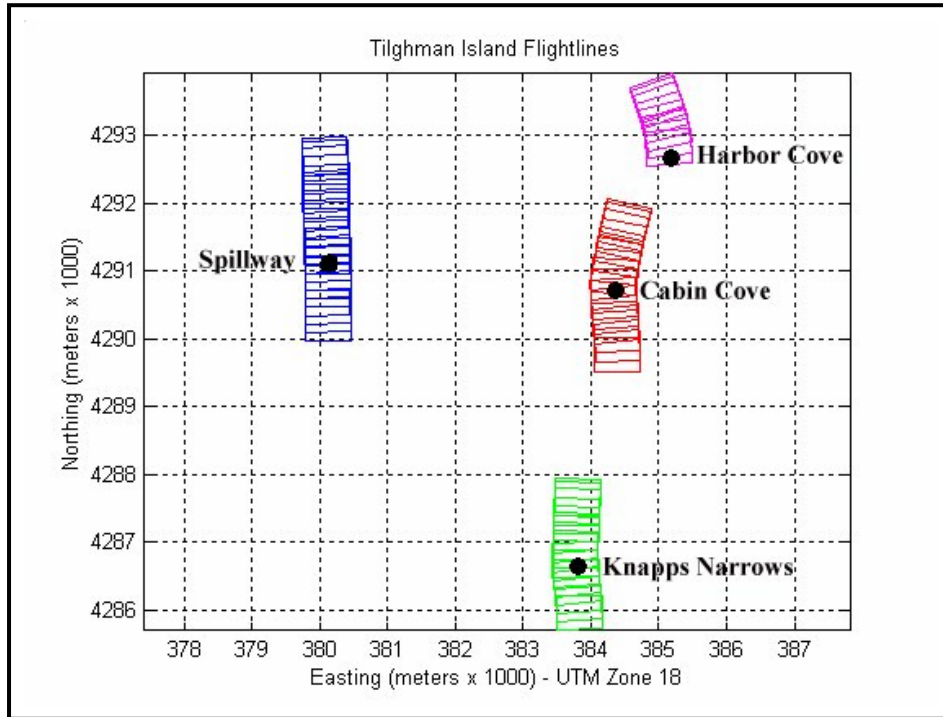


Figure 5. Location and orientation of flightlines covering sites on Tilghman and Poplar Islands

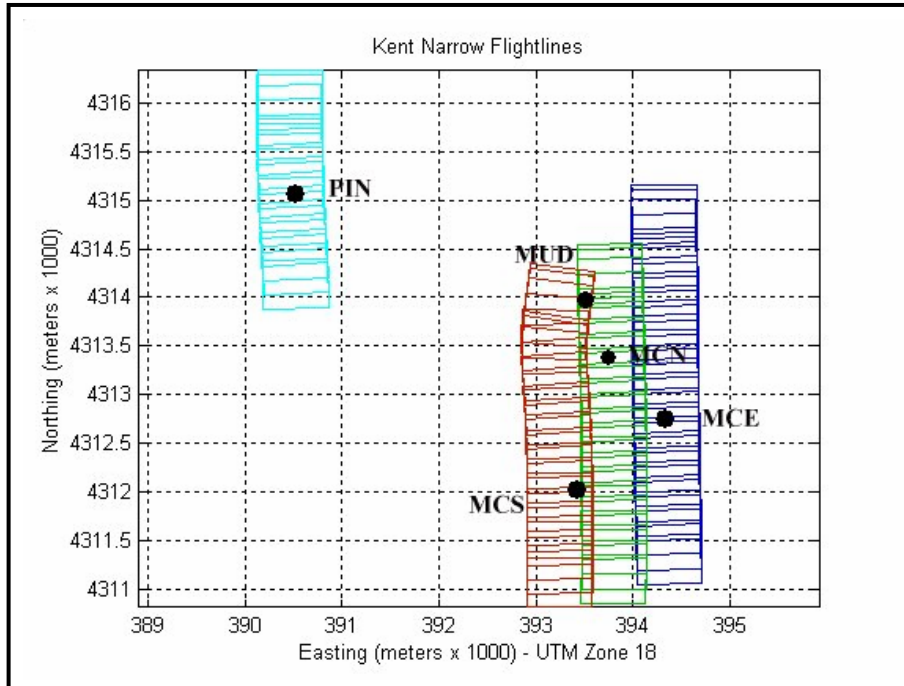


Figure 6. Location and orientation of flightlines covering Kent Narrows and Piney Creek sites.

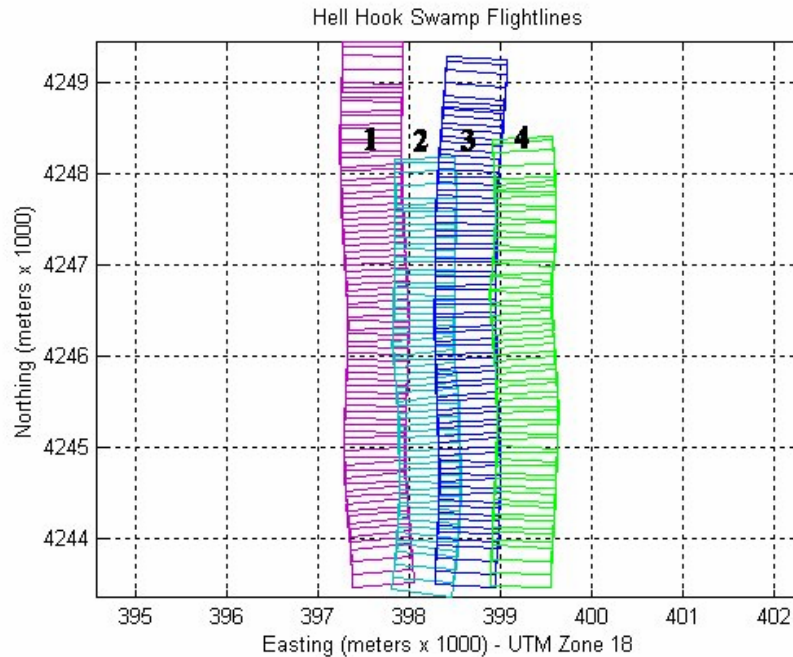


Figure 7. Location and orientation of flightlines covering Hell Hook Marsh site.

2.4 Image Post-Processing

Post-processing algorithms were applied to the imagery to address both radiometric and geometric distortions. Degradation of the radiometric (or color balance) quality of digital imagery is the result of influences from a variety of external and internal parameters. External parameters include: solar azimuth angle, solar zenith angle, atmospheric conditions (e.g., aerosols, water vapor) and surface bi-directional reflectance factors. Typical internal parameters that degrade image radiometric quality include lens distortions, lens field darkening, CCD anomalies, and system operation error (e.g., f-stop settings, shutter speed).

Software developed at TEC radiometrically corrected the complete set of CAMIS images. The first step was to band register each frame. Because the four cameras are aligned in sequence, with each lens sited parallel to the others, each band of a single frame has its center, or principle point, offset from the other bands. Figure 8 shows a single false color CAMIS frame before and after band-to-band registration.

The next post-processing step applied a single algorithm to address several of the external and internal parameters that influence radiometric fidelity. Figure 9 displays the visual impact of the correction algorithm on a true color composite. Typical radiometric distortions appear as a general darkening towards the edges of the frame and a bright area (hot spot) at the center. The same brightness shifts are present within most aerial photography, particularly the pronounced hot spot, or glaring, at the center of the photo.

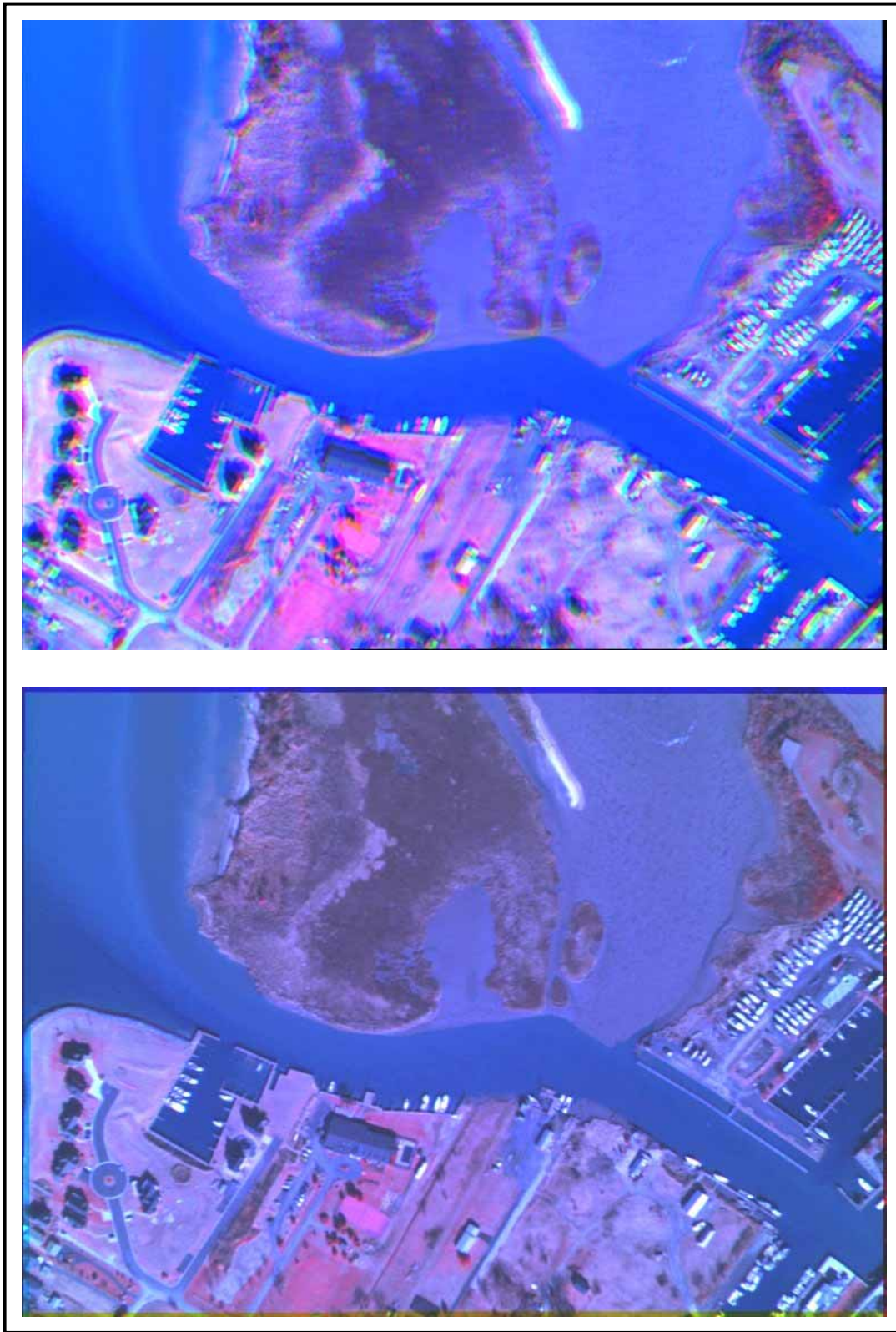


Figure 8. Raw false color CAMIS frame (top) and band registered false color CAMIS frame (bottom) Knapps Narrows, frame # 106.

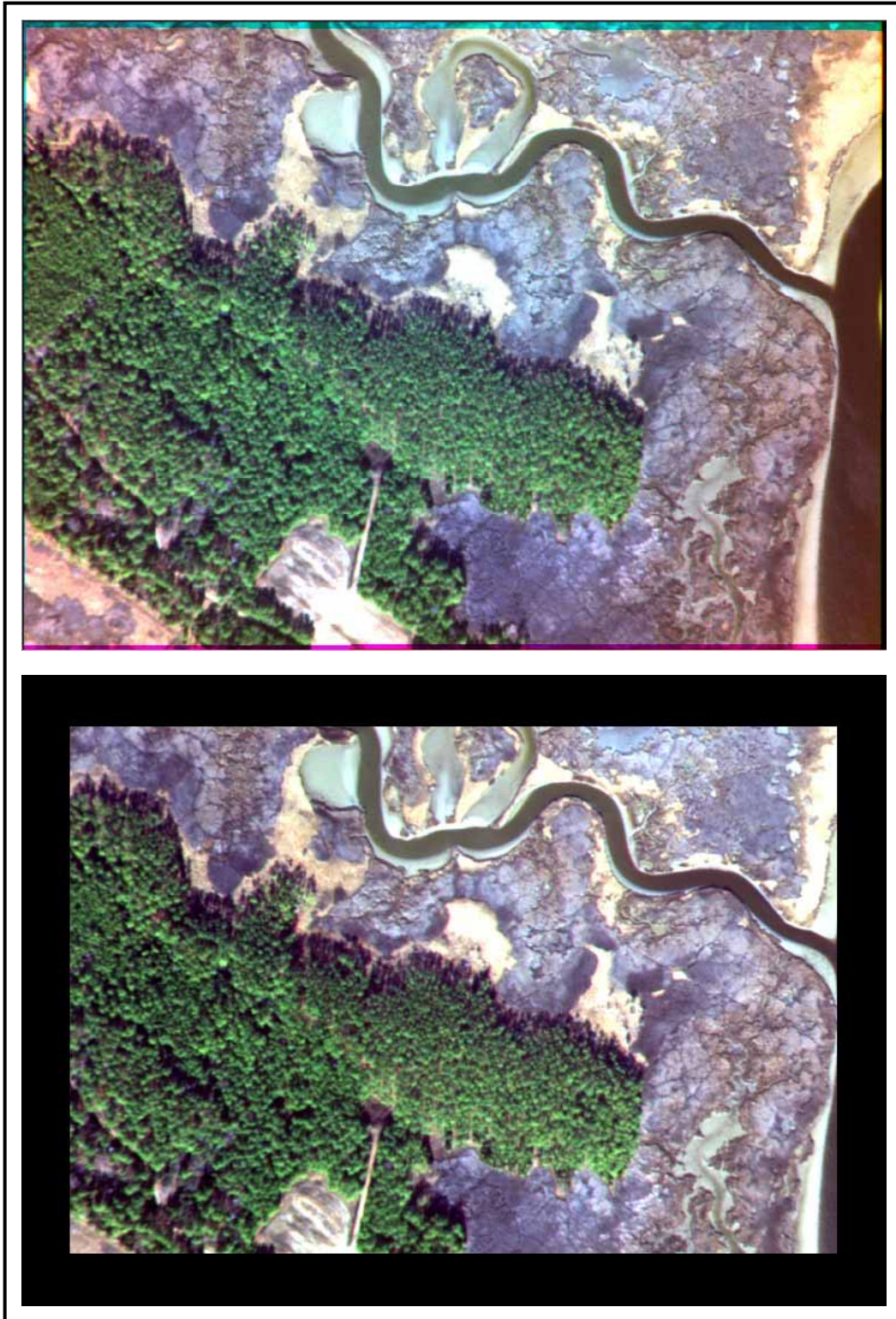


Figure 9. Band registered true color CAMIS frame (top) and radiometrically corrected true color CAMIS frame (below), Hell Hook Marsh, flightline 2, frame #108.

The corrected CAMIS frame shows greatly improved color balance throughout the entire image (Figure 9).

The next step was to create image mosaics encompassing each reference wetland. Commercial image processing software (ENVI) was used to mosaic adjacent digital frames. Figure 10 displays a mosaic of three overlapping images covering the PIN (Piney Creek) site. Geometric distortions were minimized by employing a conformal registration algorithm. In Figure 10, frame #107 served as the base image. Adding frame #106 to the bottom of frame #107 created the initial mosaic. Adding frame #108 to the top of the previous mosaic created the final three-frame composite.

The next step was to geographically register each mosaic to real earth coordinates. Commercial image processing software (ERDAS *Imagine*) geo-registered each individual mosaic to one of two digital base images. The primary source used as digital base maps were high resolution U.S. Geological Survey (USGS) Digital Orthophoto Quarter Quadrangles (DOQQ) were available for the southern research areas, including all of Tilghman Island and Hell Hook Marsh. The Root Mean Square Errors (RMSE), or registration accuracies, of the small mosaics covering the wetland sites on Tilghman Island (Knapps Narrows, Cabin Cove and Harbor Cove) were less than one pixel (< 0.87 meters). The RMSE for the much larger Hell Hook mosaic was roughly nine pixels (~ 7.83 meters). Registration accuracy is critical to the overall quality of the final map products. With good positional accuracies of the mosaics, the digital outputs can be co-registered with other data sets, including any available field data, and utilized in subsequent reference wetland investigations.

DOQQs were not available for the northern sites, including the four Kent Narrows wetlands, Piney Creek, and the Spillway site on Poplar Island. Therefore, medium resolution digital 7.5' topographic quadrangles served as base imagery for geo-registering these sites. Due to the decreased level of detail seen in the digital topo quads (e.g., generalized shore lines, generalized road locations), the registration accuracies of the Kent Narrows and Piney Creek mosaics were much poorer. RMSEs were closer to 10 pixels. Figure 11 shows the relatively minor spatial displacement of the Knapps Narrows mosaic after geo-registration to a DOQQ. Figure 12 shows the significant warping of the Piney Creek mosaic after registration to the digital topographic quadrangle. The Spillway 6 mosaic was not geometrically registered. Because this site is under construction, a reliable base image was not available.

All images were registered to Zone 18 of the Universal Transverse Mercator (UTM) coordinate system. Map coordinate units are meters, and the datum defined in the World Geodetic System 1984 (WGS 84).

The final step in preparing the individual mosaics was to clip out a rectangular image. This subsetting operation removes the majority of the background (i.e., black or blank) pixels around the uneven borders of the mosaics. Figure 13 shows the clipped, or subsetting, mosaics for Knapps Narrows and Piney Creek.



Figure 10. True color, three-frame mosaic of Piney Creek (PIN) wetland.

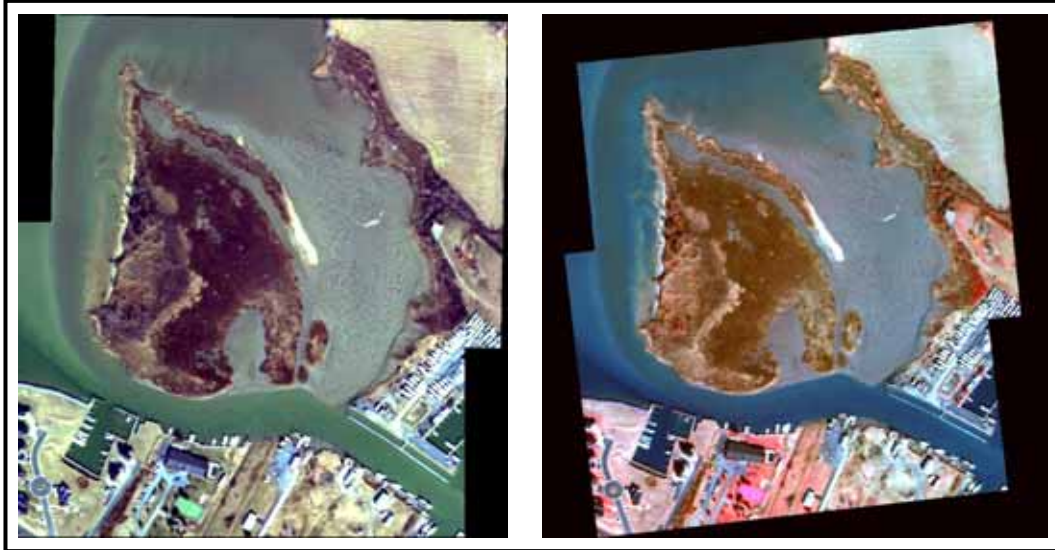


Figure 11. Knapps Narrows mosaic before and after geometric registration to DOQQ. The non-registered mosaic (left) is depicted using true-color (bands 3, 2, & 1); the geo-registered mosaic (right) is depicted using false-color (bands 4, 3, & 2)



Figure 12. Piney Creek (PIN) mosaic before (left) and after (right) geometric registration to digital 7.5' topographic quadrangle.



Figure 13. Knapps Narrows and PIN mosaics after subsetting (or clipping).

2.5 Image Classification

Ground-truth data collection, or site characterization information acquired for each reference wetland, was not included as part of this pilot project to minimize cost. Classification of remotely sensed imagery, using either manual or automated techniques, typically requires ground-truth information and accuracy assessment. Ground-truth data quantifies vegetative parameters, such as species composition and canopy densities, within discrete, geo-referenced sample plots throughout the study area. These sample data statistically train the classification of the entire data set. For image processing applications, ground-truth sample plots are precisely located within the imagery. Multivariate statistics (i.e., training statistics), that define the unique spectral responses of the vegetative classes, are extracted from the imagery at these locations. Supervised classification algorithms, a subset of a larger group of statistical techniques called discriminant analyses, use the training data to assign each pixel to one of many discrete vegetation classes.

If training data are absent, more interpretive discriminant analysis techniques are available to classify remotely sensed imagery into discrete land cover classes. Unsupervised classification, or nonhierarchical clustering, is a standard image-processing tool used to delineate spectrally unique feature classes, or clusters. This technique is more subjective than the supervised technique, relying on image analyst interpretive skill to accurately classify each spectrally unique cluster. However, since the specific objective of this preliminary effort was to delineate only three broad land cover classes, a

modified unsupervised classification technique was employed. The modified approach included:

- Segmenting each mosaic into two primary classes (vegetation vs. non-vegetation) using the Normalized Difference Vegetation Index (NDVI),
- Classifying each primary segment into eight land cover types using an unsupervised clustering routine, and
- Combining the two cluster maps into a final classification.

The resulting class maps displayed 16 land cover types ranging from deep water (typically the darkest feature), to exposed tidal mud flats, to marsh vegetation of varying density and species composition, to evergreen forests, to sand (typically the brightest feature).

No attempt was made to collapse the 16 classes into the three land cover types required for the Poplar Island restoration effort. Because of the absence of site-specific ground truth data, the 16 classes could be combined (i.e., recoded) in various combinations to produce a final class map depicting water, intertidal zones, and vegetation. Therefore, the end user has the flexibility to assign each of the 16 interpreted classes into one of the three general land cover types. Of particular concern, are the transition classes that will define the boundaries between: (1) persistent water and intertidal zones, and (2) sparsely vegetated intertidal areas and non-tidal vegetated marshland. Field personnel familiar with each site will likely accurately determine which groups of the 16 classes to collapse to produce three classes. Note that each of the individual mosaics was classified independently.

The class names were assigned based on the spectral response (i.e., cluster spectral signature statistics) of each cluster relative to its statistically adjacent clusters. This was a subjective process. Therefore, the end user must ultimately assign the most accurate cluster names during the recoding of the 16 classes to the three primary land cover types.

2.6 NDVI Mask

Figure 14 shows an example of the NDVI image for the Knapps Narrows site. The NDVI value for each pixel is calculated using the following equation:

$$\text{NDVI} = \frac{\text{CB}(4) - \text{CB}(3)}{\text{CB}(4) + \text{CB}(3)} \quad \text{Eq. 1}$$

where:

CB(4) = the infrared CAMIS band (800 nm)

CB(3) = the red CAMIS band (650 nm).

The NDVI operation outputs a single raster layer. Therefore, the pixel values are displayed using a grayscale (black and white) lookup table. The unique value assigned to each pixel ranges from -1 to +1. Values approaching -1 indicate unhealthy or dead vegetation. As live vegetative biomass increases, the index value also increases to a

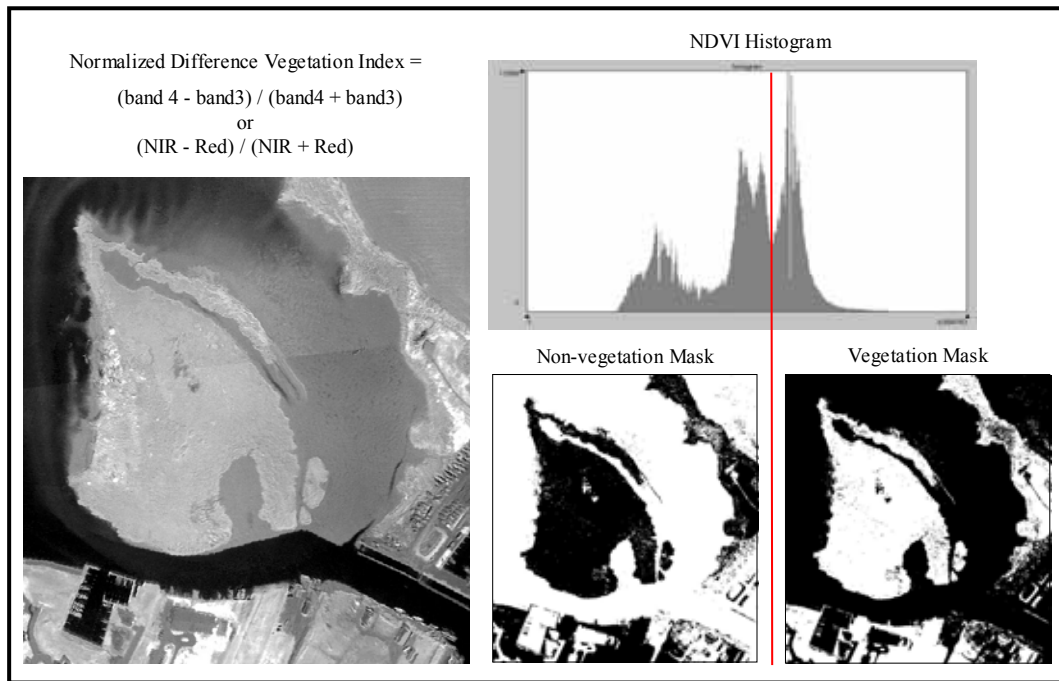


Figure 14. NDVI image (left), NDVI histogram (upper right), and primary NDVI masks.

maximum of +1. Figure 14 also shows the resulting histogram of pixel values derived from the NDVI image for Knapps Narrows. The NDVI image for each reference wetland was split into two segments by visually interpreting the NDVI histogram, the NDVI image and the original multispectral mosaic. The first image segment contained all non-vegetation areas, depicted with darker pixels; the second contained the brighter vegetated pixels. This subjective distinction was not completely accurate since pixels near the center of the NDVI histogram (i.e., near the threshold value) represented mixed pixels, or pixels displaying spectral properties of both vegetated and non-vegetated features. Leaf-off conditions during image acquisition meant that the deciduous trees and shrubs were without leaves. In addition, the reed and grass species were fully senesced. The lack of photosynthetically active vegetation may have somewhat diminished the overall interpretability of the NDVI image by reducing the contrast between vegetated and non-vegetated segments. However, the NDVI image still was able to adequately separate those pixels that were primarily vegetation from those pixels that did not include vegetation. This is based on the fact that the near infrared reflectance properties of chlorotic and necrotic vegetation is still very different from the near infrared spectral response of non-vegetated features, such as water and bare soil.

The segmented images for each mosaic were converted into two masks. An image mask assigns a value of 1 to pixels that are “switched on” and a value of zero to pixels that are “switched off” (Figure 14). The non-vegetation mask had all non-vegetation pixels

assigned a value of 1, and all vegetation pixels assigned a value of zero. The vegetation mask maintained the reverse values (i.e., veg = 0, non-veg = 1). Each mask was independently applied to the original four-band mosaic creating two unique multispectral images (Figure 15). One image contained primarily vegetated pixels and the other contained the remaining non-vegetated pixels.

2.7 Unsupervised Clustering

ERDAS *Imagine* image processing software contains a standard nonhierarchical clustering routine. This unsupervised classification algorithm was applied to both the non-vegetated and the vegetated four-band, multispectral image segments created by the NDVI masking procedure. *Imagine* allows the analyst to determine the total number of land cover classes (or clusters) classified within the input image. For this study, eight thematic classes were delineated within each of the primary segments (vegetated and non-vegetated). The selection of eight classes for each of the two image segments was based on field experience at sites similar to the reference wetlands. A subjective evaluation of the general land cover structure and relative abundances of the vegetated and non-vegetated surface features, suggested that eight clusters would sufficiently classify each segment. Using the original four-band mosaic as an interpretative replacement for ground-truth data, each of the eight unique spectral classes was assigned a land cover designation (Figure 16). Finally, combining the segmented thematic images produced a complete land cover classification of the area of interest (Figure 17).

Modifications of land cover designations were required during compilation of the final class map for each site. Many of the class names are relatively imprecise or primitive in describing the land cover features. In addition, many classes are associated with two or more cover types, with some including both vegetated and non-vegetated features.

2.8 Minimum Mapping Unit

Very high-resolution imagery typically provides far more detail than can be efficiently used in landscape mapping applications. For example, high quality, large-scale aerial photography will provide adequate clarity and detail to accurately identify surface features that are no larger than a few square feet. It is unlikely that a photo interpreter would be required to delineate image features only a few feet in diameter. Instead, the analyst will work within the limits of a predefined Minimum Mapping Unit (MMU). This two-dimensional area represents the minimum size of the polygon delineated within the aerial photo. Land use/land cover classifications commonly use a MMU of one acre to one hectare for large scale maps and much larger MMU sizes, such as 10 to 100 hectares for very small-scale land cover maps. The MMU used in this application is very small as compared to most land cover classification schemes. All reference wetland class maps were subjected to a 9-pixel ($\sim 6.8 \text{ m}^2$) minimum mapping unit filtering routine. This two-step routine first uses a simple raster GIS technique to find and remove all raster polygons that are less than or equal to 9 pixels. A raster polygon is a contiguous group of pixels that have the same land cover class designation. The thematic image is then “sieved” to remove those raster polygons below the 9-pixel minimum threshold.

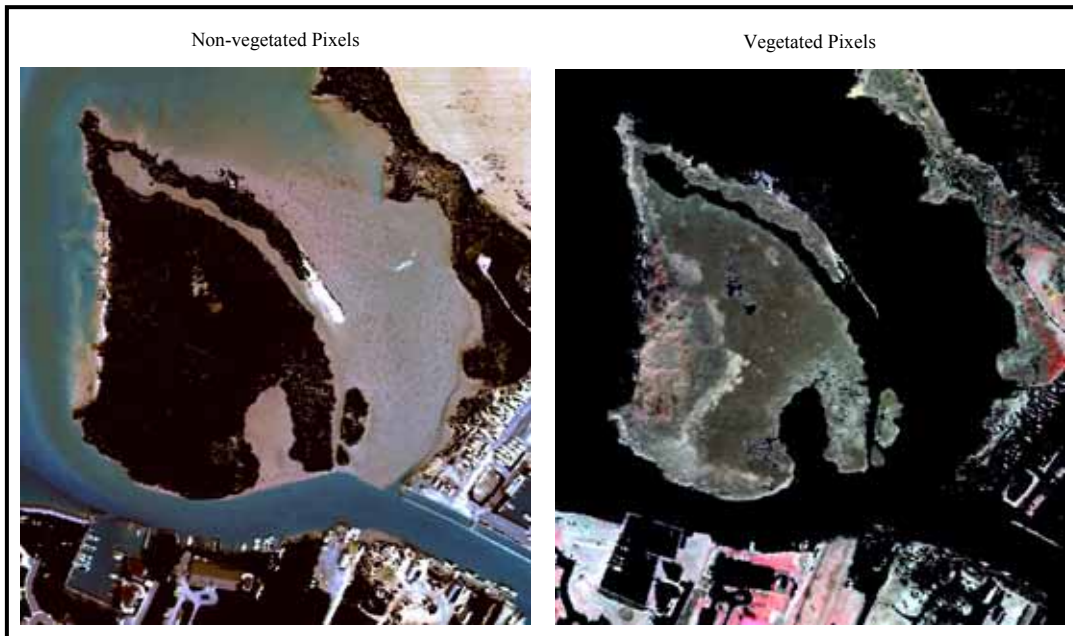


Figure 15. Primary image segments after NDVI masking.

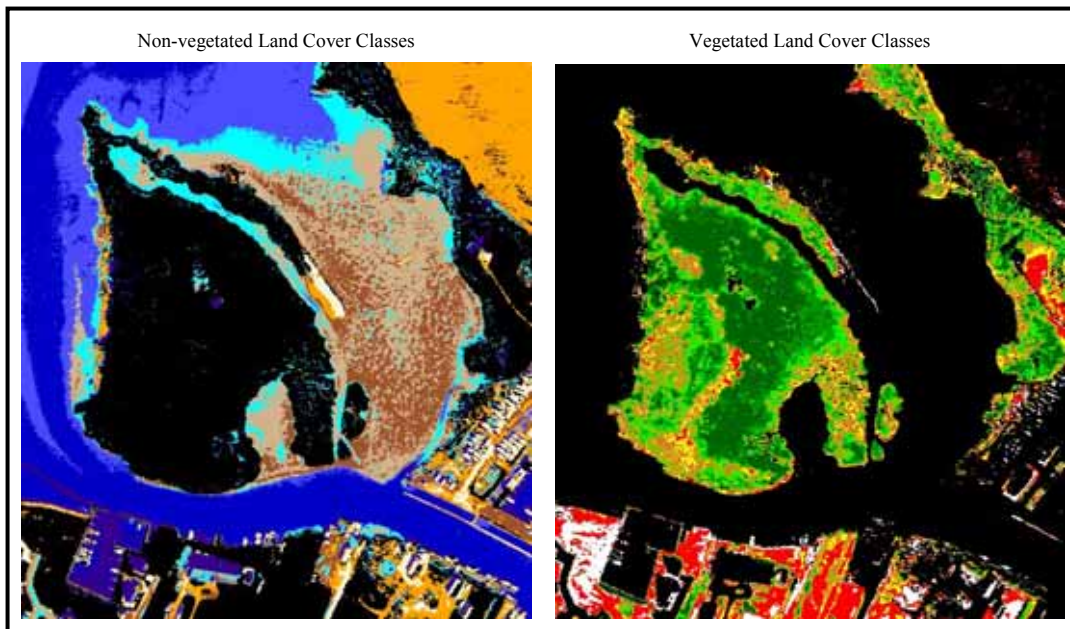


Figure 16. Results of unsupervised classification of each primary segment.

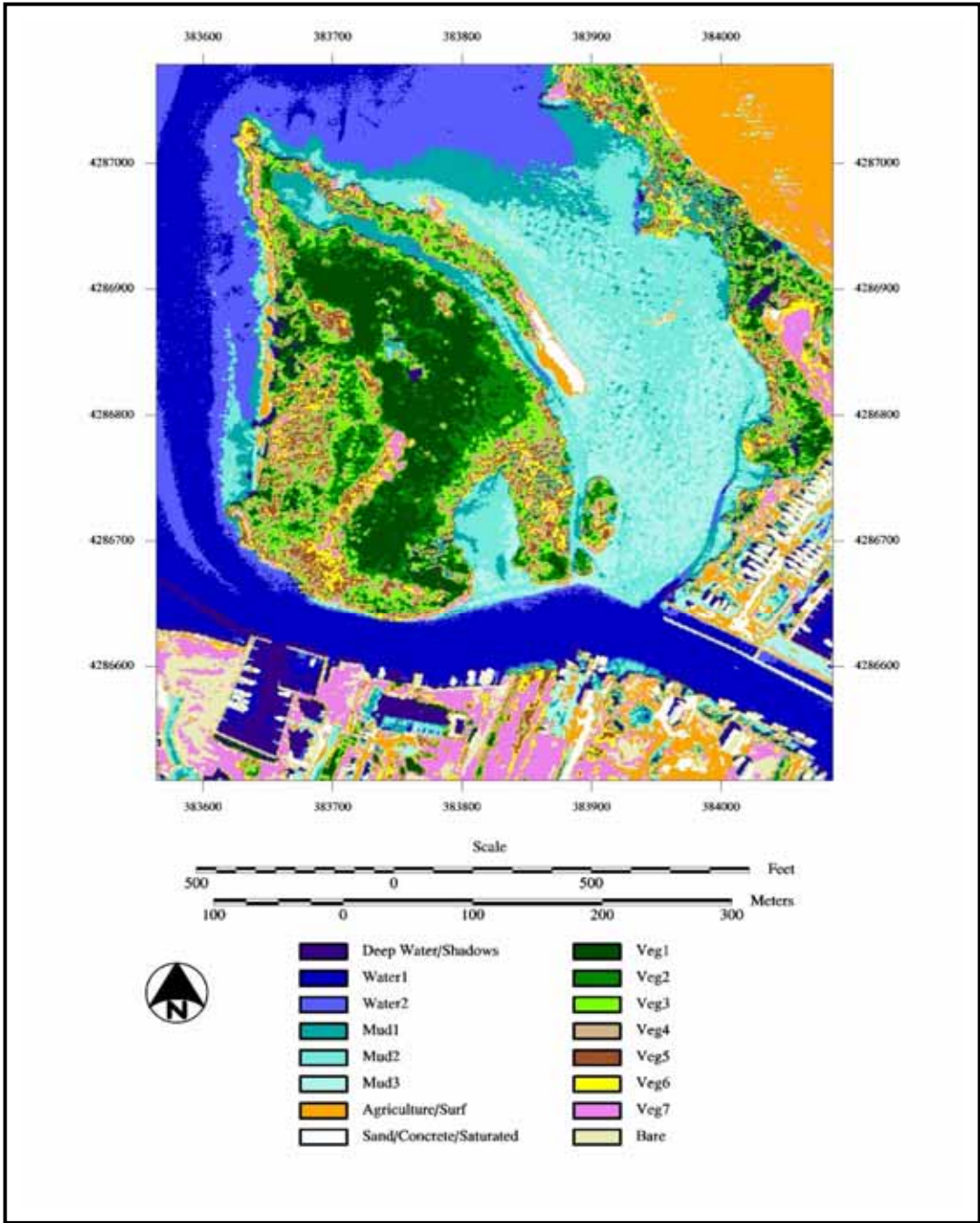


Figure 17. Class map of Knapps Narrows—full resolution.

The “holes” (removed raster polygons) are then filled by iteratively passing a 3x3 majority filter over the image until all of the deleted pixels are reassigned to a new class value.

There were two reasons for applying the MMU filter:

1. The 9-pixel “sieve” effectively removed the majority of the thematic noise in the output class maps. With high spatial resolution imagery, single pixels and small groups of adjacent pixels comprise raster polygons that are very difficult to ground truth. The very fine level of detail provided by these maps is typically not required and may actually degrade the interpretability and the overall accuracy of the classification.
2. Output products include ArcView shapefiles. Preliminary examination of shapefiles created from the full resolution class maps suggested that the interpretability of these vector files would be very difficult. File size was also a problem with the full resolution maps. The filtered class maps stored the data with greatly reduced file sizes and appeared to offer more easily interpreted data.

Figure 18 displays the result of the MMU filter on the Knapps Narrows class map. Employing an extremely small MMU for this project maintained the detail provided by the classified CAMIS images.

3.0 RESULTS

3.1 Image Quality

As described above, flying conditions were good (full sun and light winds). However, the decrease in aircraft altitude reduced the pixel dimensions (i.e., increased spatial resolution) and, more importantly, decreased the image footprint (i.e., the surface area captured within a single frame). The lower altitude did not adversely affect frame “endlap” (overlap between consecutive frames along a single flightline) but significantly decreased the “sidelap” (the amount of frame overlap between adjacent flightlines). The three flightlines covering the four sites within Marsh Creek and Muddy Creek maintained enough sidelap to adequately cover the areas of interest. However, the four flightlines acquired over Hell Hook Marsh contained “holidays” (gaps) between flightlines 1 and 2. A continuous holiday exists between flightlines 3 and 4 over Hell Hook Marsh (Figure 19).

Due to both leaf off conditions and the inclusion of large areas of open water, the color contrast of the features within the images ranged from very dark (e.g., water) to very bright (e.g., sand, concrete, healthy pine canopies). To compensate for the relatively low spectral response of these dark features, image acquisition settings included a longer

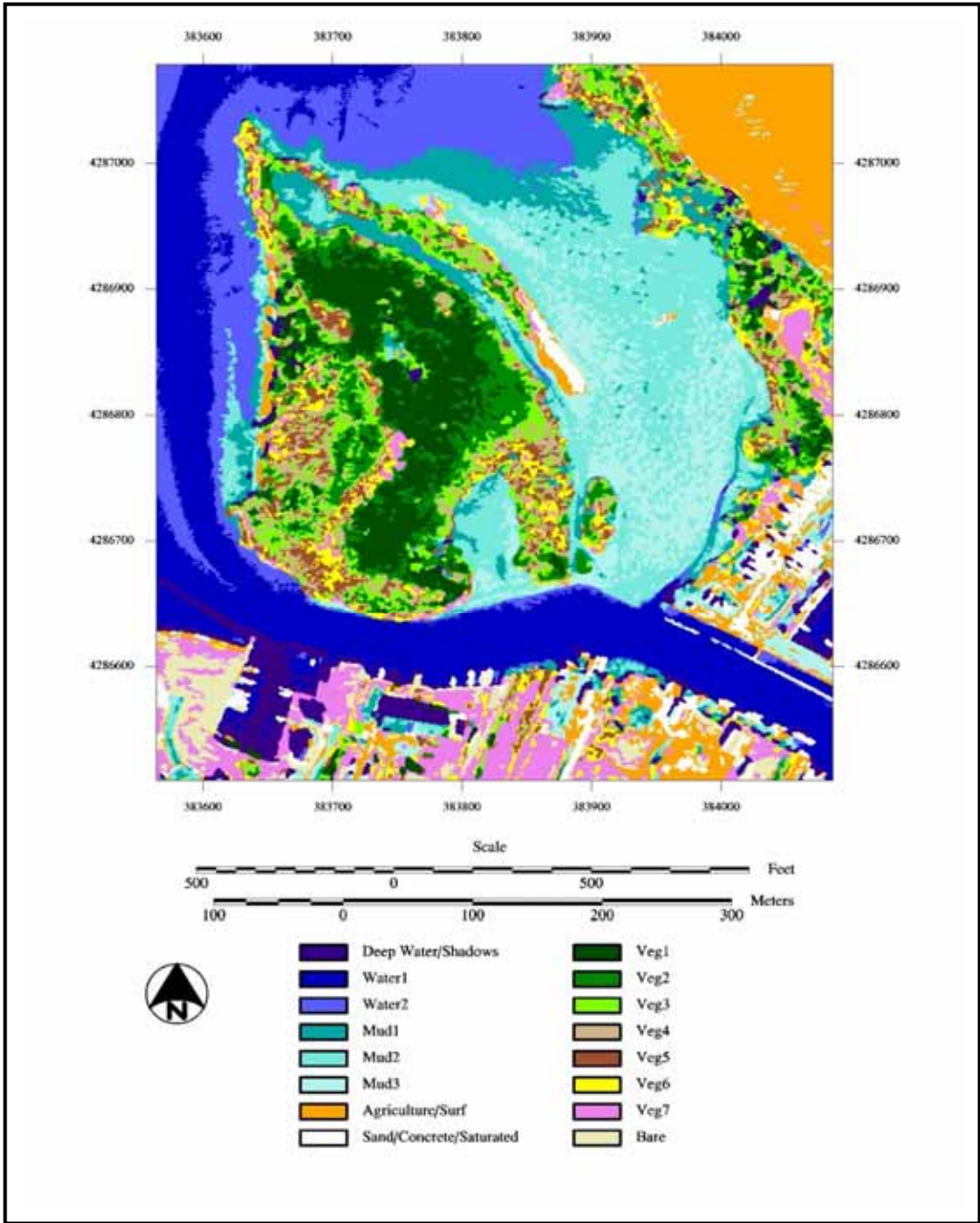


Figure 18. Class map of Knapps Narrows after application of Minimum Mapping Unit filter (MMU = 9 pixels)



Figure 19. Mosaic of Hell Hook Marsh showing significant holidays between flightlines.

integration time (or slower shutter speed). The increased integration time lead to saturation (glaring) of some of the brighter pixels. In fact, pixel saturation was apparent during acquisition. However, the system was set to acquire using a slower shutter speed, assuming that an increase in image contrast would potentially enhance the spectral differences among the darker features. Many of the frames displayed some pixel saturation. However, the overall radiometric quality of the images was acceptable with enhanced color contrast observed throughout the water, wet soil, and senesced vegetation classes.

The greatest disappointment for the project was the exceptionally poor quality of the images acquired over Spillway 6 on Poplar Island. The extreme level of saturation within these images resulted from the highly reflective disturbed soils associated with construction activities. While not evident during acquisition, pixel saturation rendered this flightline relatively useless for land cover classification. Figure 20 shows both the false color and true color mosaic for the Spillway site.

3.2 Land Cover Classification

The CAMIS image classification techniques produced detailed land cover class maps. Quantitative accuracy assessment of vegetation class identification would have required extensive field data collection at each site. As stated above, field data were not collected as part of the pilot project. However, based on previous CAMIS image interpretation over other coastal wetland study sites, the cover classes likely separated into the following general categories:

- evergreen (maritime) forests,
- tall/dense reeds,
- short/less dense reeds,
- marsh grasses,
- vegetated tidal zones,
- non-vegetated tidal zones, and
- permanent water channels of varying depth.

As described above, the assigned class names are related to spectral response (i.e., cluster spectral signature statistics) of each cluster relative to its statistically adjacent clusters. This was a subjective process. Therefore, the end user will determine the most accurate recoding of the general land categories into the three primary land cover types.

The following sections describe each wetland site.

Spillway #6

No land cover classification was performed on this site due to the extreme radiometric saturation throughout the mosaic (Figure 20).

Knapps Narrows

The processing of this wetland site is provided above as the example site for image correction and classification routines. (Of the three sites located within Tilghman Island,



Figure 20. False color (left) and true color (right) mosaics for Spillway 6 site, within Poplar Island restoration/construction area.

Knapps Narrows was the most successful. The reduced altitude of the aircraft significantly reduced the spatial coverage of both the Cabin Cove site and the Harbor Cove site.)

Cabin Cover

The single flightline for this site missed the most eastern reaches of the wetland area. Figure 21 shows the false color composite. Figure 22 shows the class map, after application of the 9-pixel MMU threshold.

Harbor Cove

Because of the difficulty of locating this site during image acquisition, only a small portion of the area was captured. Therefore, image classification was not performed at this site. Figure 23 shows a false color composite.

Marsh Creek Sites (South, East, North)

These three wetlands are all relatively narrow strips of marsh, with minimal persistent and/or tidal channels. The mosaics include significant areas of upland vegetation and open water. The relative areal coverage of both the wetland and non-wetland coastal habitats should provide adequate preliminary estimates of the proportions of each of these cover types required on Poplar Island. Figures 24, 26, and 28, respectively, show false color composites of the South, East, and North sites. Figures 25, 27, and 29, respectively show the MMU filtered class maps for each site.

Muddy Creek

With the exception of Hell Hook Marsh, this area required the greatest number of individual frames to cover the reference wetlands. Like the Marsh Creek sites, the area supports a limited system of dendritic channels. Figure 30 shows the false color composite image. Figure 31 shows the filtered class map.

Piney Creek

Figure 32 shows the false color composite of this narrow wetland. As with the other reference wetlands, the site includes both upland communities and diverse low/high marsh vegetation types, but only one relatively short tidal channel. Figure 33 shows the filtered class map.

Hell Hook Marsh

The largest of the reference sites, the full mosaic of Hell Hook Marsh (cf. Figure 19) includes diverse marsh communities and vast system of both persistent and tidal channels and guts. Unlike the previous mosaics, this class map of the mosaic subset (Figure 34) was filtered with a 25-pixel minimum mapping unit threshold. The Hell Hook wetland class map will likely provide the most useful estimates of water channel dendricity.



Figure 21. False color composite for Cabin

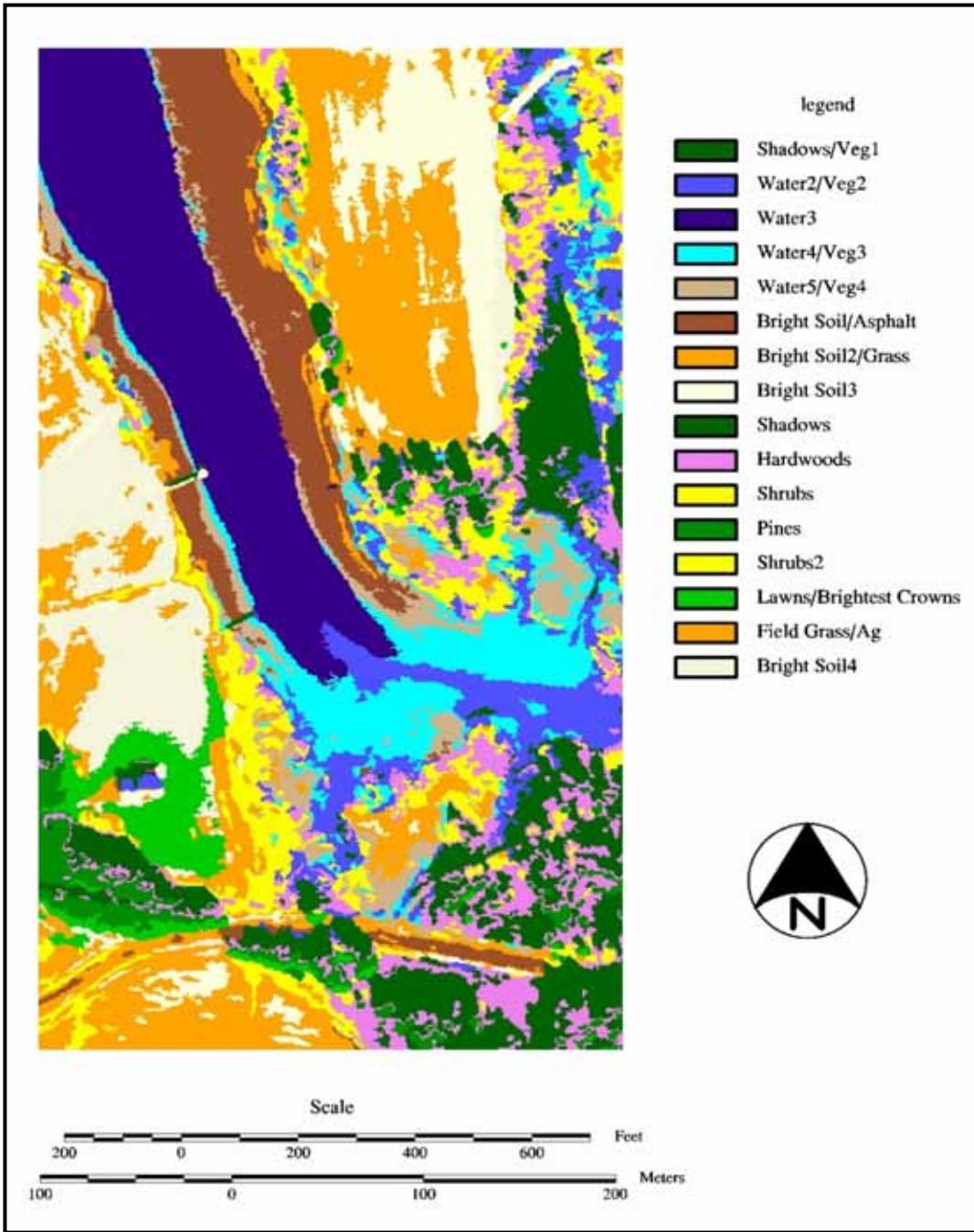


Figure 22. Class map for Cabin Cove after application of Minimum Mapping Unit filter (MMU = 9 pixels)

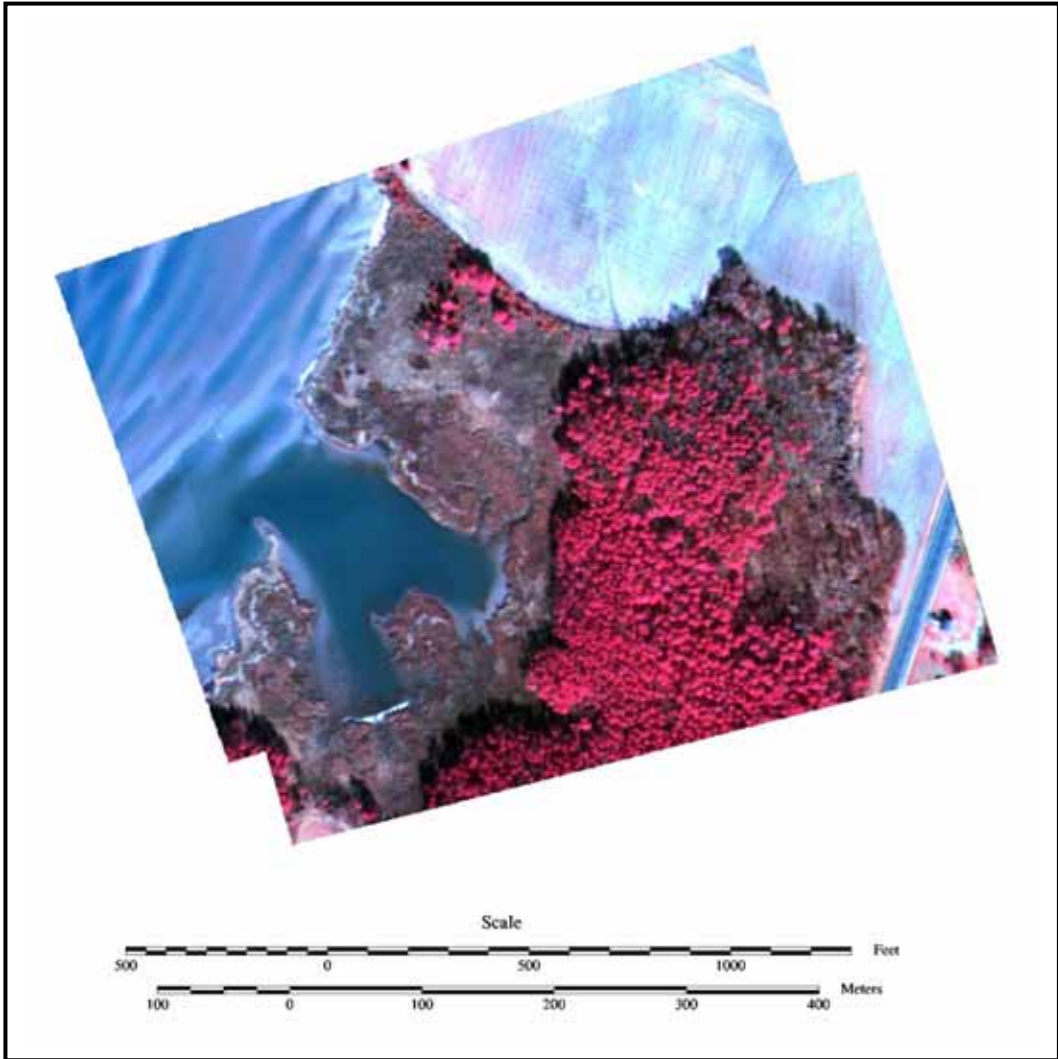


Figure 23. False color composite for Harbor Cover

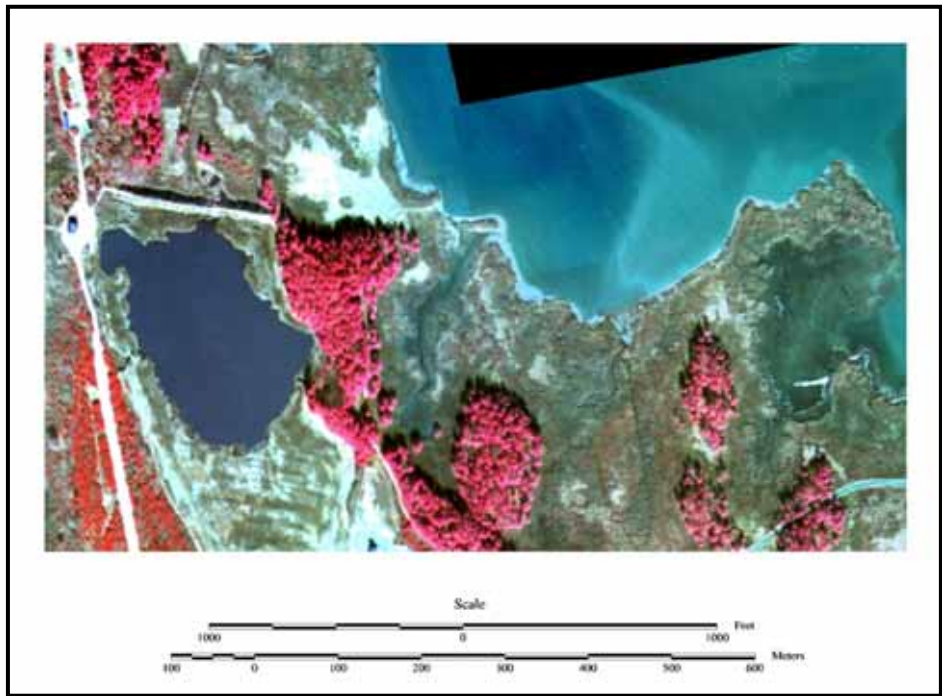


Figure 24. False color composite for Marsh Creek South.

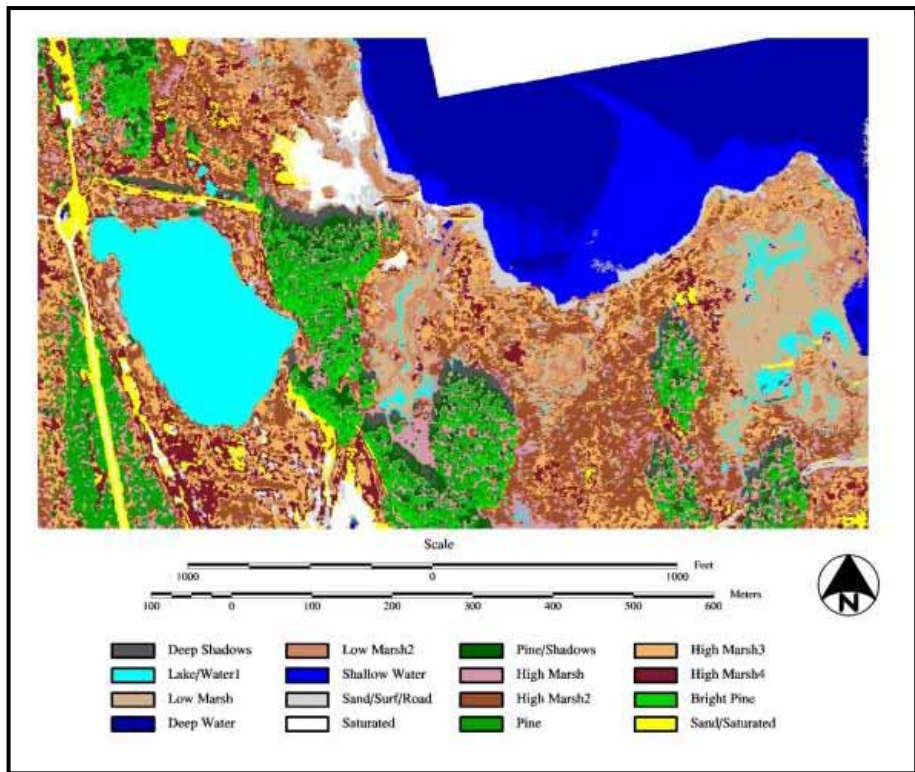


Figure 25. Class map for Marsh Creek South after application of Minimum Mapping Unit filter (MMU = 9 pixels)



Figure 26. False color composite for Marsh Creek East

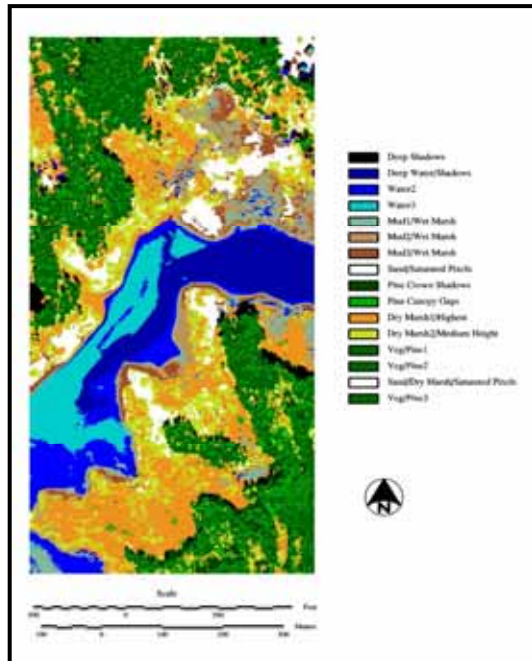


Figure 27. Class map for Marsh Creek East after application of Minimum Manning Unit filter

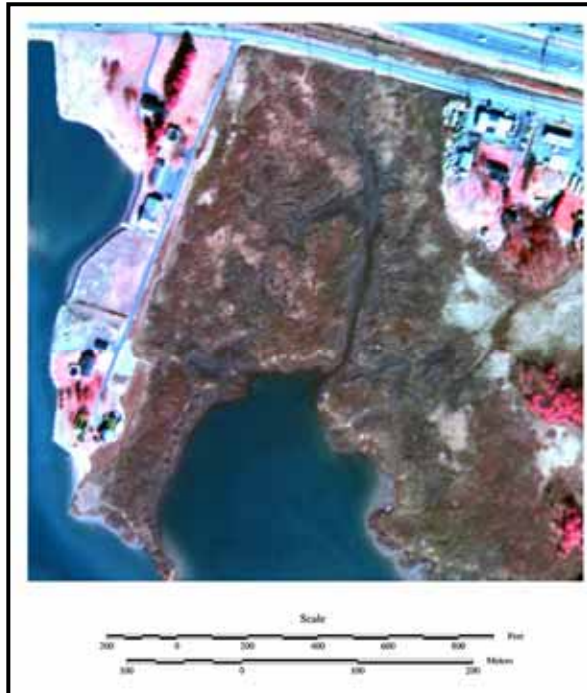


Figure 28. False color composite for Marsh Creek North.

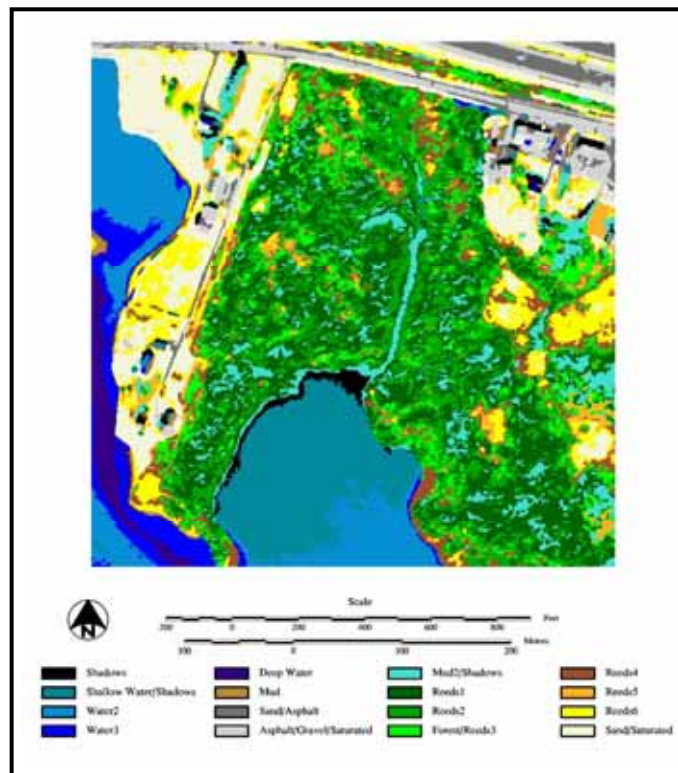


Figure 29. Class map for Marsh Creek North after application of Minimum Mapping Unit Filter (MMU = 9 pixels).

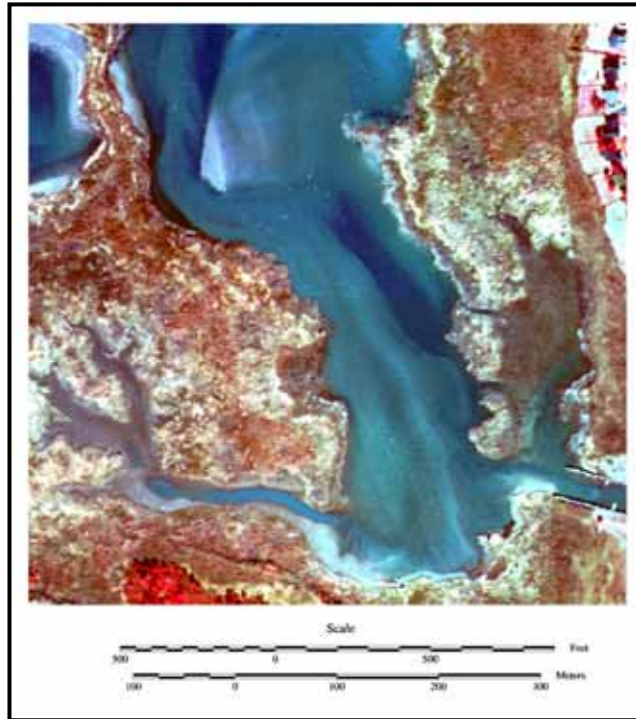


Figure 30. False color composite for Muddy Creek.

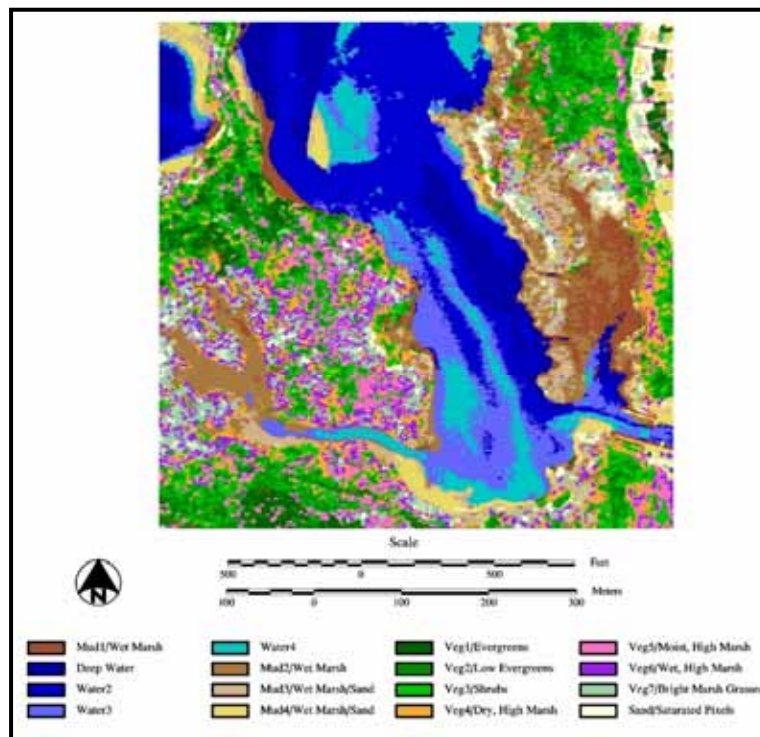


Figure 31. Class map for Muddy Creek after application of Minimum Mapping Unit filter (MMU = 9 pixels)



Figure 32. False color composite for Piney Creek.

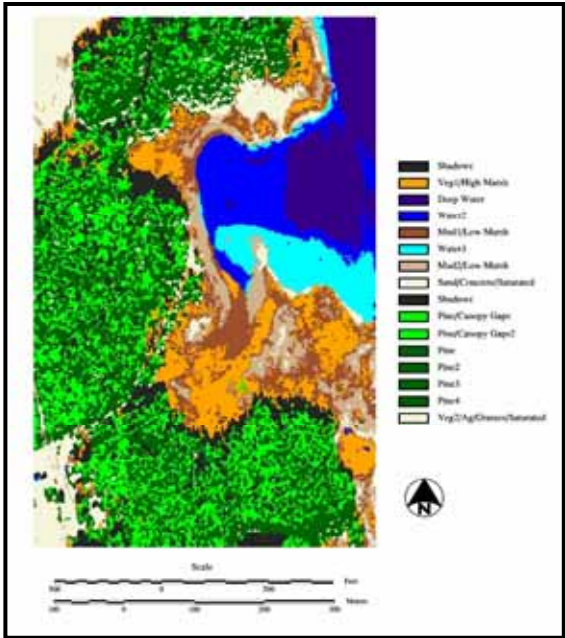


Figure 33. Class map for Piney Creek after application of Minimum Mapping Unit filter (MMU = 9 pixels)

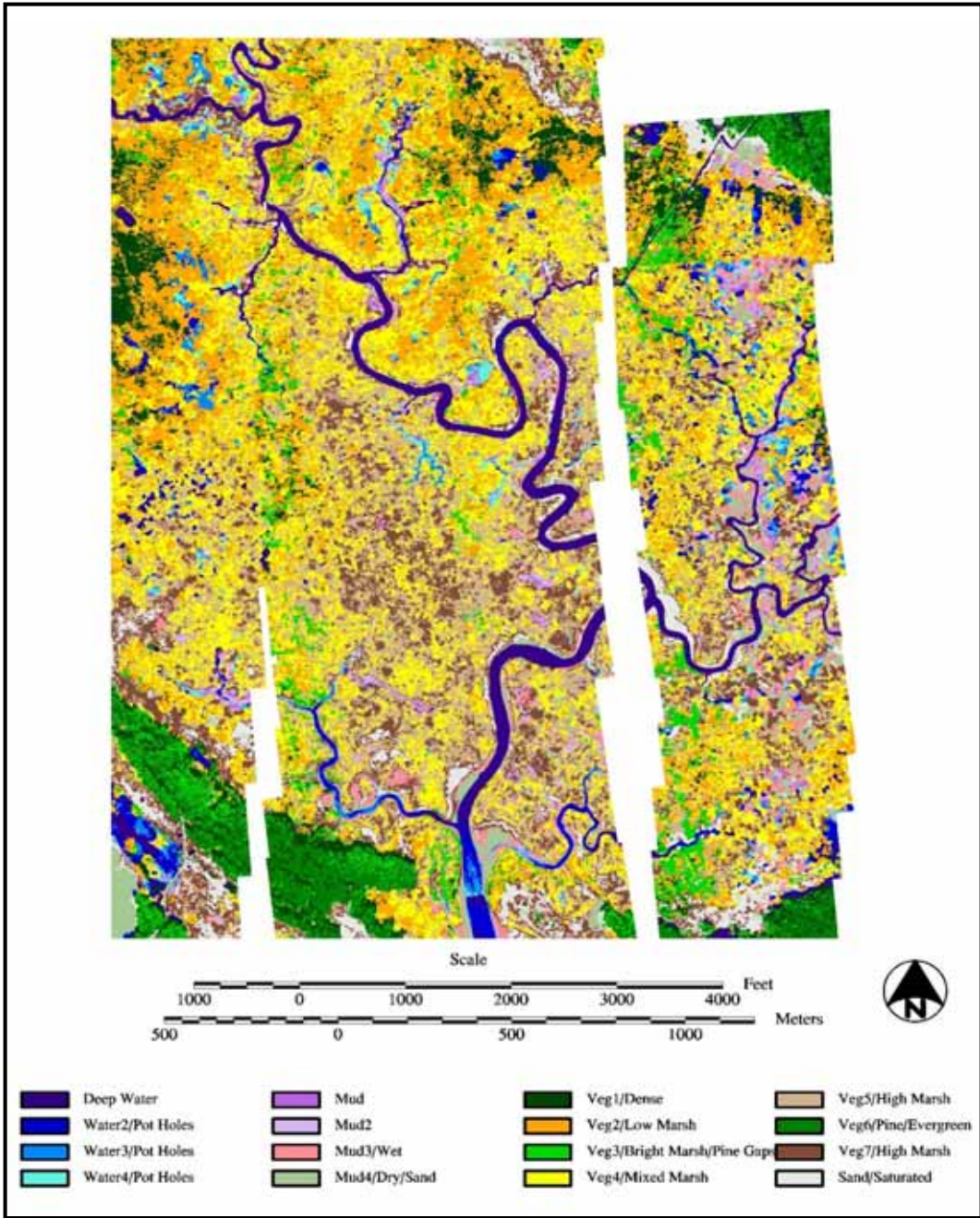


Figure 34. Class map for Hell Hook Marsh after application of Minimum Mapping Unit filter (MMU = 25 pixels)

3.3 Land Cover Area Estimates

Tables 1 through 8 list the total area (in hectares) occupied by each of the interpreted land cover classes, given for both the full resolution class maps and the minimum mapping unit filtered class maps for (respectively): Knapps Narrows, Cabin Cove, MCS, MCE, MCN, MUD, PIN, and Hell Hook Marsh.

3.4 Output Images and Shapefiles

The following sections describe the complete set of images and output map products.

3.4.1 Raw CAMIS Frames

The uncorrected CAMIS images are available. Each study site is stored in its own subdirectory. Raw CAMIS imagery is written to disk during acquisition as a pair of “tagged image file” format files (“TIF” files, which are designated by the filename extension “*.tif”). One is a three-band TIF file containing bands 2 (green), 3 (red), and 4 (near infrared). The companion TIF file contains only band 1 (blue). These files are in their raw form, with no corrections or alterations. Because these files have not been band-to-band registered, the three-band TIF will appear to be of very poor quality (cf. Figure 8).

3.4.2 Post-Processed CAMIS Frames

The full set of corrected CAMIS images is also available. Each study site is stored in its own sub-directory. Each individual image file contains all four bands, with blue in band 1, green in band 2, red in band 3, and near infrared in band 4. These data are stored in a generic binary format. The following file format information will be required to view each frame using standard image processing software:

- File Size = 768 columns (or pixels) x 576 lines (or rows)
- Number of Bands = 4
- Format = BSQ (band interleaved sequential)
- File Header Bytes = 0
- Band Header Bytes = 0
- Data Type = unsigned 8-bit.

3.4.3 Geo-Registered Mosaics

The geographically rectified mosaics for each study site are provided in an ERDAS *Imagine* format. Individual site sub-directories contain the full mosaics. These images use the following naming convention: <name>_reg.img, where <name> = site name (e.g., knapps, cabin), the suffix “_reg” indicates geometric registration, and “.img” identifies the ERDAS file extension. The subsetted, or clipped, images are also included. These images use the naming convention: <name>_sub.img, where the suffix “_sub” denotes a subset of the full, registered mosaic. The files are viewable in ArcView. The spillway #6 mosaic was not geo-registered due to the absence of a reliable reference map

Table 1. Areal extent of land cover classes for Knapps Narrows.

Class Names	All* # pixels	All hectares	All %	MMU9* # pixels	MMU9 hectares	MMU9 %
Deep Water/Shadows	13915	1.05	3.53	15089	1.14	3.83
Water1	58129	4.40	14.74	58571	4.43	14.86
Water2	37531	2.84	9.52	36637	2.77	9.29
Mud1	25854	1.96	6.56	25439	1.93	6.45
Mud2	47475	3.59	12.04	47906	3.63	12.15
Mud3	30842	2.33	7.82	29031	2.20	7.36
Agriculture/Surf	31531	2.39	8.00	32666	2.47	8.29
Sand/Concrete/Saturated	8529	0.65	2.16	10043	0.76	2.55
Veg1	24814	1.88	6.29	25139	1.90	6.38
Veg2	21159	1.60	5.37	21276	1.61	5.40
Veg3	18983	1.44	4.81	19530	1.48	4.95
Veg4	15533	1.18	3.94	13838	1.05	3.51
Veg5	14938	1.13	3.79	13944	1.06	3.54
Veg6	14381	1.09	3.65	13951	1.06	3.54
Veg7	19681	1.49	4.99	20248	1.53	5.14
Bare	10961	0.83	2.78	10948	0.83	2.78
Total		29.84	100.00		29.84	100.00

*ALL = full resolution class map; MMU9 = 9 pixel minimum mapping unit class map.

Table 2. Areal extent of land cover classes for Cabin Cove.

Class Names	All* # pixels	All hectares	All %	MMU9* # pixels	MMU9 hectares	MMU9 %
Shadows/Veg1	10163	0.77	4.67	10689	0.81	4.91
Water2/Veg2	14541	1.10	6.68	14832	1.12	6.82
Water3	25166	1.90	11.56	25163	1.90	11.56
Water4/Veg3	14602	1.11	6.71	13846	1.05	6.36
Water5/Veg4	10379	0.79	4.77	10174	0.77	4.68
Bright Soil/Asphalt	15324	1.16	7.04	15414	1.17	7.08
Bright Soil2/Grass	17889	1.35	8.22	17994	1.36	8.27
Bright Soil3	14376	1.09	6.61	14331	1.08	6.59
Shadows	12241	0.93	5.62	11970	0.91	5.50
Hardwood	15919	1.20	7.32	15948	1.21	7.33
Shrubs	11524	0.87	5.30	11730	0.89	5.39
Pines	5839	0.44	2.68	5860	0.44	2.69
Shrub2	8732	0.66	4.01	8488	0.64	3.90
Lawn/Brightest Crowns	6299	0.48	2.89	6354	0.48	2.92
Field Grass/Ag	18901	1.43	8.69	18925	1.43	8.70
Bright Soil4	15725	1.19	7.23	15902	1.20	7.31
Total		16.47	100.00		16.47	100.00

*ALL = full resolution class map, MMU9 = 9 pixel minimum mapping unit class map.

Table 3. Areal extent of land cover classes for Marsh Creek South.

Class Names	All* # pixels	All hectares	All %	MMU9* # pixels	MMU9 hectares	MMU9 %
Deep Shadows	10815	0.82	1.33	11119	0.84	1.36
Lake/Water1	64674	4.90	7.94	61909	4.69	7.60
Low Marsh	66066	5.00	8.11	66232	5.01	8.13
Deep Water	114208	8.64	14.01	115122	8.71	14.13
Low Marsh2	44892	3.40	5.51	42572	3.22	5.22
Shallow Water	57026	4.32	7.00	55870	4.23	6.86
Sand/Surf/Road	26303	1.99	3.23	24633	1.86	3.02
Saturated	16267	1.23	2.00	16355	1.24	2.01
Pine/Shadows	23346	1.77	2.86	23182	1.75	2.84
High Marsh	51254	3.88	6.29	49303	3.73	6.05
High Marsh2	101808	7.71	12.49	105768	8.01	12.98
Pine	48891	3.70	6.00	51417	3.89	6.31
High Marsh3	88250	6.68	10.83	91115	6.90	11.18
High Marsh4	54891	4.15	6.74	54607	4.13	6.70
Bright Pine	22759	1.72	2.79	22239	1.68	2.73
Sand/Saturated	23474	1.78	2.88	23481	1.78	2.88
Total		61.68	100.00		61.68	100.00

ALL = full resolution class map, MMU9 = 9 pixel minimum mapping unit class map.

Table 4. Areal extent of land cover classes for Marsh Creek East.

Class Names	All* # pixels	All hectares	All %	MMU9* # pixels	MMU9 hectares	MMU9 %
Deep Shadows	8866	0.67	1.55	8922	0.68	1.56
Deep Water/Shadows	41857	3.17	7.33	40841	3.09	7.16
Water2	38816	2.94	6.80	37198	2.82	6.52
Water3	33785	2.56	5.92	33696	2.55	5.90
Mud1/Wet Marsh	24018	1.82	4.21	21682	1.64	3.80
Mud2/Wet Marsh	23479	1.78	4.11	22325	1.69	3.91
Mud3/Wet Marsh	16929	1.28	2.97	16219	1.23	2.84
Sand/Saturated Pixels	9734	0.74	1.71	9817	0.74	1.72
Pine Crown Shadows	32836	2.49	5.75	33107	2.51	5.80
Pine Canopy Gaps	42154	3.19	7.39	41247	3.12	7.23
Dry Marsh1/Highest	101064	7.65	17.71	107776	8.16	18.88
Dry Marsh2/Medium Height	70796	5.36	12.40	72727	5.50	12.74
Veg/Pine	42266	3.20	7.41	43249	3.27	7.58
Veg/Pine	31552	2.39	5.53	29871	2.26	5.23
Sand/Dry Marsh/Saturated Pixels	30098	2.28	5.27	28873	2.19	5.06
Veg/Bright Pine	22505	1.70	3.94	23205	1.76	4.07
Total		43.20	100.00		43.20	100.00

ALL = full resolution class map, MMU9 = 9 pixel minimum mapping unit class map.

Table 5. Areal extent of land cover classes for Marsh Creek North.

Class Names	All* # pixels	All hectares	All %	MMU9* # pixels	MMU9 hectares	MMU9 %
Shadows	3844	0.29	1.24	4018	0.30	1.30
Shallow Water/Shadows	25210	1.91	8.16	24611	1.86	7.96
Water2	23516	1.78	7.61	23064	1.75	7.46
Water3	9949	0.75	3.22	9560	0.72	3.09
Deep Water	5698	0.43	1.84	5479	0.41	1.77
Mud	2338	0.18	0.76	1425	0.11	0.46
Sand/Asphalt	8310	0.63	2.69	8801	0.67	2.85
Asphalt/Gravel/Saturated	11035	0.84	3.57	11815	0.89	3.82
Mud2/Shadows	19305	1.46	6.24	18142	1.37	5.87
Reeds1	54255	4.11	17.55	57217	4.33	18.51
Reeds2	41016	3.10	13.27	41692	3.16	13.49
Forest/Reeds3	23688	1.79	7.66	21847	1.65	7.07
Reeds4	19022	1.44	6.15	18686	1.41	6.04
Reeds5	9712	0.74	3.14	8432	0.64	2.73
Reeds6	21340	1.62	6.90	21896	1.66	7.08
Sand/Saturated	30894	2.34	9.99	32447	2.46	10.50
Total		23.40	100.00		23.40	100.00
*ALL = full resolution class map, MMU9 = 9 pixel minimum mapping unit class map.						

Table 6. Areal extent of land cover classes for Muddy Creek.

Class Names	All* # pixels	All hectares	All %	MMU9* # pixels	MMU9 hectares	MMU9 %
Mud1/Wet Marsh	21133	1.60	4.75	19686	1.49	4.43
Deep Water	27923	2.11	6.28	27782	2.10	6.25
Water2	56971	4.31	12.81	58315	4.41	13.11
Water3	31539	2.39	7.09	31668	2.40	7.12
Water4	26659	2.02	5.99	25034	1.89	5.63
Mud2/Wet Marsh	36592	2.77	8.23	38144	2.89	8.58
Mud3/Drier, Low Marsh/Sandy	23559	1.78	5.30	24825	1.88	5.58
Mud4/Driest, Low Marsh/Sand	15180	1.15	3.41	14980	1.13	3.37
Veg1/Evergreens	12780	0.97	2.87	12279	0.93	2.76
Veg2/Low Evergreens	30143	2.28	6.78	31387	2.38	7.06
Veg3/Shrubs	41739	3.16	9.38	44947	3.40	10.10
Veg4/Dry, High Marsh	33340	2.52	7.50	30784	2.33	6.92
Veg5/Moist, High Marsh	22616	1.71	5.08	21751	1.65	4.89
Veg6/Wetter, High Marsh	28310	2.14	6.36	26123	1.98	5.87
Veg7/Bright Marsh Grasses	24090	1.82	5.42	24799	1.88	5.58
Sand/Saturated Pixels	12234	0.93	2.75	12304	0.93	2.77
Total		33.67	100.00		33.67	100.00
*ALL = full resolution class map, MMU9 = 9 pixel minimum mapping unit class map.						

Table 7. Areal extent of land cover classes for Piney Creek.

Class Names	All* # pixels	All hectares	All %	MMU9* # pixels	MMU9 hectares	MMU9 %
Shadows	18182	1.38	3.96	18803	1.42	4.10
Veg1/High Marsh	40415	3.06	8.81	40923	3.10	8.92
Deep Water	33978	2.57	7.40	34106	2.58	7.43
Water2	28102	2.13	6.12	27849	2.11	6.07
Mud1/Low Marsh	36749	2.78	8.01	36526	2.76	7.96
Water3	19453	1.47	4.24	19387	1.47	4.22
Mud2/Low Marsh	27317	2.07	5.95	26994	2.04	5.88
Sand/Concrete/Saturated	22759	1.72	4.96	23014	1.74	5.02
Shadows	28769	2.18	6.27	32038	2.42	6.98
Pine/Canopy Gaps	40369	3.06	8.80	51653	3.91	11.26
Pine/Canopy Gaps2	31781	2.41	6.93	24169	1.83	5.27
Pine	29728	2.25	6.48	20115	1.52	4.38
Pine2	27869	2.11	6.07	25972	1.97	5.66
Pine3	26130	1.98	5.69	22825	1.73	4.97
Pine4	31099	2.35	6.78	38977	2.95	8.49
Veg2/Ag/Grasses/Saturated	16198	1.23	3.53	15547	1.18	3.39
Total		34.73	100.00		34.73	100.00

*ALL = full resolution class map, MMU9 = 9 pixel minimum mapping unit class map.

Table 8. Areal extent of land cover classes for Hell Hook Marsh.

Class Names	All* # pixels	All hectares	All %	MMU25* # pixels	MMU25 hectares	MMU25 %
Deep Water	241403	18.27	3.57	272597	20.63	4.03
Water2/Pot Holes	192833	14.60	2.85	149579	11.32	2.21
Water3/Pot Holes	199953	15.13	2.96	100908	7.64	1.49
Water4/Pot Holes	183026	13.85	2.71	75989	5.75	1.12
Mud	158357	11.99	2.34	64440	4.88	0.95
Mud2	167939	12.71	2.48	81478	6.17	1.21
Mud3/Wet	179814	13.61	2.66	152812	11.57	2.26
Mud4/Dry/Sand	139770	10.58	2.07	145060	10.98	2.15
Veg1/Dense	395400	29.93	5.85	335090	25.36	4.96
Veg2/Low Marsh	1026064	77.66	15.18	1157459	87.61	17.12
Veg3/Bright Marsh/Pine Gaps	352034	26.65	5.21	281909	21.34	4.17
Veg4/Mixed Marsh	1268606	96.02	18.76	1479816	112.01	21.89
Veg5/High Marsh	1169190	88.50	17.29	1320982	99.99	19.54
Veg6/Pine/Evergreen	172583	13.06	2.55	192014	14.53	2.84
Veg7/High Marsh	678777	51.38	10.04	696818	52.74	10.31
Sand/Saturated	235443	17.82	3.48	254241	19.24	3.76
Total		511.75	100.00		511.75	100.00

*ALL = full resolution class map, MMU25 = 25 pixel minimum mapping unit class map.

source. All images were registered to Zone 18 of the UTM coordinate system. Map coordinate units are meters, and the datum is as defined in WGS 84.

3.4.4 NDVI Images

The Normalized Difference Vegetation Index images are also included under each study site sub-directory in an *Imagine* format. These files use the “_ndvi” suffix in the filename. As with the mosaics, these images are viewable with ArcView. However, the original digital numbers associated with each pixel were transformed to an 8-bit format. This is important since the original NDVI images are in a floating-point format. The floating-point data stored the true NDVI digital value for each pixel (min = -1, max = +1). The 8-bit version of this file has transformed these real data values to a new data range with min = 0 and max = 255. The shape of the histogram, and therefore the relative gray-scale intensity displayed for each pixel, remains unchanged in the transformed 8-bit images.

3.4.5 Class Maps

Both the full resolution and the filtered class maps are provided in the sub-directories for each site. The naming convention uses the “_all” suffix to identify the full resolution map, while a “_mmu<x>” suffix identifies the Minimum Mapping Unit class map. The “x” quantifies the Minimum Mapping Unit in number of pixels. In all cases, x = 9 pixels, except for Hell Hook Marsh where x = 25 pixels.

3.4.6 Shape Files

The two class maps (full and mmu filtered) for each study site are also available in a shapefile format under the site sub-directories. ArcView legend files (*.avl) are not included with the shape files. In addition, the land cover class names are not included as a field in the polygon attribute tables. Instead, a class code, 1 through 16, identifies the land cover class for each polygon. The class names, as interpreted by the author, are displayed in the figures provided for each study site and in the tables showing the areal coverage of each land cover class. The full resolution shape files use the following naming convention: <name>_all.*, where <name> is the first three letters of the site name, “_all” is the suffix denoting the full resolution class map, and * is one of the three ArcView file extensions (.dbf., .shp, and .shx). The naming convention for the filtered class map shapefiles are identical except that the suffix is changed to “_mmu.”

Due to the volume of the images and class maps described above, the files are not included with this report. The complete set of digital data can be obtained from the Point of Contact (POC) listed below.

4.0 CONCLUSIONS AND RECOMMENDATIONS

Based on the overall quality of the imagery in terms of spatial resolution, radiometric balance, geometric accuracy, and land cover classification, the objectives of this pilot

project were met. The ArcView shape files should provide the Poplar Island wetlands design team useful information concerning the areal coverage, distribution, and configuration of the three primary surface features (i.e., water, intertidal zone, and vegetated wetlands). Of the 10 reference wetland areas imaged, eight sites provided land cover class maps.

The images were acquired near low tide during a leaf-off season. It is recommended that follow-on work acquire remotely sensed data during the growing season and near high tide conditions. Furthermore, the smaller reference wetlands, while easily accessible from the ground, may not offer the variation in surface features seen in the much larger Hell Hook Marsh. It is also recommended that future remote sensing applications center on Hell Hook Marsh and other large, diverse estuarine wetlands. Ground-truth data will be required to complete a quantitative image classification and an objective land cover class map accuracy assessment.

5.0 COST

The overall cost of this small effort was approximately \$20,000. This total included: mission planning, image acquisition, image post-processing and image classification. Due to the fragmented locations of the eight individual study sites, the per unit area cost is relatively high at \$10 to \$15 per acre. However, high resolution satellite data, such as IKONOS imagery, would not have been more cost effective. This is due to the minimum area requirements defined by the vendors. It is estimated that three commercial satellite images would be required to cover all the reference wetlands, each costing approximately \$10,000. When combined with processing costs, the total estimated price to produce these one-meter resolution class maps using satellite imagery would be between \$40,000 and \$50,000.

Point of Contact:

Michael V. Campbell
Physical Scientist
US Army Topographic Engineering Center
ATTN: CEERD-TR-S
7701 Telegraph Road
Bldg. 2592
Alexandria, Virginia 22315
Phone: 703-428-6802 ext. 2367
Fax: 703-428-6425
Email: Michael.V.Campbel@erdc.usace.army.mil

REPORT 2

Enhanced Levee Inspections Using High Spatial Resolution Digital Airborne Multispectral Imagery

1.0 INTRODUCTION

The Corps of Engineers is responsible for the construction and maintenance of thousands of miles of levees throughout the continental United States. The Rock Island District maintains more than 546 combined miles of levees and concrete flood walls along the Mississippi and Illinois Rivers and their tributaries. Periodic inspections of these flood control structures are mandatory. The District has recently developed and implemented an ArcView GIS application to assist with levee inspections. The mapping system is built around a suite of vector layers depicting a variety of cultural features, including: roads, waterways, and municipal boundaries. A Global Positioning System (GPS) is integrated into the system to record the geographic position of damage or other anomalies as inspectors slowly drive along the crest of the levee. A raster background image, included as an ArcView layer, assists in navigation and provides a visual point of reference for the inspectors. Currently, this imagery is limited to USGS 7.5' panchromatic (i.e., black and white) orthorectified quadrangles. These inexpensive sources of geographically registered imagery are cost effective and easily procured, but are typically out-of-date by the time they become available. While color infrared (i.e., false-color) photos are sometimes available, this ArcView application employed panchromatic images.

1.1 Objective

The objective of this applied research effort was to evaluate the cost effectiveness of utilizing high spatial resolution airborne digital multispectral imagery to enhance levee inspection procedures. Cost effectiveness was evaluated based on total cost to acquire and post-process the airborne images, and the benefit that the mosaics provided to the levee inspection procedures as enhanced background layers in the ArcView application.

2.0 METHODS

2.1 Project Site

The project site was the Sny levee. Located on the east bank of the Mississippi River, near East Hannibal, IL, the Sny levee includes roughly 28 miles (~ 45 km) of earthen flood control structures.

The coordination of this project was accomplished with Kevin Carlock of the Rock Island District. Mr. Carlock provided the ArcView project over the Sny levee which contained 11 vector layers and the background geo-registered, panchromatic ortho-photos (Figure 1). Detail of the areas adjacent to the flood control structure is shown in Figure 2.

2.2 Instrumentation

The sensor used in the effort was the Computerized Airborne Multicamera Imaging System (CAMIS) model 4768P, developed by Flight Landata (Lawrence, Massachusetts). This airborne digital multispectral imagery is unlike other airborne digital camera systems, which employ a single charge-coupled device (ccd) technology, in that the

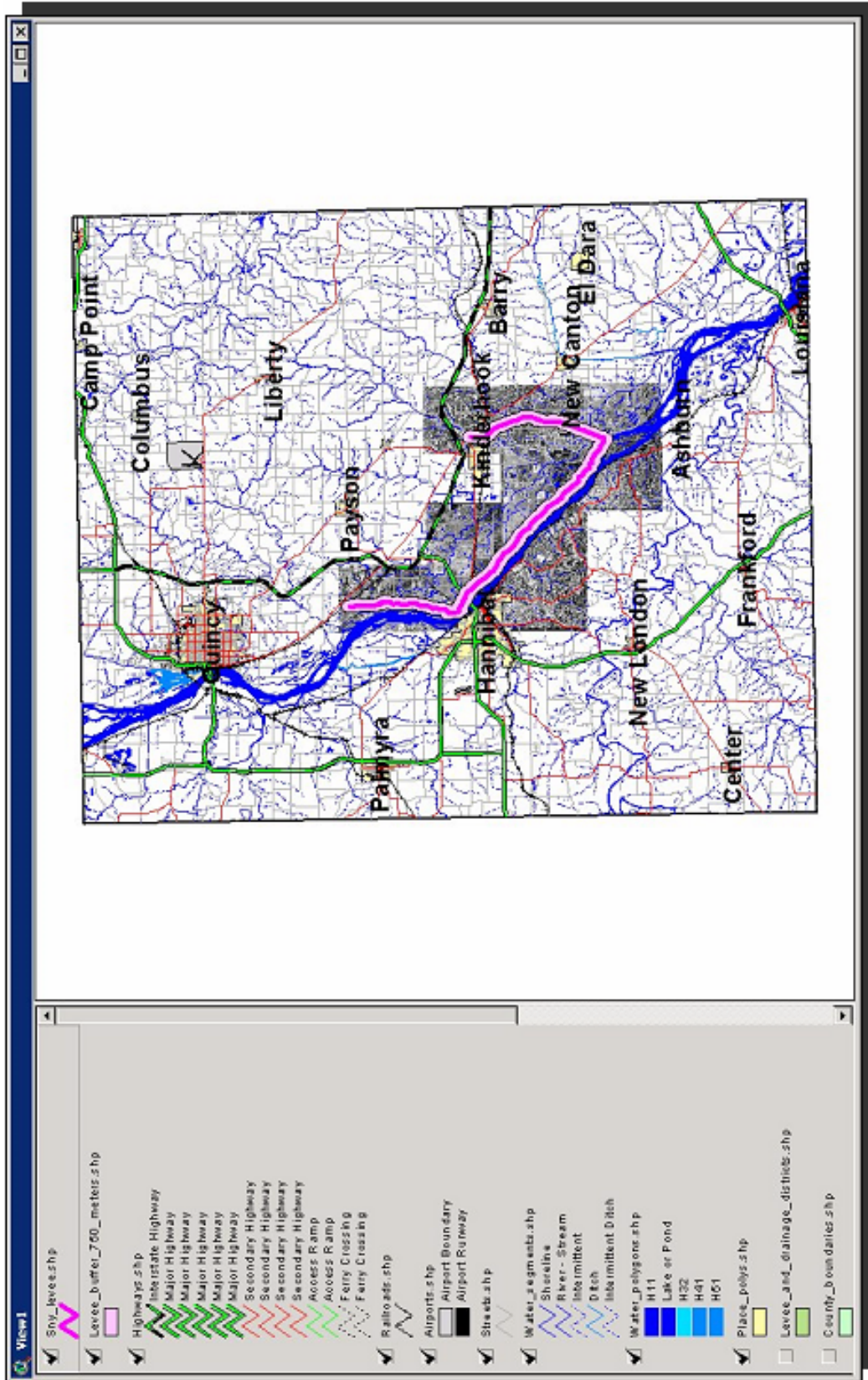


Figure 1. ArcView project provided by Rock Island District depicting project area.

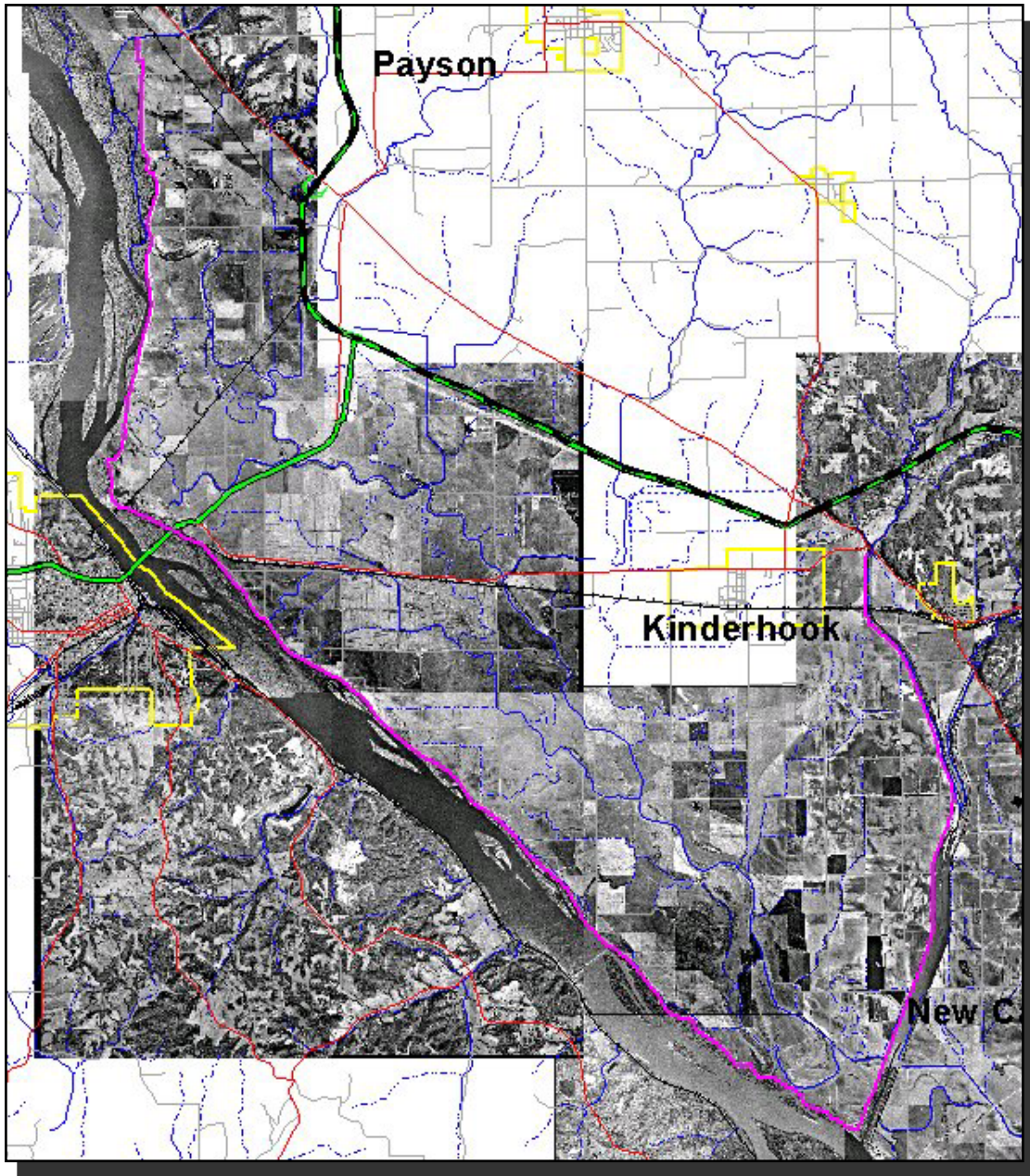


Figure 2. Detail of project site. The Sny levee is shown as the magenta line.

optical head consists of four independent Sony XC8500 progressive scan cameras mounted on a sited solid base (Figure 3). Each camera is sensitive in the range of 350–1100 nm. Bandpass interference filters determine the wavelength interval recorded by each camera. The standard wavelength configuration was used for this mission: 25 nm bandpass filters centered at 450 nm (blue), 550 nm (green), 650 nm (red), and 800 nm (near infrared). The CCD dimensions in each camera are 768 x 576 square pixels with 8-bit radiometric resolution. An aircraft altitude of 6115 ft (1865 m) above ground level (agl) produces a nominal spatial resolution of 1 m² per pixel.

The CAMIS processing unit consists of a 233 MHz Pentium processor with 64 MB of RAM, 23 GB hard drive, and a Matrox Genesis Image Processing Card with 24 MB onboard memory. A Motorola Oncore GT GPS receiver obtains absolute code phase positions for the center pixel of each image. The system was mounted and flown onboard a Cessna 172 Skyhawk. The pilot navigated along each flightline using an onboard moving map with code phase global positioning system (GPS).

2.3 Mission Planning and Image Acquisition

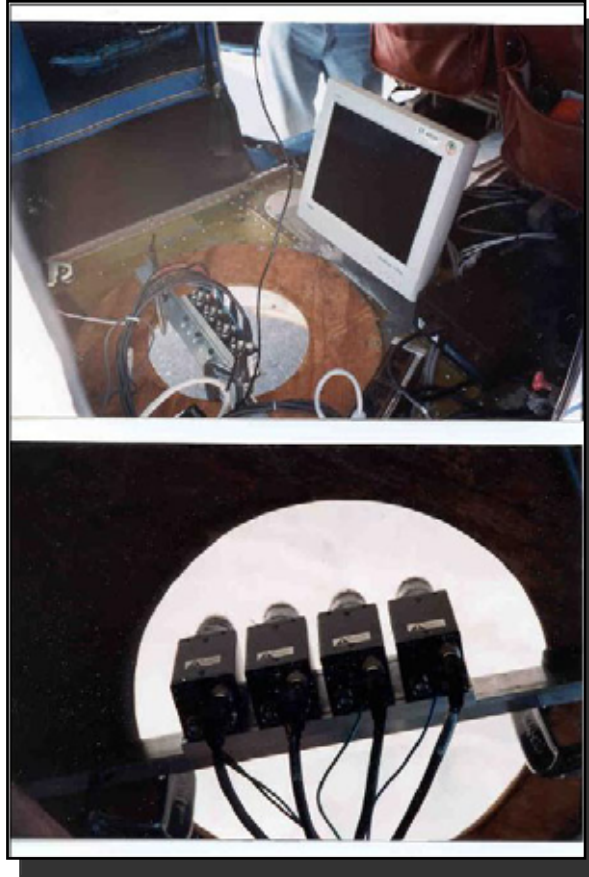
The mission consisted of a series of flightlines covering the length of Sny levee. Since the CAMIS sensor acquires images as discrete four-band, rectangular digital frames, flightline calculations are similar to those used for standard aerial photographic missions. For this mission, nominal frame-to-frame overlap (or endlap) was 60%, while nominal flightline sidelap was at 20%. As shown in Figure 4, the levee was divided into four segments, with flightlines oriented parallel to the azimuth of the main axis of each segment. A total of nine flightlines were developed to collect a complete set of images over the levee (Figure 4).

CAMIS images were collected on two dates: 4 September 2001 and 17 July 2002. The first mission was only marginally successful in acquiring cloud free images. A lingering mid-summer weather pattern resulted in the formation of low-altitude strato-cumulus clouds by 10:00 AM every morning during the week of 2 September 2001. Therefore, a second mission was flown in mid-July 2002. Weather conditions were much more favorable resulting in cloud-free frames of the entire levee. Image acquisition for both missions occurred within +/- 1.5 hours of solar noon to provide optimal solar illumination and to minimize shadows.

2.4 Image Post-Processing

The same post-processing algorithms used in the Poplar Island project were applied to the Sny levee images (see Report 1, pages 11 – 19). These techniques are used to correct both radiometric and geometric image distortions. The steps include:

- Band-to-band registration (a geometric correction),
- Removal of frame edge darkening and frame center hot spots (a radiometric correction),



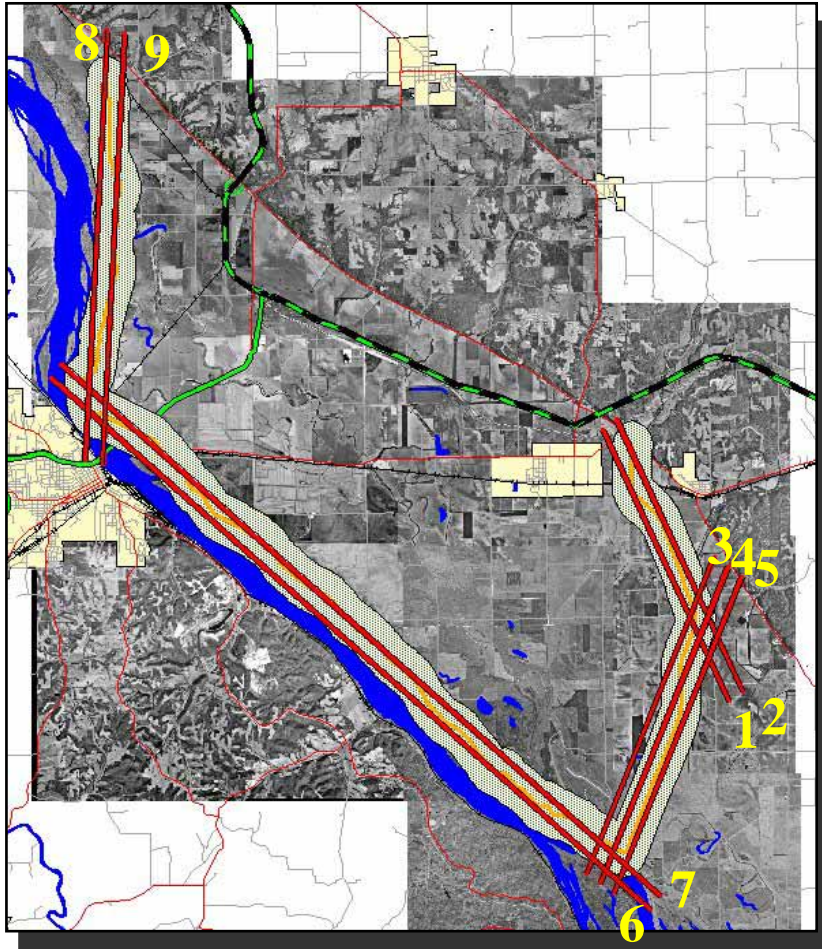
Onboard Configuration:

- Cameras
- Pentium II PC with vendor software
- Flatscreen monitor for real-time image display
- Code phase GPS antenna to record nominal coordinate for each frame center
- DC to AC power inverter

Typical Aircraft:

- Cessna 172 Skyhawk
 - Navigation using code phase GPS with moving map
 - Static camera mount
- (Photo displays CAMIS mounted in a Cessna 208 using standard large format aerial camera port.)

Figure 3. The CAMIS model 4768P airborne digital multispectral sensor.



Flightline #	Start Easting	Start Northing	Stop Easting	Stop Northing
1	659264.3916	4390101.125	655580.1479	4398242.823
2	659664.3916	4390401.125	655980.1479	4398542.823
3	655113.3409	4384947.855	658831.8637	4394422.831
4	655513.3409	4384647.855	659231.8637	4394122.831
5	655913.3409	4384347.855	659631.8637	4393822.831
6	656955.4189	4383861.694	639449.6886	4399796.944
7	657255.4189	4384261.694	639749.6886	4400196.944
8	640463.6834	4397300.535	641110.1209	4410189.985
9	640953.6834	4397200.535	641600.1209	4410089.985
Flightline #	Start Longitude	Start Latitude	Stop Longitude	Stop Latitude
1	-91.143811026	39.645881946	-91.184810225	39.719882335
2	-91.139078979	39.648509043	-91.180074504	39.722510993
3	-91.193375211	39.600235055	-91.147810387	39.684881970
4	-91.188788939	39.597460759	-91.143220541	39.682105824
5	-91.184203036	39.594686289	-91.138631065	39.679329504
6	-91.172187673	39.590117740	-91.372603389	39.736669282
7	-91.168600841	39.593665071	-91.369018743	39.740222777
8	-91.361306938	39.714018814	-91.351000000	39.830000000
9	-91.355614047	39.713037349	-91.345297764	39.829017854

Figure 4. Orientation of the nine flightlines required to acquire a complete CAMIS image set over the Sny levee. The flightlines are depicted in red, with flightline numbers are in yellow. The table, shown above, lists both the UTM coordinates and the Lat/Long's for the starting and stopping point of each flight path.

- Frame-to-frame mosaicking (a geometric correction), and
- Mosaic geometric registration (a geometric correction).

All mosaics were registered to panchromatic orthoquads provided in the ArcView project (Zone 15 of the Universal Transverse Mercator coordinate system).

3.0 RESULTS

The band-to-band registration procedure worked well for both acquisition dates. The radiometric correction algorithm worked poorly for the 2001 acquisition date due to excessive clouds and cloud shadows. The resulting images showed significant shifts in the intensity and hue of colors when comparing overlapping frames. The 2002 images showed excellent color balance along flightlines after application of the radiometric correction technique.

The frame-to-frame mosaicking step created the initial multi-image mosaics within their own “pixel space.” This process was completed manually using the ENVI image processing software. Visually interpreted control points are employed to “stitch” together overlapping images. Therefore, as the mosaics were built by adding one frame at a time, the X and Y coordinates are assigned to each pixel as the row and column numbers of expanding digital file. This frame-to-frame registration procedure used a rotation, scale, and translation (RST) geometric transformation to sequentially combine the overlapping images. The use of the RST transformation is important to maintain the rectangular shape of each individual frame the construction of the “pixel space” mosaics. Figure 10 from Report #1 provides an example of a three frame pixel space mosaic. This method of frame-to-frame mosaicking is extremely labor intensive. However, the image analyst has complete control over the geometric fidelity of the initial mosaics.

After completing the preliminary mosaic for a section of levee (e.g., flightlines 1 and 2), the next step was to assign real world coordinates to the linear image. The mosaics were geometrically registered to the panchromatic orthophotos provided in the ArcView project. First, second, and sometimes third order polynomial transformations were employed to register each mosaic. This second, and final, geometric registration step was also labor intensive. The 2001 mosaics were poorly registered to the orthophotos. The poor output from the geometric registration was due to the linear nature of the pixel space mosaics. Significant warping (i.e., distortion) was observed at the ends of the flightlines (Figure 5). Results were improved for the 2002 images by geo-registering smaller clusters of four to five frames to the orthophotos (Figure 5).

The final CAMIS images included three overlapping mosaics (Figures 6 through 9). Flightlines 1 through 5 comprise the first group, covering the southern and eastern stretches of the levee system. Flightlines 6 and 7 cover the longest portion of the levee running along the east bank of the Mississippi River. Flightlines 8 and 9 portray the north-western run of the levee, also along the eastern bank of the Mississippi. The September 2001 mosaics display an overall poor image quality in flightlines 1 through 7.

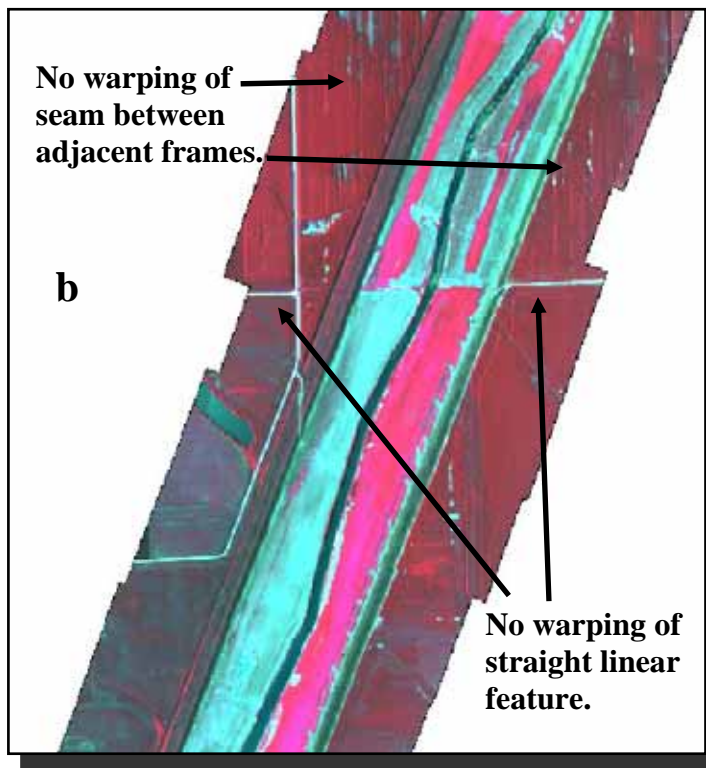
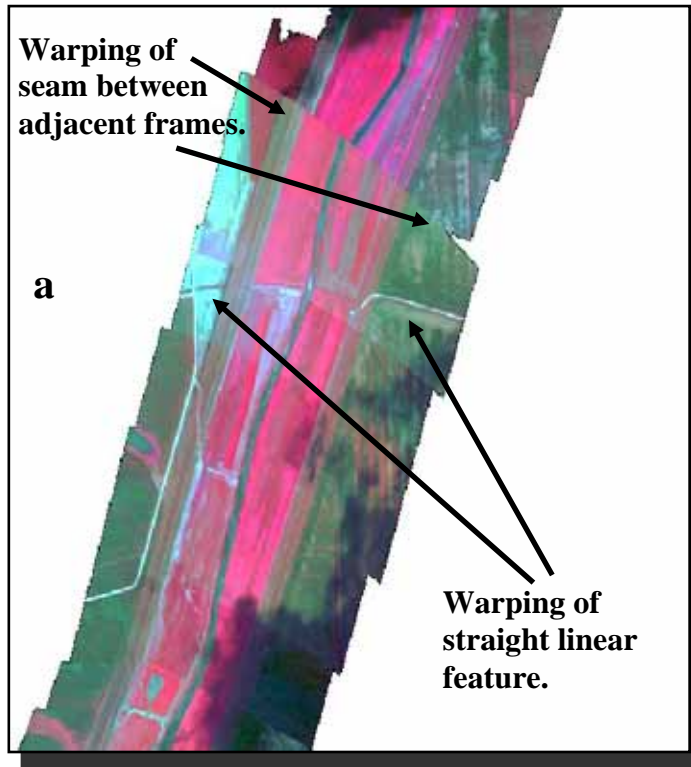


Figure 5. Examples of: (a) poor geometric registration, and (b) good geometric registration.



Figure 6. 4 September 2001 geo-registered, false-color mosaic.

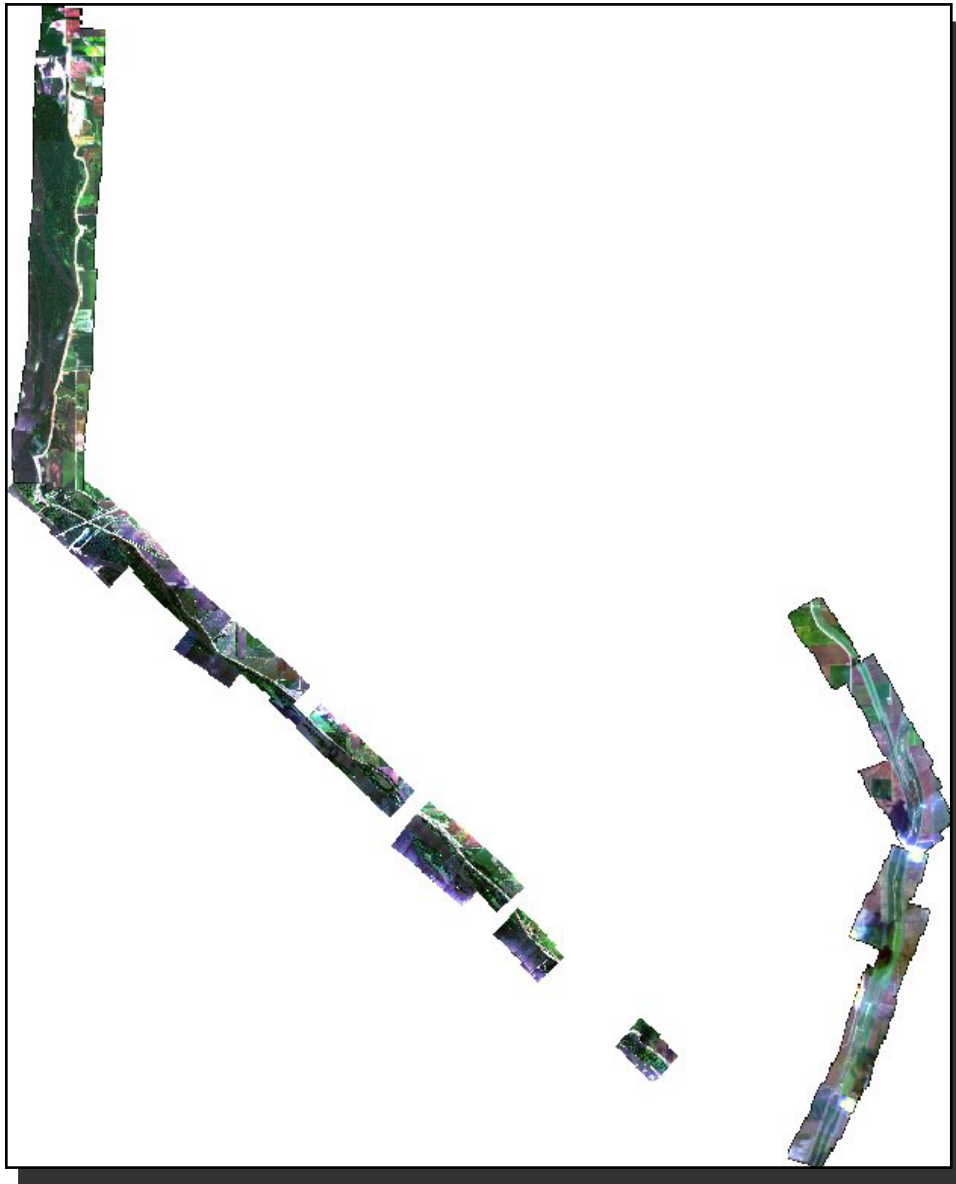


Figure 7. 4 September 2001 geo-registered, true-color mosaic.



Figure 8. 17 July 2002 geo-registered, false-color mosaic.



Figure 9. 17 July 2002 geo-registered, true-color mosaic.

The frames omitted from lines 6 and 7 are due to excessive cloud cover. Flightlines 8 and 9, however, are cloud-free and show better radiometric balance. The July 2002 imagery shows generally good radiometric balance with only one small area of cloud shadows near the center of flightlines 6 and 7. Approximately 160 CAMIS frames were used in the creation of each mosaic.

4.0 UTILITY FOR ARCVIEW APPLICATION

Both sets of CAMIS mosaics were provided to the District for evaluation in assisting levee inspections. Their review was based primarily on the ability of the one-meter multispectral mosaics to provide useful information for the inspection process. Their conclusion was that the spatial resolution would need to be significantly higher to enhance the inspections. The one-meter images depicted adequate detail for features adjacent to the levee. The detection of very small anomalies directly on the control structure, such as seepage or boils, was not reliable. This disappointing conclusion suggests that high resolution satellite data would likely not be a useful source of remotely sensed data for levee inspections. Even with application of the pan-sharpening routine, IKONOS imagery reaches its highest spatial resolution at one meter. The QuickBird commercial satellite, operated by DigitalGlobe (Longmont, Colorado), offers a pan-sharpened multispectral product with a 0.6 m spatial resolution. This slightly smaller pixel is beginning to approach the desired pixel size. Communications with the District has set the desired spatial resolution at 0.25 m or higher (i.e., smaller than 25 cm).

The CAMIS system can easily provide 0.25 m imagery by decreasing flying height during acquisition. However, the costs of post-processing and mosaicking approximately 2,560 frames would be prohibitive. Perhaps the best source of very high resolution remotely sensed imagery would be a single-ccd digital aerial imaging system. These widely used digital cameras can produce cost-effective very high resolution imagery with excellent geometric fidelity. The primary shortcoming of the single-ccd cameras is their limitation to only three spectral bands. Thus, a decision must be made to choose either true-color or false-color images. In addition, the output images are generally not suitable for advance processing such as supervised classification. This is due to the techniques required to generate three complete color planes from only one ccd array per image. Advantages provided by these systems also include typically larger focal arrays, which translates to much larger frames and fewer pictures needed to cover the area of interest. Also, when equipped with a highly precise differential GPS (dGPS) receiver, used to generate very accurate aircraft positions (X, Y, and Z), along with an inertial measurement unit (IMU), to record aircraft attitude parameters (pitch, roll, and yaw), the frames can be rapidly post-processed to produce geometrically accurate mosaics. Assuming that for this levee inspection application, the images would be used as enhanced background data in the ArcView application, there would not be a need for a higher level of radiometric fidelity required for advanced image processing techniques. The cost to acquire, geometrically post-process, and mosaic three-band digital aerial camera images covering the Sny levee with a 0.25 meter spatial resolution is estimated to be the roughly same as the one meter CAMIS mosaics (\$30,000 to \$40,000).

5.0 COST

Project costs can be segregated into: (1) image acquisition and (2) image processing. Image acquisition costs differed slightly between the two collection dates. The September 2001 acquisition employed a CAMIS sensor owned by TEC (originally purchased from Flight Landata in 1998). TEC contracted with a local flight services company, with TEC personnel operating the CAMIS system during acquisition. Due to a number of unavoidable constraints, image capture was limited to a two-day window. The total mission costs were roughly \$12,000, including \$8,000 for flight services and \$4,000 for labor and travel. Image post-processing costs, including data archiving, geometric/radiometric corrections, and data transfer, are estimated at approximately \$18,000. This estimate assumes a rate of \$80/hour for 225 hours. Therefore, the total cost for creating the relatively poor mosaics, shown in Figure 6 and 7, was ~ \$30,000. The failure of this initial mission can be attributed to the limited time allowed for image acquisition coupled with the poor atmospheric conditions.

Flight Landata, using their CAMIS equipment (identical to TEC's sensor) acquired the July 2002 image data. Because their contract stipulated cloud-free imagery, the contractor did not set a rigid schedule and timed the image acquisition with favorable weather conditions. The total cost for the second acquisition mission was \$20,000. Post-processing costs, assuming the same number of hours and the same labor rate, remained at \$18,000. Therefore, the total cost of the more successful second mission was ~ \$38,000. The CAMIS frames cover approximately 44 km² (~ 11,000 acres). Using an average of the total estimated costs for the two missions, including acquisition and processing (given above), the price per square km is roughly \$750. This converts to approximately \$3.00 per acre.

The CAMIS images have a much higher cost per unit area relative to high spatial resolution satellite imagery. The vendors of high resolution satellite imagery require a minimum area for purchase. Using IKONOS imagery as an example, Space Imaging (Thornton, Colorado) has set the minimum area at 10 x 10 km. The price for this minimum window, assuming only basic geometric registration (i.e., not ortho-rectified), is roughly \$55/ km² or \$5,500. This price includes both one-meter panchromatic and four-meter multispectral data. A rectangle measuring 20 km wide (east/west) by 25 km long (north/south) is required to cover the Sny levee as shown in Figures 1 and 2. Therefore, cost for acquiring high resolution IKONOS imagery for this 500 km² area would be approximately \$27,500. The price tag for acquiring and post-processing the same 500 km² area using one-meter CAMIS imagery would exceed \$375,000. The satellite data is much cheaper and generally does not require significant radiometric or geometric corrections. The IKONOS imagery must be run through a "pan-sharpening routine." The process, available as built-in routine in both ENVI and *Imagine* software packages, merges higher resolution (e.g., one-meter pixels) panchromatic imagery with slightly lower resolution (e.g., four-meter pixels) multispectral data to produce a simulated one-meter multispectral product. These images are excellent for manual interpretation but, with questionable radiometric fidelity, may not always be suitable for classification with quantitative image processing routines.

Compared with traditional aerial photography, digital imaging systems have several cost effective advantages. The primary benefit of CAMIS-like systems is that the raw data are provided in a digital format. Aerial photos must be transformed, through scanning, from an analogue format (either paper or transparency) to a digital format. The scanned aerial frames can then be post-processed as digital files, requiring similar radiometric and geometric post-processing steps as with CAMIS frames. The second benefit of multi-camera digital systems is their ability to acquire more than three spectral bands. The aerial photo mission would have to be flown twice, with appropriate film and camera lens, to provide both true-color and false-color images. A third benefit is total time needed to provide a completed digital mosaic. Assuming that the appropriate hardware and software tools are available, the multispectral imaging system could produce a radiometrically balance, geometrically corrected mosaic within two weeks. The analogue photos require film developing and digital scanning just to prepare the imagery for the digital post-processing steps. These steps are completed twice to produce mosaics with more than three spectral bands. Assuming that the film developing and scanning adds one additional dollar per acre over the cost of the CAMIS imagery (i.e., \$4.00 per acre), the total cost to produce a true-color digital mosaic would be approximately \$44,000. The false-color mosaic would double the price to \$88,000.

The one advantage that scanned hardcopy photos have over the CAMIS imagery is the potential to produce digital frames with very high spatial resolution. Depending on the original scale of the photography, the pixel dimensions of the scanned print can be very small (e.g., less than 0.25 m). CAMIS imagery can also be acquired with extremely high spatial resolution by lowering the altitude of the aircraft. A decrease in pixel size results in a decrease in the areal coverage of each frame. The addition of frames needed to fully cover the site requires larger digital file sizes. For example, to increase the spatial resolution from one meter to 0.5 meters, the total number of frames required to cover the same area increases by a factor of four. To further increase the resolution to 0.25 meters requires 16 frames for every frame with one meter pixels. The costs of post-processing and mosaicking these higher resolution imagery increases at the same exponential rate, but would easily double if pixel dimensions were decreased to 0.5 meters and would more than double with the decrease to 0.25 meter pixels.

6.0 IMAGE DATA

The output mosaics were initially supplied to the Rock District in ERDAS *Imagine* image file format (*.img). While providing both the highest spectral resolution (all four bands) and the best radiometric (8-bit data) resolution for the completed mosaics, the *Imagine* formatted files were extremely large. The six final mosaics, three mosaics for each acquisition date, totaled roughly 2.3 gigabytes of data. Furthermore, ArcView 3.2 cannot turn off, or make transparent, the excessive number of background pixels (i.e., black pixels containing no data). Therefore, the District asked for single-band geo-tiff files. This file format drastically reduced the required disk storage space. Also, ArcView is able to make the background pixels transparent. The translation from four-band images, with 8-bits in each band, to one-band images, with a limit of 256 colors, only slightly

reduced the overall interpretability of the geo-tiff images. Both false-color and true-color renditions of each geo-registered mosaic were provided in the one-band geo-tiff format. Also, the mosaic representing flightlines 6 and 7 was cut into three smaller rectangles to further reduce the number of background pixels required to store and display these images. The final suite of single-band geo-tiff images, including both false- and true-color frames, required only 662 megabytes of disk space.

7.0 CONCLUSIONS AND RECCOMENDATIONS

This application of high-resolution imagery to enhance levee inspections showed that one-meter multispectral imagery was of only marginal utility. The District's evaluation clearly showed a need for even smaller pixels. It is recommended that a single-CCD digital aerial camera system be employed to acquire data with very high spatial resolution (e.g., 0.25 m). The estimated costs to receive a complete mosaic covering the 45 km (28 miles) of the Sny levee, including an acceptable buffer region of 500 meters on each side of the structure, would be between \$30,000 and \$40,000.

REPORT 3

Application of High Resolution Airborne and Satellite Multispectral Imagery for Invasive Species Mapping at Lake Okeechobee, Florida

1.0 INTRODUCTION

Western Lake Okeechobee supports a complex system of freshwater wetland and aquatic plant communities. Invasive and undesirable plant species are a significant problem throughout Southern Florida, especially within the diverse communities that characterize Lake Okeechobee. Examples of invasive exotics include: *Hydrilla verticillata*, water hyacinth (*Eichhornia crassipes*), water lettuce (*Pistia stratiotes*), and Brazilian pepper (*Schinus terebinthifolius*). Invasive species management practices, such as control and eradication, require the initial step of delineating the areal extents of plant populations.

The Jacksonville District houses the Aquatic Plant Control Operations Support Center (APCOSC). The following description of the Center is from the APCOSC web site:

“Headquarters, U.S. Army Corps of Engineers established the Aquatic Plant Control Operations Support Center (APCOSC) within the Jacksonville District to serve as the Corps-wide center of expertise in the operational aspects of aquatic plant management [ER 1130-2-500 (dated 27 Dec 1996)]. Staff knowledge and expertise, gained through the administration of the largest and most diverse aquatic plant management program within the Corps, enables APCOSC personnel to professionally execute the mission of assisting our customers in the planning and operational phases of aquatic plant management activities.

The APCOSC is part of the Construction-Operations Division, located at the Jacksonville District Office in Jacksonville, Florida. The APCOSC and Aquatic Plant Control Section are permanently staffed by program administrators, field biologists, airboat operators and herbicide applicators.

The APCOSC (Center) serves as the Corps consultant on invasive plant issues and furnishes technical expertise and/or personnel and equipment to respond to localized, short term critical situations caused by excessive growths of aquatic and other invasive plants throughout the nation. The Center assists HQUSACE in the training and certification of Corps pesticide application personnel. Staff serves as national contact and distribution point for information exchange and technology transfer with Federal, state and local agencies. Center staff also serves as focal point and public/customer interface on matters related to assigned programs and conducts a wide-range of outreach and public educational activities in addition to work for others.

The Aquatic Plant Control (APC) Section provides guidance, administration and technical support for the Aquatic Plant Control Operations Support Center (APCOSC); the Removal of Aquatic Growth Project (RAGP); the Aquatic Plant Control Program (APCP) cost-share agreements with the State of Florida and the Commonwealth of Puerto Rico; all noxious and exotic plant control programs; the Melaleuca management program; and prepares and manages the annual budgets for these programs.

The APC Section has a field biologist located in Orlando and field staff in Palatka. The North Florida APC Field Unit, located in Palatka, conducts hired-labor APC operations in the St. Johns River as well as O&M snagging and clearing operations in the Withlatchoochee and Ocklawaha Rivers, subject to appropriate funding. District office staff includes 3 biologists and the APC Section secretary.”

1.1 Objective

The objective of this applied research effort was to employ high spatial resolution digital airborne and satellite-borne multispectral imagery to identify and delineate various exotic and native plant communities within selected study sites over western Lake Okeechobee. Specifically, the APCOSC is responsible for the management (i.e., delineation, monitoring, and control) of two invasive species: water hyacinth (*Eichhornia crassipes*) and water lettuce (*Pistia stratiotes*). The resulting vegetation maps are focused on classifying the spatial extent of these two floating aquatic plants. The quality of the final vegetation maps are quantified using the overall accuracy of the thematic products. The costs and benefits of both the airborne and satellite image processing are also discussed.

The project was coordinated with Jon Lane of the APCOSC. Mr. Lane also arranged cooperation and assistance from staff at the Clewiston (Florida) Field Office.

2.0 METHODS & RESULTS

2.1 Image Acquisition and Post-Processing

The Computerized Airborne Multicamera Imaging System (CAMIS) acquired one-meter spatial resolution imagery over several rectangular (5 x 2 km) sites on two dates: (1) 31 January 2001 and (2) 9 December 2001 (Figure 1). The January 2001 data were acquired with TEC’s in-house CAMIS equipment. The acquisition of the December 2001 was contracted out to Flight Landata (Lawrence, MA). The specifications and operation of the CAMIS sensor were identical to acquisition parameters used for the Poplar Island project (Report 1) and the Sny levee project (Report 2). To reiterate, the four-CCD system was fitted with same 25 nm bandpass filters centered at 450, 550, 650, and 800 nm. The spatial resolution was one meter. All images were acquired within 1.5 hours of local solar noon. The complete suite of post-processing routines, as described in Report 1 (pages 11 - 19) were applied, including band-to-band registration, radiometric correction, pixel-space mosaic creation, geometric registration of the completed mosaics, and clipping the mosaics to rectangular dimensions. Color infrared USGS 7.5’ orthophoto quadrangles were used as the base imagery for final geometric registration.

The January 2001 CAMIS data proved to be of little utility to this project. South Florida was experiencing a very dry period and the water levels in Lake Okeechobee were extremely low. During field data collection (see below), it was determined that the distribution of invasive species, either terrestrial or aquatic, was so low that delineation would be impractical with remotely sensed data. The imagery was post-processed, with

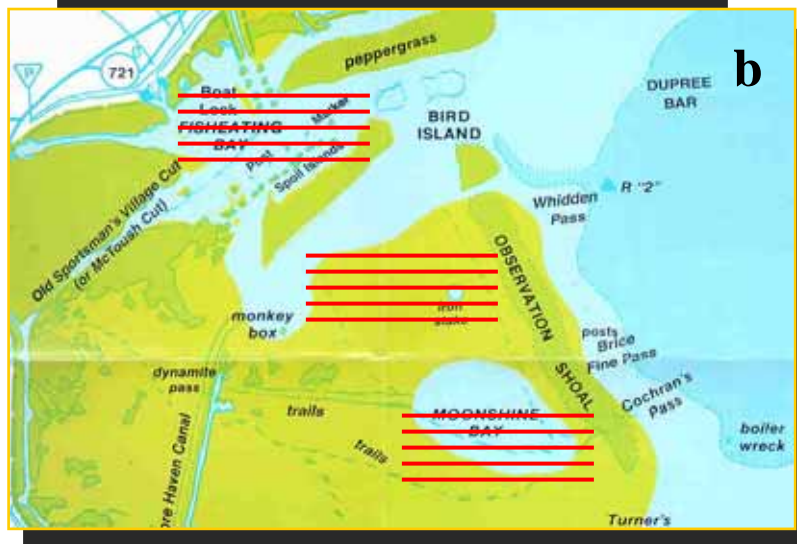


Figure 1. (a) Overview of western shore of Lake Okeechobee and the IKONOS image area. (b) Location and orientation of CAMIS flightlines.

two of three mosaics completed (Fisheating Bay and Monkey Box). Figures 2 and 3 show true-color and false-color representations of these low water level mosaics, respectively.

Figures 4 and 5 display the three CAMIS mosaics built from the imagery acquired in December 2001. Invasive species, particularly water hyacinth, were distributed throughout the study sites (Figures 6a and 6b).

A multispectral IKONOS image was acquired over a larger area of western Lake Okeechobee, which included the CAMIS study sites, on 17 July 2002 (Figure 1). This commercial satellite, operated by Space Imaging (Thornton, Colorado), acquires four-band multispectral imagery with four-meter spatial resolution (Figures 7 and 8). The spectral band widths of the IKONOS imagery are wider as compared to the CAMIS bands, but are centered in the same regions, thus providing blue, green, red, and near infrared data. Also, IKONOS imagery is acquired with 11-bit radiometric resolution, as compared to 8-bit radiometric resolution with the CAMIS data. The commercial satellite data were purchased to provide a comparison to the airborne images. The mid-summer collection date allowed for a seasonal comparison of vegetation signatures with the CAMIS winter images.

Both image sets, CAMIS and IKONOS, were reprojected to the UTM coordinate system with the datum set to NAD27 to match the current GIS database used by the Jacksonville District.

2.2 Field Data Collection

Field data were acquired during acquisition of both the CAMIS missions. Additional field data were not collected at the time of IKONOS acquisition. Plant species associations were recorded at point locations throughout the three study areas. Differentially corrected GPS coordinates were recorded at each sample plot. Terrestrial photos were also taken to qualitatively document the density and distribution of the emergent and submerged plant species. During the January 2001 mission, a total of 22 sites were sampled. During the December 2001 mission, a total of 36 sites were sampled (Figure 9). Considering the Corps' primary mission is to manage water hyacinth and water lettuce, areas supporting these two species were more intensively sampled. None of the January 2001 field data were applicable to the December 2001 imagery due to significant changes in vegetation distributions between the dates.

2.3 Image Analysis

Two different image processing techniques were used to develop vegetation class maps for each of the two image sources:

1. The CAMIS airborne mosaics were processed using a supervised classification algorithm, which requires the use of the field data.
2. The IKONOS satellite image was processed using an unsupervised cluster routine that did not require the use of coincident ground truth data.

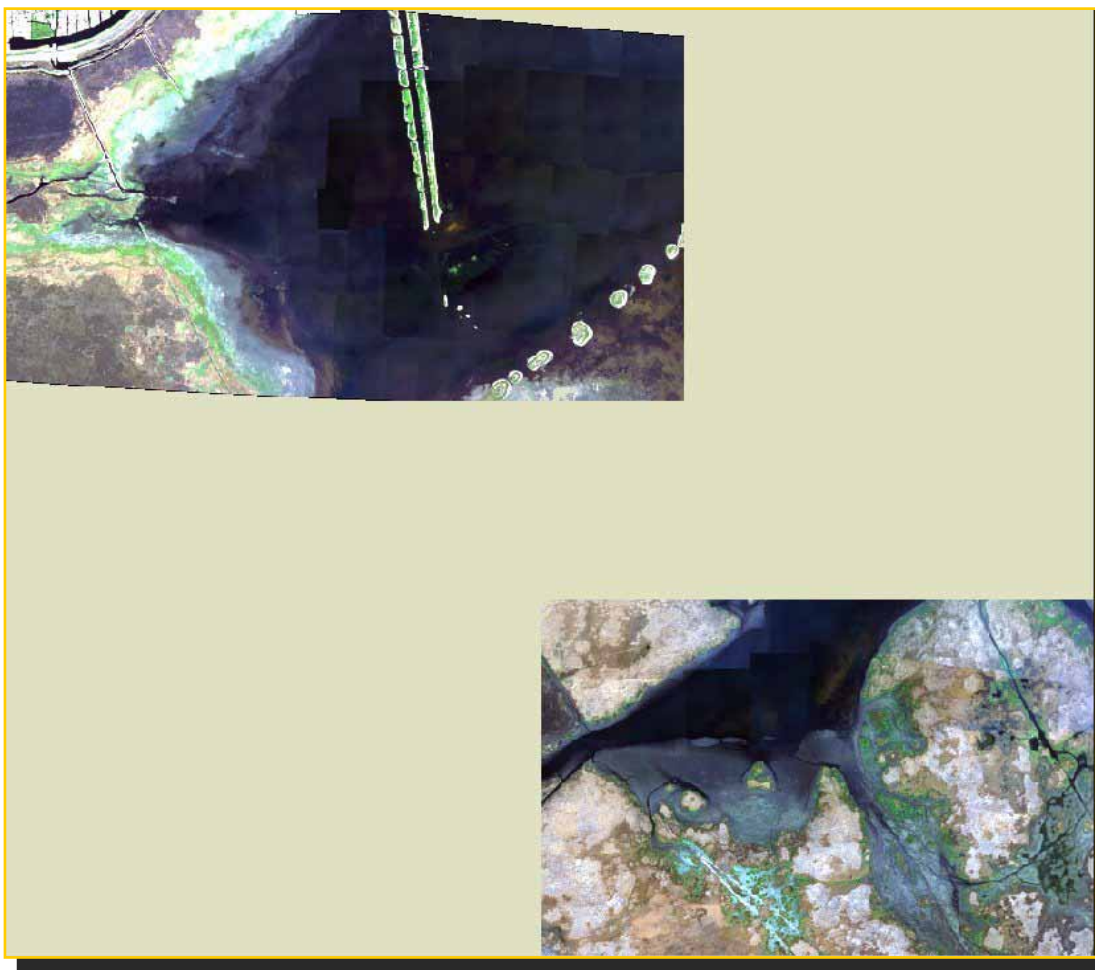


Figure 2. True-color composite mosaics of Fisheating Bay and Monkey Box with imagery acquired 31 January 2001.



Figure 3. False-color composite mosaics of Fisheating Bay and Monkey Box with imagery acquired 31 January 2001.



Figure 4. True-color composite of Fisheating Bay, Monkey Box, and Moonshine Bay acquired 9 December 2001.

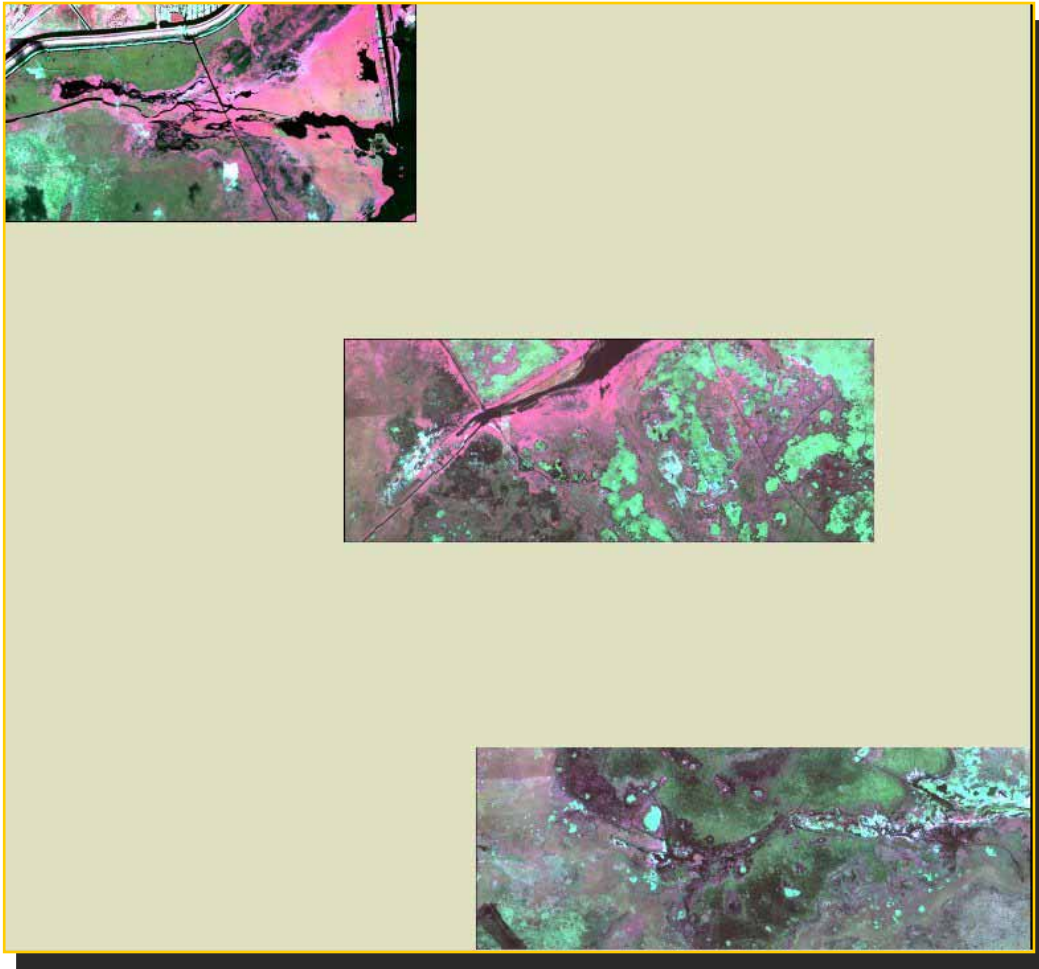
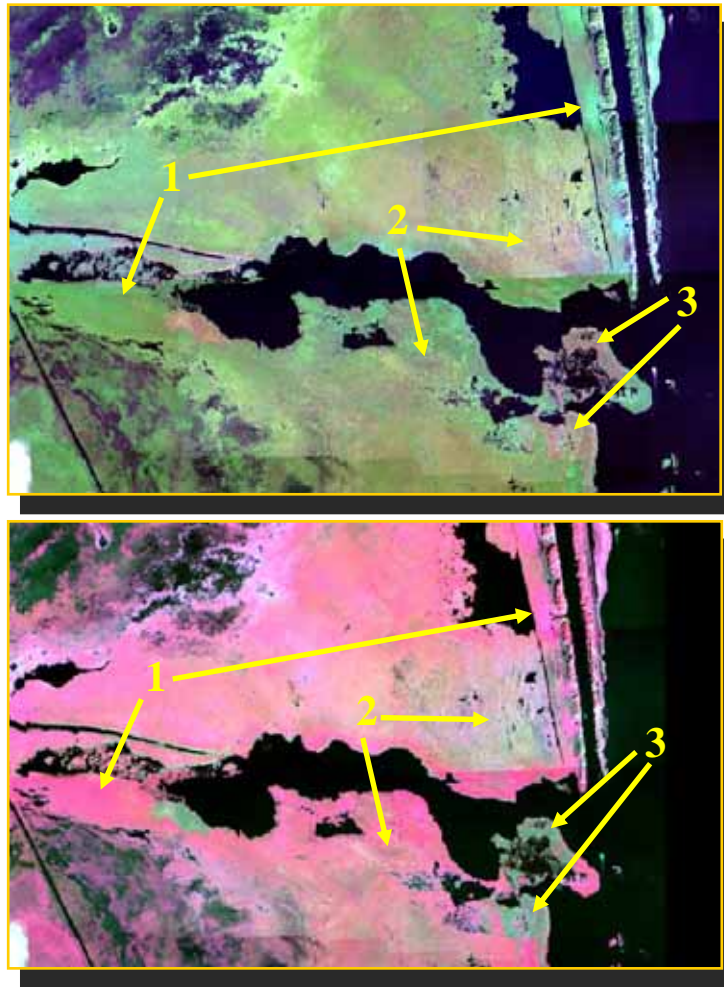


Figure 5. False-color composite of Fisheating Bay, Monkey Box, and Moonshine Bay acquired 9 December 2001.



1 – pure water hyacinth

2 – mixed hyacinth

3- herbicide treated hyacinth

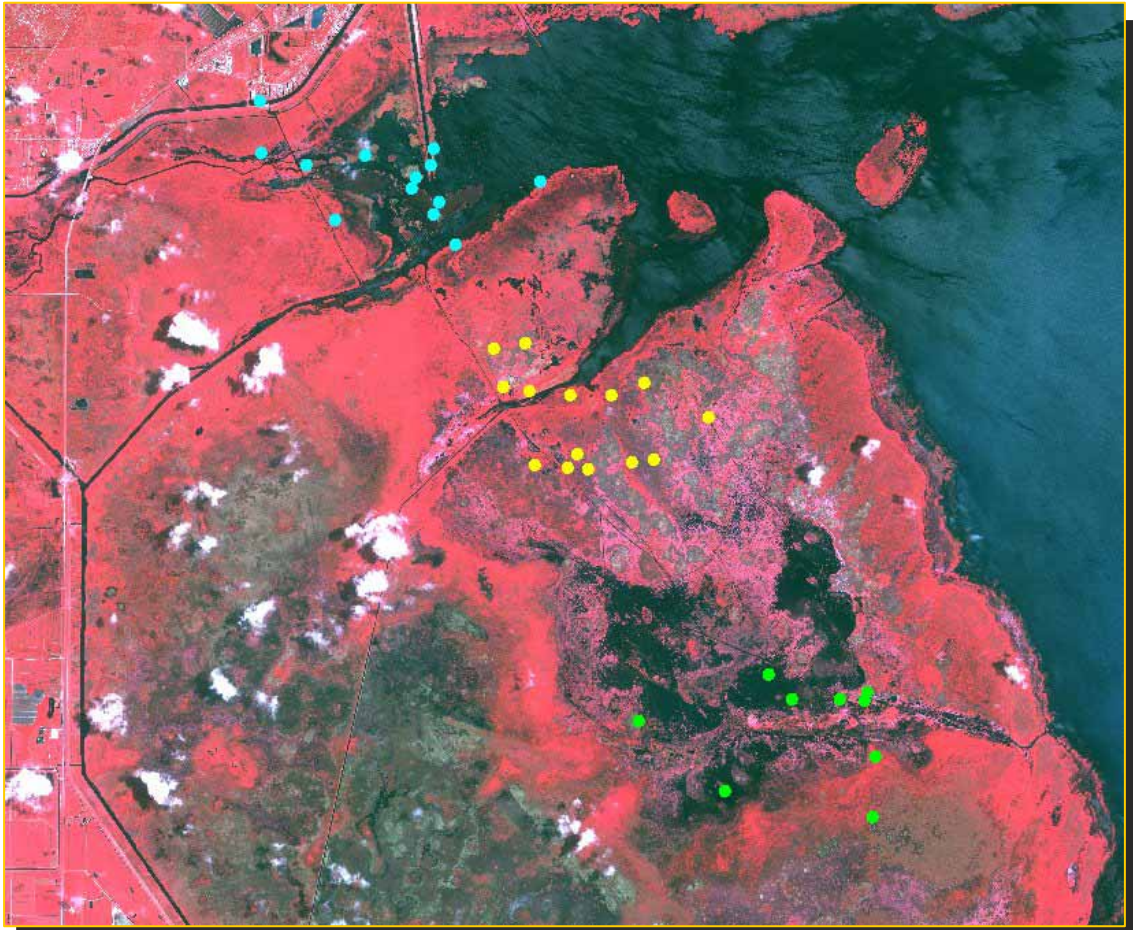
Figure 6. Examples of extensive distribution of healthy water hyacinth and herbicide treated water hyacinth within Fisheating Bay. (a) True-color composite showing pure hyacinth and mixed hyacinth as shades of green and greenish-brown. (b) False-color composite showing pure hyacinth and mixed hyacinth as shades of bright pink and pale yellow.



Figure 7. IKONOS image of western Lake Okeechobee, acquired July 2002; false-color composite.



Figure 8. IKONOS image of western Lake Okeechobee, acquired July 2002; true-color composite.



 **Fisheating Bay**

 **Monkey Box**

 **Moonshine Bay**

Figure 9. Location of field plots established during 9 December 2001 CAMIS image acquisition.

2.3.1 CAMIS Imagery

The goal of most applications of digital remotely sensed data is to assign each multispectral pixel to predefined, discrete class (or group). This foundation for classification techniques begins with statistically-based multivariate discriminant functions that determine the most likely group membership for each pixel. There are a variety of supervised classification algorithms. The maximum-likelihood classifier is one of the most frequently employed discrimination techniques. This algorithm uses the class-conditional probability density functions to calculate the likelihood that a given pixel, possessing its unique spectral vector, belongs to each of the pre-defined classes. The equation used with the maximum likelihood/Bayesian classifier is:

$$D = \ln(a_c) - [0.5 \ln(|Cov_c|)] - [0.5 (X - M_c)T(Cov_c^{-1})(X - M_c)]$$

Where:

- D = calculated weighted distance (i.e., the likelihood estimate),
- c = a unique class,
- X = the measurement vector of the candidate pixel (i.e., the unique spectral vector),
- M_c = the mean vector of class c (calculated from the training statistics for that class),
- a_c = percent probability that any candidate pixel is a member of class c (commonly the analyst accepts the default value of 1.0)
- Cov_c = the covariance matrix of the pixels in class c (calculated from the training statistics for that class),
- $|Cov_c|$ = the determinant of Cov_c matrix,
- Cov_c^{-1} = the inverse of Cov_c matrix,
- Ln = natural logarithm function, and
- T = transposition function used in matrix algebra.

[This maximum likelihood equation, including notations and descriptions for each variable, is copied directly from the ERDAS *Imagine* Field Guide (5th Edition, 1999, page 250).]

There are a number of slightly different versions of the maximum-likelihood classifier published in various multivariate statistical textbooks and image processing textbooks. All variations calculate the same weighted distance estimate (D) for every pixel. Actually, D is calculated c times for each pixel; that is, if there are five classes, then D is calculated five times for every pixel. The weighted distance estimates for a single pixel are then sorted, with that pixel assigned to the class with the lowest D value (i.e., the smallest weighted distance).

2.3.1.1 Signature Collection

The supervised classification algorithm must have multivariate statistics to calculate several variables in the equation above, including: M_c , a_c , and Cov_c . The multivariate statistics represent *a priori* information and, therefore, train the classification algorithm concerning the means and ranges of pixel values that define each class. These training

statistics were generated from the 36 training sites (i.e., the sample plots). Using ERDAS *Imagine*, pixel values (integer values for each of the four CAMIS spectral bands) were extracted from the December 2001 CAMIS images at each sample site by navigating to the X,Y coordinates collected in the field. Typically, at least 25 pixels comprised the training site. The training pixel values were stored in a separate database. Training statistics were then generated from each of the 36 sample sites. A number of plots were replicates of the same vegetation type. These statistics were combined to generate a total of 24 initial classes (Table 1). Table 2 lists the mean values for each class. Figures 10 and 11 provide graphs of the mean pixel values. It is clear that many of the signatures are overlapping.

2.3.1.2 Signature Separability

Before applying the newly created spectral signatures as training data to the CAMIS mosaic, the signatures were evaluated for separability. Signature separability is a standard tool in commercial image processing software packages. The Transformed Divergence algorithm was used, although a variety of algorithms are available within *Imagine*. The four-dimensional mean vectors and covariance matrices are computed for the training statistics. A transformed divergence score is calculated to estimate the magnitude of the pair wise differences, or separabilities, of each of the 24 class mean vectors. The results of the signature separability tests highlighted those classes that, while supporting unique vegetation species associations (as observed in the field), were not distinct with respect to their spectral properties. The lack of separability among several classes suggested that different species associations with similar plant canopy architectures (e.g., height, density) maintain closely related vegetative textures. In addition, plant associations with similar amounts of senescent biomass tended to have similar spectral responses. The following bullets summarize the observations from the signature separability analyses:

- Floating mats of water hyacinth mixed with other species are spectrally similar to mixed vegetation types without hyacinth.
- Tall reeds, such as *Phragmites* and *Typha*, are spectrally similar to shorter species that have senescent biomass, including herbicide treated water hyacinth.
- Sample sites that include both green vegetation and open water are spectrally similar regardless of the species present.
- Dense mats of pure water hyacinth showed the same reflectance characteristics as dense stands of smartweed.

With nearly 5,000 hectares (~ 12,000 acres) depicted within the three CAMIS mosaics, 36 training sites (i.e., sample plots) provided a relative limited vegetation characterization.

Table 1. Vegetation descriptions of training sites.

Class Name	Description
Alligator	Alligatorweed (<i>Alternanthera philoxeroides</i>)
Duck	Duckweed (<i>Lemna valdiviana</i>)
Eleocharis	<i>Eleocharis cellulosa</i>
Hyacinth 1	Water Hyacinth High Density
Hyacinth 2	Water Hyacinth Medium Density
Hyacinth/Grass	Water Hyacinth/Grasses Mix
Hyacinth/Treated	Herbicide Treated Water Hyacinth
Lettuce	Water Lettuce
Lily	Water Lily (<i>Nymphaea odorata</i>)
Melaleuca	<i>Melaleuca quinquenervia</i>
Mixed Veg 1	Mixed Vegetation High Density
Mixed Veg 2	Mixed Vegetation Medium Density
Pepper	Brazilian Pepper (<i>Schinus terebinthifolius</i>)
Phrag	<i>Phragmites australis</i>
Smartweed	Smartweed (<i>Polygonum spp.</i>)
Smartweed/Panicum	Smartweed/ <i>Panicum</i> Grass Mix
Taro	Wild Taro (<i>Colocasia esculenta</i>)
Torpedo 1	Torpedo Grass (<i>Panicum repens</i>) Mature High Density
Torpedo 2	Torpedo Grass Young Medium Density
Torpedo 3	Torpedo Grass Mature Low Density
Typha/Dead	Dead Cattails
Typha/Mix	Cattail (<i>Typha spp.</i>)/Mixed Vegetation
Water	Water
Water/Veg Mix	Water/Vegetation Mix

Table 2. Training statistics for each of the defined classes.

Class Name	Mean Band 1 (blue)	Mean Band 2 (green)	Mean Band 3 (red)	Mean Band 4 (near IR)
Alligator	51.3	82.5	45.6	129.9
Duck	66.3	105.5	77.1	101.5
Eleocharis	27.3	44.2	27.8	64.2
Hyacinth 1	45.3	89.6	38.5	167.0
Hyacinth 2	35.8	88.6	49.1	130.2
Hyacinth/Grass	36.8	85.1	40.8	173.9
Hyacinth/Treated	41.2	69.4	48.7	95.2
Lettuce	62.4	126.3	71.8	165.0
Lily	34.4	78.1	42.6	122.2
Melaleuca	59.9	97.9	52.3	133.3
Mixed Veg 1	45.6	87.3	41.4	162.3
Mixed Veg 2	34.4	57.8	43.0	91.6
Pepper	46.1	78.0	40.6	178.7
Phrag	44.0	72.6	53.9	100.3
Smartweed	37.3	85.6	40.8	169.8
Smartweed/Panicum	36.3	68.6	42.7	121.3
Taro	53.4	98.4	44.3	190.8
Torpedo 1	37.1	57.1	39.6	82.7
Torpedo 2	41.3	74.2	43.9	104.1
Torpedo 3	35.6	71.1	41.0	105.9
Typha/Dead	57.5	80.9	75.2	93.0
Typha/Mix	47.6	77.1	53.1	156.3
Water	23.9	35.0	22.4	52.8
Water/Veg Mix	31.6	59.6	35.6	88.1

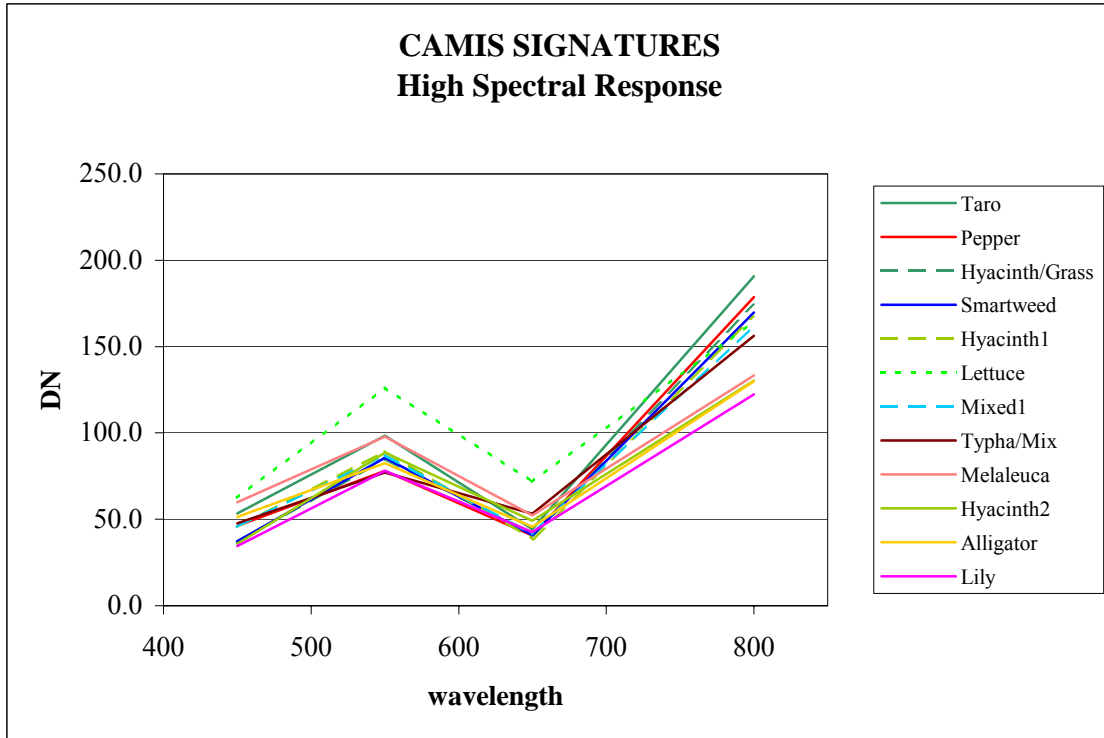


Figure 10. Training signatures extracted from CAMIS mosaics. Vegetation types with high spectral response (i.e., brighter pixels).

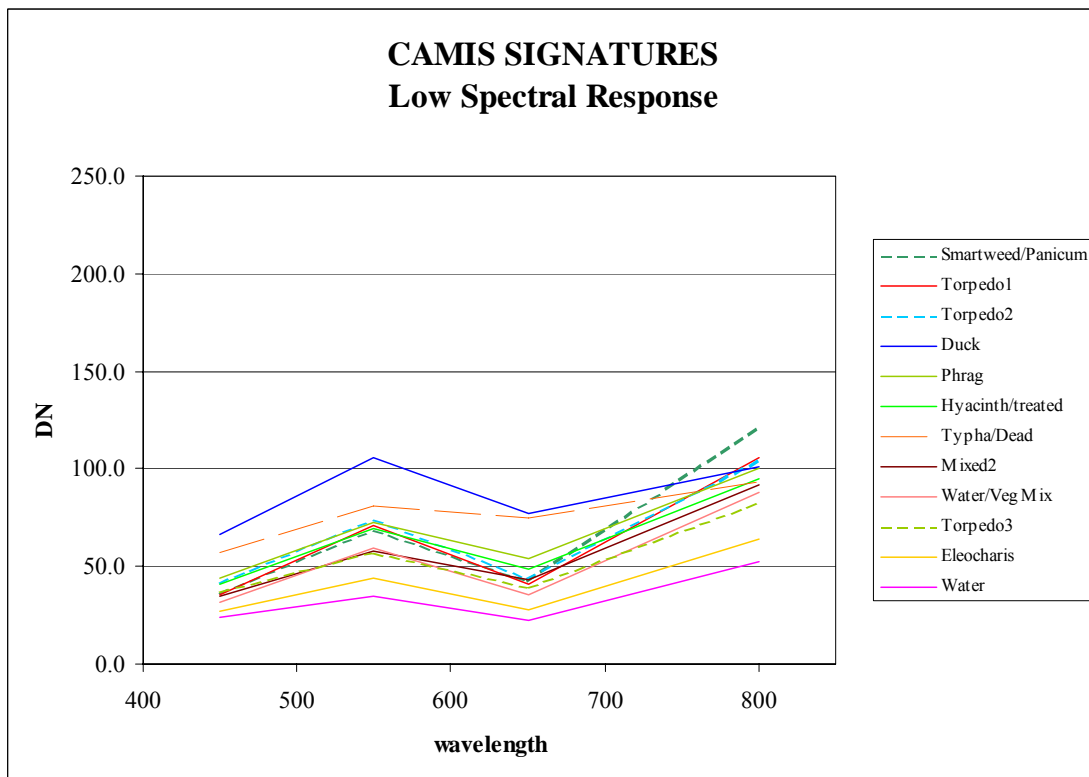


Figure 11. Training signatures extracted from CAMIS mosaics. Vegetation types with lower spectral response (i.e., darker pixels).

Two options were available to minimize the negative impacts associated with the inseparability of the vegetation classes described above. One option was to aggregate the signatures to create fewer classes. This step would hopefully improve the separability of the training statistics. However, lumping classes together would reduce the potential detail in the final thematic map. A second option was to employ all 24 classes in the maximum likelihood classifier and then combine the spectrally similar thematic classes. The second option was selected in an attempt to maintain the greatest level of spatial detail in the final thematic product.

The 24 classes in the supervised classification product were aggregated to a final 18 classes.

2.3.1.3 Minimum Mapping Unit

A minimum mapping unit (mmu) filtering routine was also applied to the full resolution class map. This filtering algorithm first delineates all of the raster polygons throughout the thematic image. A raster polygon is defined as a group of adjacent (i.e., connected) pixels with the same thematic class value. The adjacency criteria defines the polygon using pixels joined along the four flat edges of the square pixel and joined at the corners. The second step is to define an appropriate mmu. For this research effort, a minimum mapping unit of 144 pixels (144 m²) was selected. This unusual size was selected since it covers the same two-dimensional area as nine 4 x 4 m IKONOS pixels. The next step is to delete all raster polygons that are less than 144 pixels. This operation is synonymous with applying a polygon sieve to the thematic image, where all raster polygons below the mmu threshold size are “dropped.” The final step in the technique is to iteratively apply a majority filter to the sieved image. This majority filter, usually a 3x3 pixel matrix, uses a neighborhood operation to fill in the now empty pixels that were lost in the sieving step. As the center pixel of the 3x3 matrix passes over each dropped pixel, the class values for the eight surrounding pixels in the matrix are tallied. The blank center pixel is then assigned the same class value as the majority of the pixels within the matrix. The filter then moves to the next sieved pixel and repeats the operation. The filter is passed over the image many times until all pixels that were deleted in the sieving operation are reassigned a new class value. The operation ignores any background pixels that were already present in the full resolution thematic map.

Figure 12 shows the aggregated vegetation class map after application of the mmu filter.

2.3.1.4 Accuracy Assessment

The field data sample size was inadequate to provide for a thorough assessment of the thematic accuracy of either the full resolution or mmu filtered vegetation class maps. However, a pseudo-accuracy calculation was completed using the actual training site locations. This step is typically performed as a preliminary procedure in assessing the quality of the thematic map. In this case, the accuracy of the 24 class, mmu filtered map was ~80%. The aggregated 18 class, mmu filtered map was only ~70% correct. These results suggest that a number of the sample sites were incorrectly classified.



Alligator Weed	
Brazilian Pepper	
Duckweed	
Eleocharis/Shallow Water	
Hyacinth	
Lettuce	
Lily	
Mixed Veg 1	
Mixed Veg 2	
Phragmites	
Smartweed/Mixed	
Taro	
Torpedo Grass	
Treated Hyacinth/Dead Typha	
Typha Dead	
Typha Mixed	
Water	
Water/Veg	

Figure 12. Supervised classification results of CAMIS mosaics after application of the 144 pixel minimum mapping unit filter.

For example, the areas of mixed hyacinth shown in Figures 6a and 6b are classified as *Phragmites* and/or *Typha/Mix*. Also, much of the *Phragmites* classified throughout Moonshine Bay (the southern most mosaic) is actually mixed vegetation. A more thorough visual interpretation of the thematic product, combined with additional analyses of the inseparability among the training signatures, suggests that the final CAMIS-derived vegetation class map is no greater than 60% accurate.

2.3.2 *IKONOS Image*

As described above, the primary post-processing step applied to the IKONOS image was to reproject its coordinates to the NAD27 datum. Additional post-processing steps included:

- Masking out (i.e., removing) cloud pixels,
- Clipping (i.e., removing) the area outside the Lake Okeechobee levee, and
- Rescaling the 11-bit data to 8-bit data.

2.3.2.1 Histogram Matching

As stated above, no field data were acquired at the time of the acquisition of the four-band multispectral, four-meter spatial resolution IKONOS image. The classification of these data, therefore, had to rely on analyst interpretation to develop unique vegetation signatures needed for classification. An attempt was made to use the signatures acquired from the CAMIS mosaics. This procedure required that the spectral histograms from the July 2002 IKONOS image be matched to the December 2001 CAMIS spectral histograms. An exhaustive analysis of the two sets of four histograms (i.e., blue, green, red, and near infrared) was unsuccessful in developing IKONOS bands with 8-bit distributions similar to that of the CAMIS bands. The primary reason for the failure of this technique is assumed to be the date of acquisition of each image set. South Florida does experience a subdued senescence of vegetation during the winter months. The CAMIS images were captured during this period. The IKONOS satellite data was collected during high summer, when the vegetation is actively growing. In addition, water levels within Lake Okeechobee significantly impact the distribution of vegetation types, particularly the areal extent of water hyacinth and water lettuce. Water levels had changed between the two acquisition dates. The differences in plant phenology and species distributions resulted in a very poor matching of the IKONOS histograms to the CAMIS histograms. The supervised classification technique was abandoned.

2.3.2.2 Unsupervised Classification

An unsupervised classification technique was employed to develop a class map from the IKONOS data. The cluster techniques applied to the IKONOS imagery over Lake Okeechobee were similar to those applied to the CAMIS mosaics for the Poplar Island Reference Wetlands Mapping project (Report 1, pages 19 - 26). At Poplar Island, the

images were first segmented into two primary data sets using the Normalized Difference Vegetation Index (NDVI). One segment represented primarily non-vegetated surface features, while the other segment represented primarily vegetated pixels. Then each segment was classified using an unsupervised clustering routine within the *Imagine* software. Next, the classes from the two independent segments were labeled with vegetation or non-vegetation types using visual interpretation of the original multispectral CAMIS frames. Finally, the segments were combined and the classes were logically aggregated to create final land cover maps.

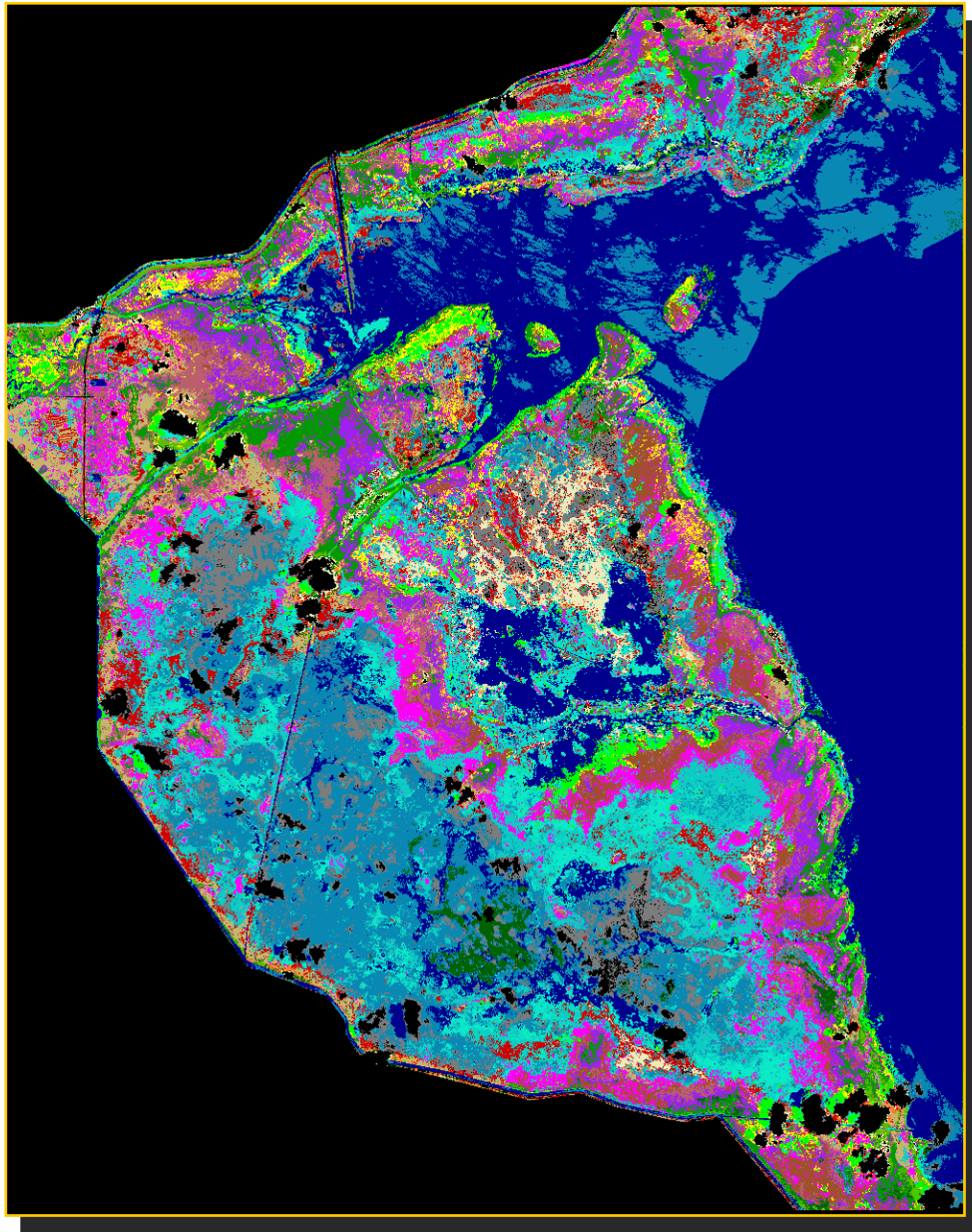
For the IKONOS scene over Lake Okeechobee, an NDVI image was again used to stratify the multispectral image, but this time into four segments. The objective of increasing the number of segments was to enhance the separability of the classes derived from the unsupervised classifications. The first segment included the lowest NDVI values and thus represented features with the least amount of vegetation. Examples of classes with the lowest NDVI values include: open water, low density vegetation surrounded by water (e.g., *Eleocharis*), and stands of dead *Typha*. The second segment, with NDVI values from the lower middle portion of the histogram, included low to medium density vegetation types, such as: veg/water mixed and herbicide treated hyacinth. The third NDVI segment comprised pixels with medium to high density vegetation, including: mixed vegetation, hyacinth/grass mix, and *Phragmites*. The last segment contained the brightest (i.e., greatest green biomass) vegetation pixels. Pure water hyacinth, dense areas of water lilies, and dense stands of smartweed are included in the fourth NDVI segment. A total of 18 clusters were classified within each of the four segments. The spectral signatures were plotted and, along with visual interpretation of the original multispectral IKONOS scene, were used to assign a descriptive class name to each cluster. Similar clusters were aggregated within each segment. Then, the four segments were combined, with similar clusters again aggregated. The final IKONOS derived vegetation map contained 18 thematic classes (Figure 13). Table 3 lists the names and qualitative descriptions of each class.

2.3.2.3 Minimum Mapping Unit

A nine-pixel mmu threshold was applied to the IKONOS class map to remove the thematic speckle and improve the utility of the final product (Figure 13).

2.3.2.4 Accuracy Assessment

Without either ancillary field data or training sites, a quantitative accuracy assessment was not possible. A subjective evaluation of the statistical overlap among spectral mean vectors of the final 18 classes confirms the results reported for the CAMIS derived thematic map. Mixed vegetation classes were difficult to separate, including species mixes that contained water hyacinth and water lettuce. Also, areas that support pure vegetation types, such as dense stands of smartweed, were confused with pure mats of water hyacinth. Therefore, it is assumed that the overall thematic accuracy of the IKONOS-derived vegetation map is approximately 60%.



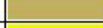
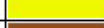
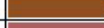
Hyacinth	
Broadleaf	
Grass	
Duckweed/Soil	
Typha - Dead	
Phragmites	
Dying Veg1	
Dying Veg2	
Mixed Lettuce	
Mixed Grass	
Mixed Lily	
Mixed Hyacinth	
Mixed Low Density	
Submerged Veg	
Water/Veg1	
Water/veg2	
Water/veg3	
Water	

Figure 13. Unsupervised classification results of IKONOS image after application of the 9 pixel minimum mapping unit filter.

Table 3. Description of vegetation classes developed from the segmented unsupervised classification of the IKONOS multispectral image.

Class Name	Description
Hyacinth	Floating mats of pure water hyacinth
Broadleaf	Stands of dense broadleaf species (smartweed, alligator weed)
Grass	Stands of dense grass species (Panicum)
Duckweed/Soil	Very bright areas of floating duck/sparse areas of exposed sand
Typha – Dead	Dense stands of necrotic cattails
Phragmites	Dense stands of Phragmites
Dying Veg1	Chlorotic/necrotic veg including treated hyacinth, high density
Dying Veg2	Chlorotic/necrotic veg including treated hyacinth, low density
Mixed Lettuce	Areas of water lettuce mixed with other species
Mixed Grass	Areas of mixed grasses
Mixed Lily	Areas of water lily mixed with other species
Mixed Hyacinth	Areas of water hyacinth mixed with other species
Mixed Low Density	Areas of low density mixed vegetation
Submerged Veg	Water with dense, slightly submerge aquatic vegetation
Water/Veg1	Shallow water with some aquatic vegetation
Water/Veg2	Water mixed with aquatic vegetation
Water/Veg3	Water mixed with aquatic vegetation
Water	Open water

2.3.2.5 Final Product

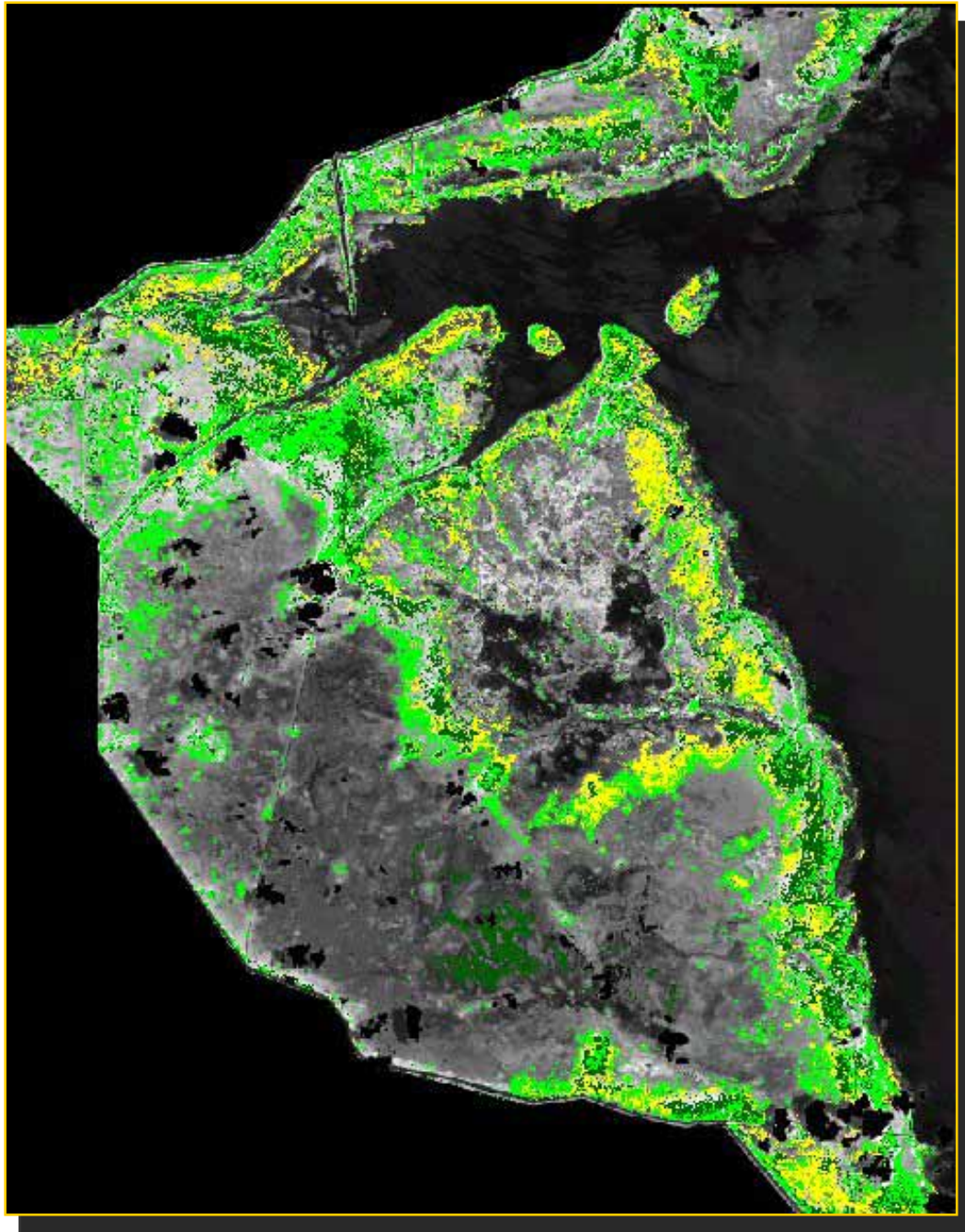
The District's primary objective is to control the distribution of water hyacinth and water lettuce throughout the Lake Okeechobee. The IKONOS vegetation map, with its complete coverage of the western wetlands, may actually depict too much information for the Districts' needs. Figure 14 shows a three class vegetation map displayed on top of a single IKONOS spectral band. The near-infrared band was selected as the grayscale background image. The three vegetation classes were aggregated from the complete set of 18 classes. The objective of this product is to provide the District, Field Office, and spray contactors with the optimal level of vegetative information needed to direct herbicide application methods. This two layer map would be stored in a digital format and provide valuable spatial information for seasonal (or long-term) monitoring of hyacinth and lettuce growth and movement within the Lake. The map could also be plotted to a large map sheet and provided directly to spray crews with the intent of increasing the efficacy of herbicide application.

3.0 COST

The cost to acquire the December 2001 CAMIS frames was \$20,000. Image post-processing and mosaicking costs were estimated at approximately \$16,000 (200 hours @ \$80/hour). Field data collection costs, including travel and labor, are estimated at \$10,000. Image classification required another \$6,400 (80 hours @ \$80/hour). At a total cost of \$52,400, the completion of the CAMIS vegetation classification required roughly \$10/hectare (\$4.50/acre).

The IKONOS image acquisition costs were \$33,000. With no post-processing steps necessary, image analysis was focused on developing the vegetation class map. At total of 80 hours were used to develop the final map, for a total cost of \$6,400. The four-meter satellite image covers roughly 35,000 hectares (85,500 acres) of marshland. At a total cost of almost \$40,000, the IKONOS class map cost little over \$1 per hectare (~\$0.50/acre).

The total costs for both of the vegetation class maps reflects an inadequate amount of field data collection. The IKONOS data was processed without any concurrent on-site observations. Based on the cost to visit the limited number sample sites used to classify CAMIS mosaics, a more thorough field data campaign would require at least three times the sample size. The number plots would again increase to collect an adequate number of accuracy sample sites within the CAMIS mosaic areas. The IKONOS image, covering seven times the area shown by the CAMIS frames, certainly would require an extensive network of field plots, distributed over the entire 35,000 hectares, to produce a reliable thematic product. However, remembering that the District is primarily interested in mapping the distribution of only two specific species, the number of field observations could be significantly reduced.



-  **Hyacinth**
-  **Mixed Hyacinth**
-  **Mixed Lettuce**

Figure 14. The final three class thematic product depicting the distribution of the invasive species of interest to the District. The background image is the near infrared channel (band 4) and is included to assist with navigation to areas supporting hyacinth and lettuce.

Perhaps as a general “rule-of-thumb,” this investigation at Lake Okeechobee suggests that the project budget for creating a reliable vegetation map from high resolution multispectral imagery should include roughly equal dollars for image acquisition and field data collection. Reliability is quantified for this remote sensing application as an overall thematic accuracy of approximately 80%. Image post-processing (if required) and image analysis costs, including supervised and/or unsupervised classification, should be included as separate items.

4.0 CONCLUSIONS AND RECOMMENDATIONS

This project expended a significant amount of planning and execution with respect to the airborne multispectral imagery. The satellite imagery offered a much more cost effective data source for mapping the relatively large study area. The District was periodically updated throughout the project. Their evaluation of the thematic maps suggested that remotely sensed imagery could potentially offer a cost effective source for monitoring hyacinth and lettuce distributions across all of Lake Okeechobee. A rough estimate of the cost of acquiring four-meter IKONOS imagery over the entire Lake was well over \$100,000. A less expensive image source was identified as the SPOT sensor. With 10-meter multispectral and 2.5-meter panchromatic imagery, a pan-sharpened four-band product would cost between \$20,000 and \$25,000. The price range assumes that some post-processing will be required to radiometrically balance (or equalize) the several SPOT scenes required to cover all of Lake Okeechobee. Image classification costs, including the collection of the required minimum amount of field data, would be reduced by employing an unsupervised clustering routine to identify hyacinth and lettuce pixels. Field data collection could then be limited to verification of areas mapped as hyacinth and lettuce. Depending on the available budget, SPOT imagery could be acquired and processed seasonally (i.e., three to four times per year), providing valuable invasive species monitoring data by mapping the distribution of hyacinth and lettuce over the whole of Lake Okeechobee.

REPORT 4

Detailed Wetland Vegetation Mapping Over Blackwater Wildlife Refuge using High Resolution Digital Airborne Hyperspectral Imagery

1.0 INTRODUCTION

The newest digital airborne remote sensing systems combine the multispectral and hyperspectral spectral properties of commercial satellite sensors with the temporal and spatial flexibility of traditional aerial photographic systems. The high spatial resolution imagery provided by these systems greatly enhances environmental monitoring strategies. Sub-meter pixel dimensions enhance the detail of surface features. However, too much data can degrade the accuracy and the utility of the final map product. Therefore, the effective use of high-resolution digital airborne imagery, both multispectral and hyperspectral, requires improved processing techniques that ensure accurate representation of the land cover classes of interest. The development and application of post-processing algorithms to remove both radiometric and geometric distortions, which are typically present in all airborne images, are essential.

The Corps of Engineers Baltimore District has recently initiated the Blackwater Refuge, Dorchester County, Maryland Section 206 Small Ecosystem Restoration project. The following project description is taken directly from the District's website.

“Blackwater National Wildlife Refuge, located approximately 10 miles South of Cambridge, is one of the largest and most significant wildlife refuges on the Eastern Shore of Maryland and plays a key part in the overall ecology of the Chesapeake Bay. It contains over 17,000 acres of wetlands, woodlands, and croplands. The refuge is critical winter habitat for thousands of migratory birds, including numerous species of swans, snow geese, and ducks. The refuge also provides year-round habitat for a number of species, including the bald eagle, shore birds, otters, and the endangered Delmarva Fox Squirrel. The refuge also provides spawning habitat for blue crab, striped bass, oysters, shad, and other aquatic wildlife.

Project History:

At present, the Blackwater refuge, along with many areas of the Chesapeake Bay, is rapidly losing marsh habitat, with an estimated 7,000 acres out of 17,000 being severely impacted. The causes of degradation include altered hydrology, sea level rise, land subsidence, increased salinity, and the damage from the non-native Nutria. Additionally, eroded sediment has been linked to the decline of submerged aquatic vegetation (SAV) in the Tangier Sound area. The Corps, with the assistance of federal and local partners, proposes to implement a project to restore the damaged marshland. The Corps' emphasis will be on restoring the degraded marsh habitat, using fill material to offset subsidence and prevent future damage from rising sea levels. Native salt-marsh vegetation will likely be re-planted to anchor the added sediment and provide nutrients and nesting grounds for the native animal species. In conjunction, the U.S. Fish and Wildlife Service (USFWS) plans to implement a Nutria control program, designed to prevent the future degradation of the restored and remaining habitat. Overall, this project represents a critical initiative in preserving and managing the fragile wetlands of the Chesapeake Bay. The project site is on federal land, managed by the USFWS.

Status:

The feasibility study was begun in January 2001. The Corps is working with a number of government agencies and non-profit organizations to facilitate the restoration project, including the USFWS, MDNR, Department of Agriculture, the Chesapeake Bay Foundation, National Audubon Society, Sierra Club, and Ducks Unlimited. The Corps is also coordinating closely with the Marsh Restoration/Nutria Control Partnership.

At present, the Corps is focusing on three different activities, the fix of the hydrologic breach at Parson's Creek, a comprehensive hydrologic analysis of the marsh system, and the design and construction of a marsh restoration demonstration project. The breach at Parson's Creek has led to severe saltwater intrusion within the Fishing Bay Watershed requiring immediate action. The hydrologic study is being conducted by the Waterways Experiment Station and will be used to design the restoration project."

Accurate and detailed land use/land cover base maps are critical to the monitoring and evaluation of both the short-term and long-term environmental impacts of these three initial activities.

Blackwater National Wildlife Refuge (USFWS) purchased digital airborne hyperspectral imagery covering the entire refuge. Acquisition and post processing of the airborne Imaging Spectroradiometer for Applications (AISA) data was conducted by 3Di, LLC (Easton, Maryland) during the summer and fall of 2000. Advanced processing, both image mosaic and classification, on the 3.0-meter resolution imagery was performed by the US Army Topographic Engineering Center (Fort Belvoir, Virginia)

1.1 Objective

The objective of this applied research effort is to employ industry standard techniques to create a detailed vegetation classification of the entire refuge. Innovative hyperspectral image processing algorithms and techniques may be developed and implemented, as necessary.

2.0 BACKGROUND

The Airborne Imaging Spectrometer for Applications (AISA) is a commercially produced hyperspectral pushbroom type imaging spectrometer. The following system description is adapted from the website of sensor manufacturers: SPECIM, Spectral Imaging Ltd., P.O.Box 110 (Teknologiantie 9A), FIN-90571 Oulu, FINLAND. [<http://www.specim.fi/>]

"AISA is a very compact system, consisting only of two units, the sensor head (frontend) and a rugged portable PC. The graphical user interface (GUI) provides the sensor flexibility and easy-of-use. The image data are stored as a default to a large capacity hard disk.

The basic operation of the direct-vision, dispersing prism-grating-prism (PGP) spectrograph is illustrated in Figure 1. The PGP is composed of a specially designed volume type transmission plane grating made of dichromated gelatin (DCG) and cemented between two symmetrical or nearly symmetrical prisms. The grating is designed to operate under Bragg condition and the prism angles change accordingly. A collimated light beam is dispersed at the PGP so that the center wavelength passes axially through the grating and prisms. Shorter and longer wavelengths are dispersed symmetrically on both sides of the central wavelength. [The Bragg condition is named after Nobel Prize English physicists Sir W.H. Bragg and his son Sir W.L. Bragg. Their work involved explaining why the cleavage faces of crystals appear to reflect X-ray beams at certain angles of incidence. In this application, the AISA system utilizes Bragg's Law to control the "splitting" of the solar illumination into individual wavelengths.]

A spectrograph based on the PGP element is composed of a narrow slit, a collimator lens, a PGP element, and a focusing lens (Figure 1). Radiation entering the spectrograph through the slit is collimated by the first lens and refracted at the prism surface to the right incident angle of the holographic grating. The grating disperses the light according to the common grating equation. Spatial information on the entrance slit is transferred to the image plane at the axis parallel to the slit length direction. The spectrum is formed perpendicular to the optical axis with a good spectral linearity. The tubular direct vision (on-axis) construction leads to low geometrical aberrations in both the spatial and the spectral axes. The optical properties are further guaranteed by using very high quality triplet lenses that are specially designed for imaging purposes.

Operating Modes:

AISA provides a very flexible way to select parameters for different operating modes. There are four operation modes, which are programmable through configuration files. The 384 spatial pixels include 360 ground-target and 20 downwelling irradiance pixels.

Mode A: Provides full spatial (384) and full spectral (288 pixels) information. Neither spectral channel bandwidth modification nor spatial binning is available, but each pixel of the focal plane is digitized as single pixel. Therefore, mode A requires long integration times. This mode is mainly for calibration, testing and demonstration purposes. However, it can be used in low velocity and/or high-altitude aerial surveys.

Mode B: Provides full spatial resolution (i.e., smallest pixels) with reduced spectral resolution. This mode offers 384 spatial pixels with no binning, although spatial binning (i.e., summing of 2, 4 or 8 pixels to output larger pixels) is available for low signal level measurements.

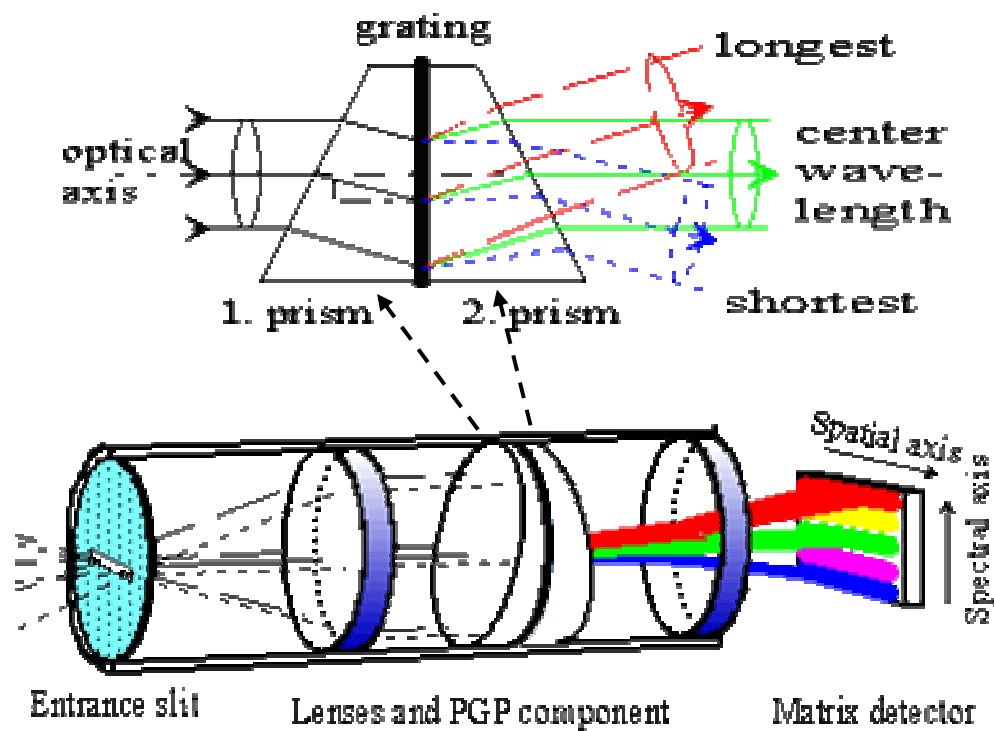


Figure 1. Configuration of the direct-vision, dispersing prism-grating-prism (PGP) spectrograph used in the AISA sensor.

Spectral sampling is programmable between 1.5 to 9.4 nm bandwidths within a total wavelength range of 450 nm. Individual spectral bands are programmable. Therefore, the total number of channels is controlled by the selected spectral bands and selected bandwidths.

Mode C: Provides full spectral resolution, with reduced spatial resolution. This mode utilizes the full hyperspectral capabilities of the sensor (288 bands), but with only 47 pixels in the cross-track direction (as compared to 384 with Mode B). Further spatial binning (i.e., decreased spatial resolution) is still available. Mode C is suitable for hyperspectral applications that require varied spatial resolutions.

Mode D: Provides the greatest variation in both spectral resolution and spatial resolution. While Mode D minimizes the amount of data to be collected and allows high frame rates, it does not offer the highest spatial resolution.

Downwelling irradiance measurement:

The quality of the airborne remotely sensed data could be improved by using downwelling irradiance measurements together with the actual target measurements. In AISA this is implemented using a hemisphere (or flat) reflector attached to the aircraft roof receiving direct solar radiation. In best case there is a clear, sunny sky. The correction is more difficult if atmospheric conditions are cloudy or partly cloudy. The resulting signal is fiber-optically connected to the spectrograph such that it covers a few pixels from the swath width (i.e. a few columns on the detector). Thus, there is a simultaneous measurement of downwelling irradiance with the same wavelength range as is captured by the CCD. This is a great advantage to systems requiring mechanical movement of the instrument or even separate instrument to measure the signal representing the downwelling irradiance. Naturally even in the best case the measurement is only an approximation of the downwelling irradiance on the ground due to various atmospheric effects.”

It was assumed that the vendors used Specim software tools to calculate at-sensor-reflectance values for each pixel using the raw irradiance images and the downwelling solar radiance data. The reflectance-calibrated data were then provided to Blackwater staff.

3.0 METHODS

3.1 Image Acquisition

Hyperspectral imagery was collected over four flights, each flight on a different day. Flights 1 and 2 were on 7 June and 30 June 2000, respectively. Flights 3 and 4 were on 15 September and 12 October, respectively. The aircraft maintained an altitude of

approximately 3050 m (~ 9842 ft) above –ground level (agl). The nominal spatial resolution of the data is documented as 3 meters (3 x 3 meter pixels = 9 m² per pixel).

Parameters set within AISA operating mode B, as described above, produced hyperspectral imagery with 38 spectral bands. The band center for the minimum wavelength was at 461 nm, while the maximum band center was at 891 nm. The width of each of the individual bands varied: bands 1 through 14 maintained a band width of 4.86 nm, bands 15 through 32 maintained width of 5.2 nm, and bands 33 through 38 at 5.32 nm.

The thermoelectrically stabilized charge-coupled device (CCD) output images with a 12-bit radiometric resolution. Therefore, assuming a minimum digital number (DN) value of 0 (i.e., no reflected electromagnetic radiation detected by the CCD), the maximum DN in the raw imagery during acquisition was theoretically 4096. After reflectance calibration, the DN's were transformed to a signed 16-bit radiometric quantization. Atmospheric conditions during image acquisition were not documented. The images show very few clouds; therefore it is assumed that skies were clear.

The majority of the images were acquired in either an east-to-west or a west-to-east flightpath. Several ancillary flightlines were acquired using either north or south flightpaths. Figure 2 depicts each flightline and its default filename. In general, the east/west lines are numbered from 1 to 20, with path 1 at the north extreme of the study site and path 20 at the south. It is assumed that the trailing character in the filename (i.e., E, W, N, or S) indicates the direction the aircraft was flying during acquisition.

3.2 Post-Processing

The reflectance data were provided on a set of nine (9) CDs. Each flightline included a suite of files including: a reflectance calibrated image file (*.dat), an ENVI formatted header file (*.hdr), a sensor information/calibration file (*.dsc), an instrument calibration file (*.fod), and an aircraft navigation file (*.nav).

*.dat – This is the large file containing the reflectance calibrated, 38-band imagery. The file was provided in an ENVI compatible format.

*.hdr – This header file passes all required image format data to the ENVI software package.

*.dsc – This text file presented the only form of metadata, or background information, provided by the vendor. Critical data extracted from each of the .dsc files were compiled in a spreadsheet. Table 1 displays a subset of the information in the spreadsheet file, specifically the date, time, and geographic coverage of each flightline. Additional information provided in the .dsc files included characteristics uniform to all images:

Table 1. Subset of flightline header data provided in *.dcs files. Information is sorted by ascending date and time. ULX = Upper Left easting, ULY = Upper Left northing, LRX = Lower Right easting, LRY = Lower Right northing (projection – UTM, zone – 18N, datum – WGS84, units – meters).

Flightline Name	CD #	Date (dd-mon-yy)	Julian Day	Time (24-hr)	UL X (m)	UL Y (m)	LR X (m)	LR Y (m)	# Samples (columns)	# Lines (rows)
BLINE20E	4	07-Jun-00	158	11:23	388660	4247490	413857	4245594	8400	633
BLINE17W	3	07-Jun-00	158	11:33	388044	4249685	409722	4246946	7227	914
BLINE19E	4	07-Jun-00	158	11:43	388815	4248047	413412	4246292	8200	586
BLINE14W	3	07-Jun-00	158	11:54	387981	4252021	412992	4250251	8338	591
BLINE18E	4	07-Jun-00	158	12:05	388262	4248897	413345	4247097	8362	601
BLINE15E	3	07-Jun-00	158	12:16	388019	4251223	412889	4249327	8291	633
BLINE12E	2	07-Jun-00	158	12:27	387439	4253857	413284	4252201	8616	553
BLINE16W	3	07-Jun-00	158	12:39	388039	4250483	412741	4248752	8235	578
BLINE13E	2	07-Jun-00	158	12:52	388353	4252982	413274	4251371	8308	538
BLINE8W	1	07-Jun-00	158	13:02	388016	4257079	412820	4255111	8269	657
BLINE11E	2	07-Jun-00	158	13:13	388120	4254622	413380	4252975	8421	550
BLINE7E	1	07-Jun-00	158	13:23	388004	4257882	413033	4256043	8344	614
BLINE10E	2	07-Jun-00	158	13:47	388303	4255513	413323	4253779	8341	579
BLINE9E	1	07-Jun-00	158	14:18	388415	4256255	413315	4254569	8301	563
BWS21	7	30-Jun-00	181	10:46	388148	4264327	390035	4247251	630	5693
BWS23	7	30-Jun-00	181	12:01	412031	4263820	413978	4246774	650	6683
BW22N	7	30-Jun-00	181	12:11	411223	4263370	413152	4244299	644	6358
BWW8	6	30-Jun-00	181	12:25	387967	4257022	413419	4255483	8485	514
BW1E1	5	30-Jun-00	181	12:35	388108	4262761	413368	4261180	8421	528
BW5W	6	30-Jun-00	181	12:45	388023	4259449	411888	4257868	7956	528
BW2E	5	30-Jun-00	181	12:55	387858	4261949	413325	4260374	8490	526
BW4W	5	30-Jun-00	181	13:05	387609	4260302	413517	4258733	8637	524
BW3E	5	30-Jun-00	181	13:16	386372	4261110	413870	4259505	9167	536
BW17W	7	30-Jun-00	181	13:27	387628	4249634	414247	4248020	8874	539
BW6E1	6	30-Jun-00	181	15:07	387191	4258691	404783	4257152	5865	514
BW6E1A	6	30-Jun-00	181	15:12	408845	4258665	414488	4257141	1882	509
BLK1S	8	15-Sep-00	258	18:42	410776	4262376	412489	4252092	572	3429
BLK2W	8	15-Sep-00	258	18:50	401555	4250029	412316	4247329	3588	901
BLK3W	8	15-Sep-00	258	19:01	387046	4249164	395035	4247628	2664	513
BLK4E	8	15-Sep-00	258	19:09	387485	4258756	414446	4257139	8988	540
BLK1E	9	12-Oct-00	285	13:03	387572	4258775	394187	4257197	2206	527
BLK1W	9	12-Oct-00	285	13:16	387264	4258817	413862	4257152	8867	556

The AISA operating mode was B.
Spatial Resolution = 3.0 x 3.0 meters (pixel size)
Image File Format = BIL (band interleaved by line)
Image Radiometric Range = signed 16-bit (min = -32768, max = 32768)
Number of Bands = 38
File Header Length = 1024 bytes
Map Projection and Coordinate System: UTM-WGS84
UTM Map Zone = 18 North

Additional flightline specific information provided in *.dsc file includes:

Sun Angle = xx.x degrees above horizon
Sun Azimuth = xx.x degrees from map north
Destination file base name = 'YEARjuliandate_uniquename_refl'
{Example = '2000158_BLINE7E_refl'}

**fod* – This text file holds the downwelling solar radiation values as measured by the radiometer mounted on top of the aircraft. A measurement of solar radiation is acquired for each of the 38 bands. The numbers appear to be measured as irradiance in an unsigned 16-bit format.

**nav* – This text file contains aircraft navigation data used to photogrammetrically rectify and register each scan line. The data include: time stamp (seconds), start UTM easting coordinate, start UTM northing coordinate, aircraft altitude (meters), aircraft heading (azimuth degrees), aircraft pitch (degrees from true), aircraft roll (degrees from true), and aircraft yaw (degrees).

3.2.1 Geometric Correction

The raw reflectance data were unzipped and individually displayed to ensure the images were not corrupt. Based on the development of the flightline diagram (Figure 2), combined with an assumption of radically different vegetation phonologies that would be observed in June as compared to a September/October timeframe, post-processing of the AISA images were limited to the 7 and 30 June data.

Several test mosaics of a two to three adjacent flightlines, using only a subset of bands to minimize processing time, were created to evaluate the geometric fidelity of the AISA imagery. The mosaics showed acceptable georegistration of the reflectance-calibrated images, with horizontal errors no greater than three to four pixels. Certainly a higher level of geometric accuracy would be desirable. However, considering the volume of data acquired and the intended purpose of the imagery, this level of geometric accuracy was considered to be acceptable. Figure 3 shows two examples of the typical departure of linear features between adjacent flightlines. The area shown is in the southern portion of the study area, along Route 336 north of Crapo, Maryland.

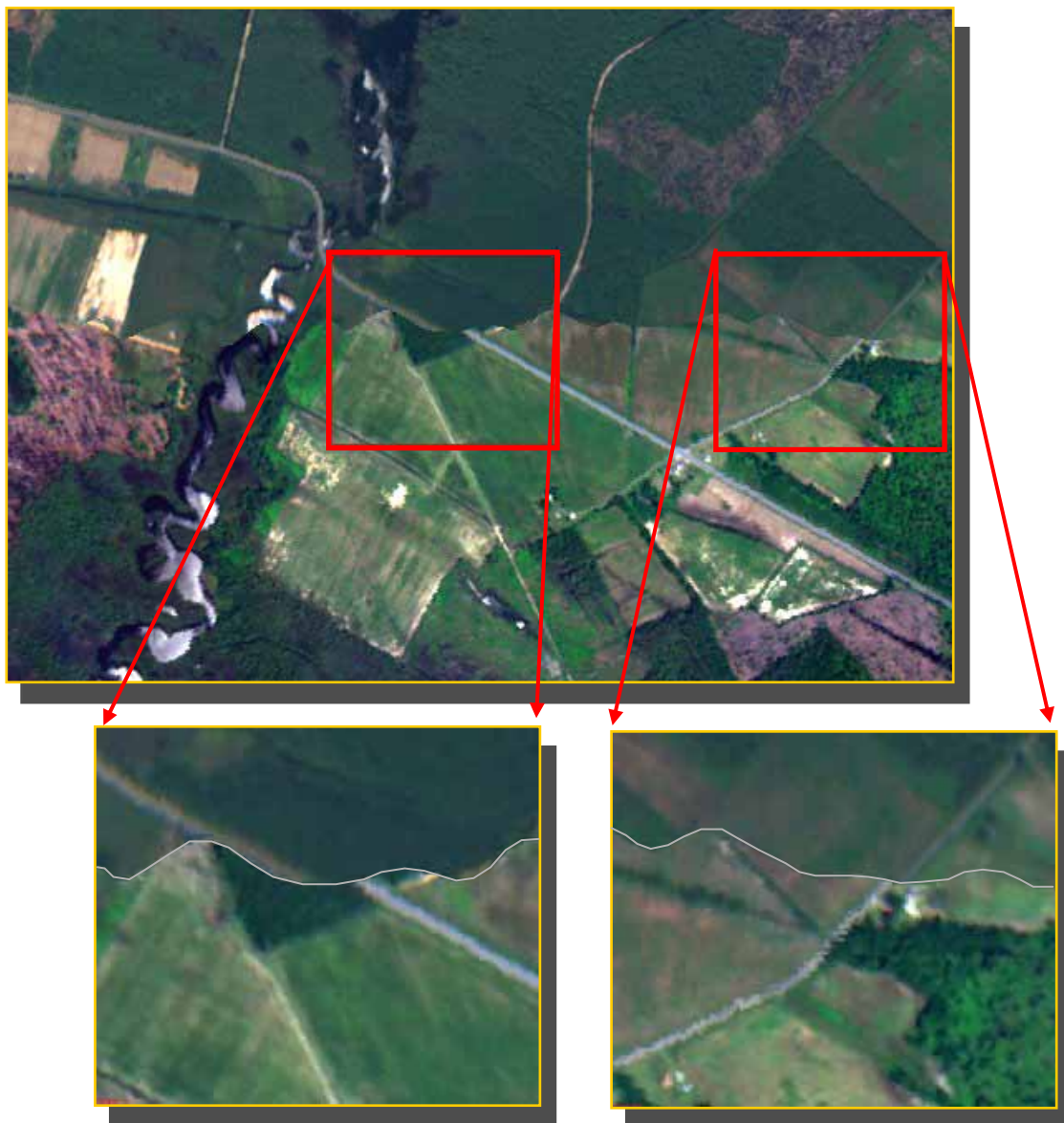


Figure 3. Examples of the geometric quality of the AISA imagery. No quantitative assessment of the actual error in registration was performed or provided by the vendor. A qualitative evaluation suggests that the georectification processes used to rectify the AISA flightlines are adequate for this application. The gray line, within the insets, defines the boundary (or seam) between the two adjacent flightlines. The area shown is along Route 336 north of Crapo.

3.2.2 Radiometric Correction

3.2.2.1 Histogram Evaluation and Adjustment

During the construction of the preliminary mosaics, the radiometric fidelity of adjacent flightlines was observed to be relatively poor. Figures 4 and 5 show the radiometric departure between two adjacent flightlines. It was clear that some form of radiometric normalization or equalization would be needed to minimize the dramatic brightness shifts between overlapping images. At the beginning of this research effort it was assumed that little if any radiometric corrections would be required given that the hyperspectral imagery was calibrated, or corrected, to at-sensor-reflectance values. This suggests that the identical land surface features (e.g., dominant loblolly pine crowns, soybean fields at the same stage of development) should have identical, or nearly identical, DN's across all flightlines acquired on the same Julian Date. If the land surface feature signatures were equal across flightlines after the reflectance calibration, adjacent images (e.g., BLINE7E and BLINE8W) would produce nearly seamless hyperspectral mosaics. This was not the case with the Blackwater images. Consistently, the seam between two adjacent images was visually detectable. Radiometric normalization or equalization involves manipulation of the image histograms.

Histogram analyses generally involves both statistical and graphical tools, as well some general understanding of the anticipated minima, maxima, and distribution of possible data values (i.e., DN's) within an image-based data set. Table 2 presents the minimum, maximum, mean, and standard deviation of the DN's of two overlapping flightlines: BLINE7E and BLINE8W. Nearly all 38 bands show a minimum value of zero, corresponding the background pixels within each image file. Raster data, such as digital imagery, must be stored in matrix (i.e., rectangular) file formats. Therefore, with non-rectangular output image types, such as AISA data acquired using a pushbroom scanner system, a rectangle with dimensions (and accompanying geographic coordinates) slightly larger than the actual image is created to store the data. The empty, or blank, pixels surrounding the image data become background pixels, and are generally assigned an output DN of zero (0). From an image processing perspective, background pixels add to the overall complexity of the image statistical characteristics. Figure 6 shows flightlines BLINE7E and BLINE8W and their associated mean reflectance spectra including the background pixels. It is good practice to, when possible, remove background pixels by trimming the original file using a slightly smaller rectangle. Some data pixels will likely be lost during the resizing of the file. If the pixels to be clipped are critical, removing the background pixels may not be possible. Such was the case with the AISA images. The amount of overlap, more accurately defined as flightline sidelap, between adjacent flightpaths was too small to accommodate background pixel clipping since gaps would have been created. In fact, the percent sidelap was so uniformly small that many between flightpath holidays, or holes, can be seen throughout the completed mosaics. Table 3 provides image statistics after exclusion of the background pixels. Note that band 1 of BLINE7E and two bands in BLINE8W (bands 1 and 38) maintain negative values as minimum DN's. Figure 7 shows flightlines BLINE7E and BLINE8W and their

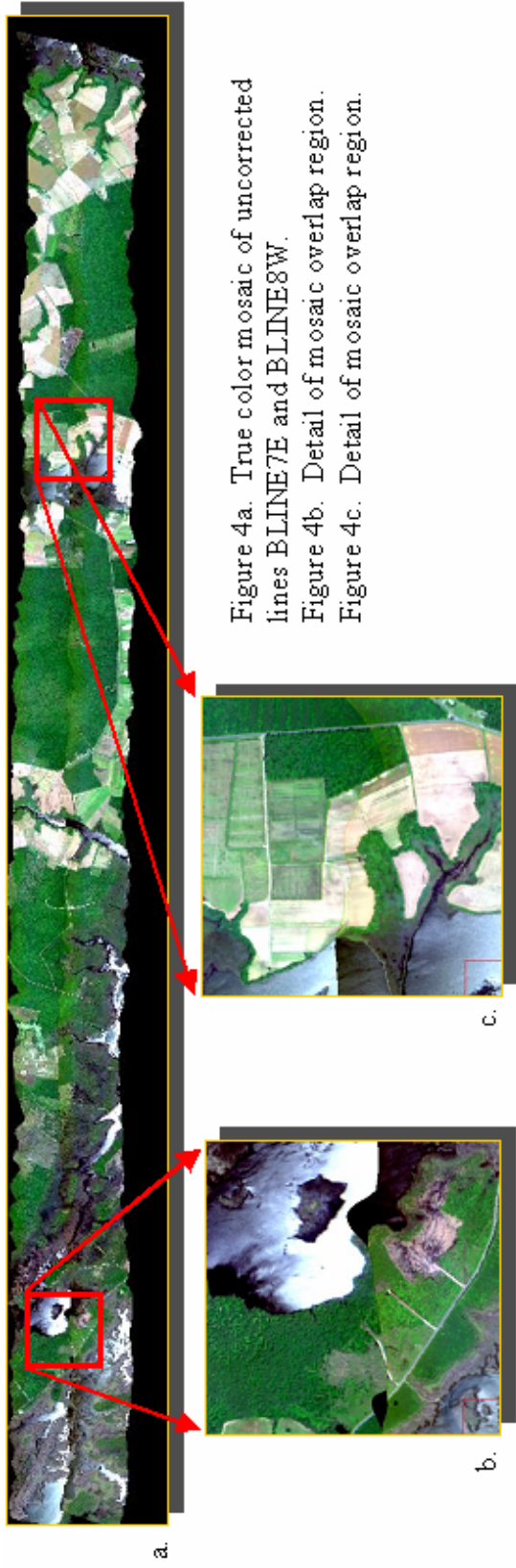


Figure 4a. True color mosaic of uncorrected lines BLINE7E and BLINE8W.

Figure 4b. Detail of mosaic overlap region.

Figure 4c. Detail of mosaic overlap region.

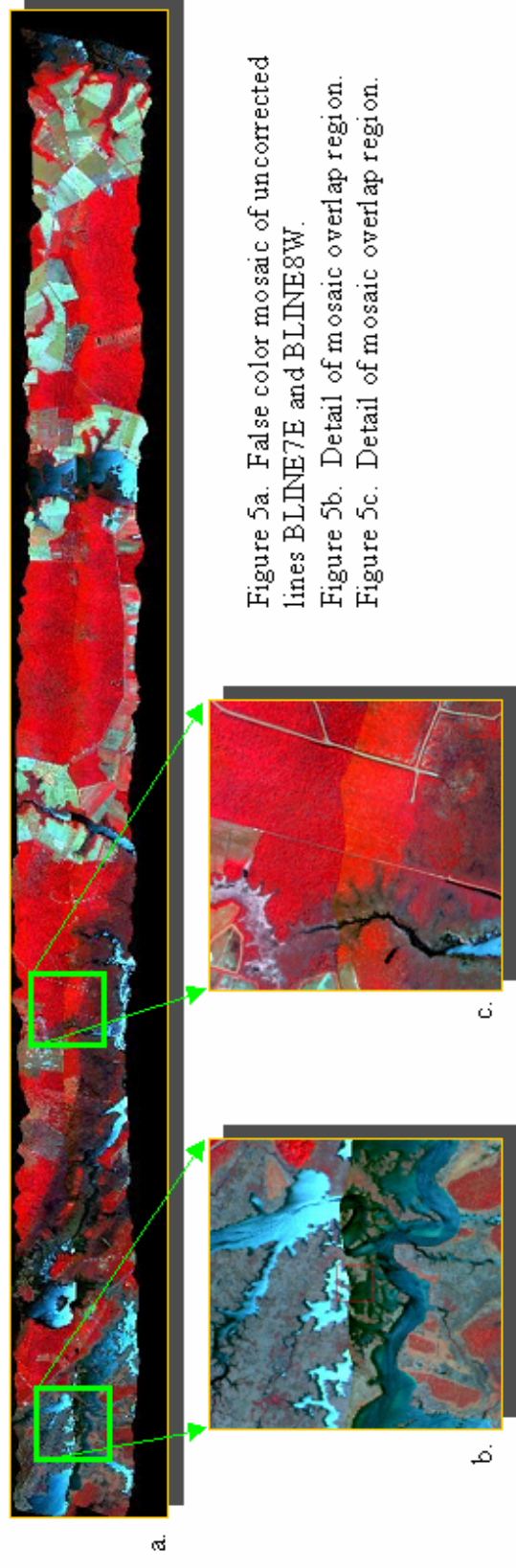


Figure 5a. False color mosaic of uncorrected lines BLINE7E and BLINE8W.

Figure 5b. Detail of mosaic overlap region.

Figure 5c. Detail of mosaic overlap region.

Table 2. Minimum and maximum reflectance values for flightlines BLINE7E and BLINE8W including background (i.e., zero) pixels. Note negative minimums for band 1 of 7E and bands 1 & 37 of 8W.

AISA Band	Wavelength (nm)	BLINE7E				BLINE8W			
		Min	Max	Mean	Stdev	Min	Max	Mean	Stdev
1	461	-41	11436	298.6	305.2	-34	3616	274.4	297.4
2	469	0	11514	305.8	316.3	0	14406	279.5	306.5
3	474	0	11290	306.1	319.4	0	10631	279.0	308.5
4	480	0	11043	312.9	330.5	0	4675	284.8	318.4
5	492	0	9163	311.1	334.1	0	4643	282.2	320.4
6	498	0	8651	322.1	348.2	0	4937	292.2	333.3
7	505	0	7839	316.3	343.1	0	4829	286.1	327.7
8	511	0	7302	337.1	364.4	0	5129	305.3	348.4
9	526	0	6302	377.1	394.5	0	5201	339.9	377.6
10	532	0	5919	397.1	411.1	0	5328	358.0	394.7
11	539	0	5850	412.9	425.8	0	5405	371.4	408.1
12	552	0	5628	425.2	438.5	0	5423	381.8	419.8
13	560	0	5711	421.2	437.9	0	5372	376.8	417.1
14	568	0	5511	411.9	436.0	0	5491	365.9	410.6
15	581	0	4849	400.6	439.9	0	5702	355.3	410.7
16	586	0	4781	389.0	430.9	0	5739	344.6	400.3
17	602	0	4914	384.5	434.7	0	5719	339.7	402.3
18	614	0	4987	380.0	440.2	0	5890	334.4	403.9
19	640	0	5555	365.8	438.7	0	5875	323.0	401.5
20	652	0	6095	358.7	440.4	0	5889	316.9	401.4
21	664	0	5806	358.2	452.2	0	5987	310.9	405.1
22	671	0	5543	354.8	455.3	0	6118	308.2	406.3
23	680	0	5258	368.1	474.1	0	6259	318.9	420.8
24	692	0	5126	386.6	465.5	0	5720	336.5	418.2
25	702	0	5261	515.9	550.0	0	5887	456.0	514.7
26	711	0	5502	654.6	664.7	0	6009	582.8	640.4
27	739	0	5691	1050.9	1106.1	0	5858	953.6	1120.1
28	744	0	5933	1155.4	1228.0	0	6143	1048.2	1244.9
29	751	0	6362	1200.3	1287.6	0	6166	1095.0	1313.5
30	782	0	9161	1239.8	1335.3	0	6054	1130.1	1360.4
31	793	0	10389	1220.1	1311.6	0	5949	1112.3	1335.5
32	798	0	10779	1215.2	1305.0	0	5941	1106.2	1326.7
33	805	0	11605	1229.4	1318.6	0	5954	1116.2	1336.7
34	817	0	12859	996.6	1064.6	0	4739	905.0	1078.6
35	842	0	14629	1252.3	1343.4	0	5885	1125.7	1348.2
36	852	0	16844	1264.2	1355.5	0	5922	1142.4	1367.2
37	872	0	20458	1204.9	1290.2	-31	5617	1075.1	1284.0
38	891	0	19244	1171.3	1246.6	0	5516	1052.3	1247.7

BLINE7E



BLINE8W

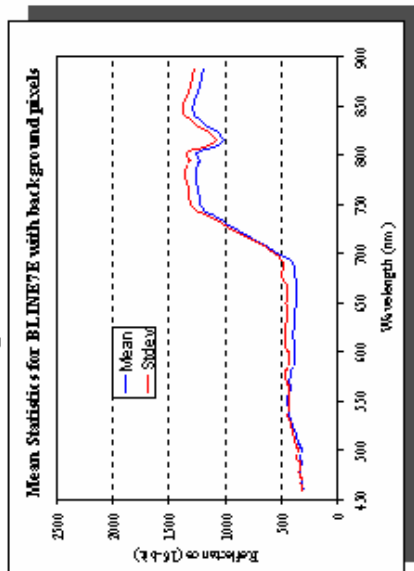


Flightline: BLINE7E

Date: 7 June 2000

Size: 614 rows x 8344 columns
(5,123,216 pixels)

Number of Background Pixels: 2,360,266



Flightline: BLINE8W

Date: 7 June 2000

Size: 657 rows x 8269 columns
(5,432,733 pixels)

Number of Background Pixels: 2,701,404

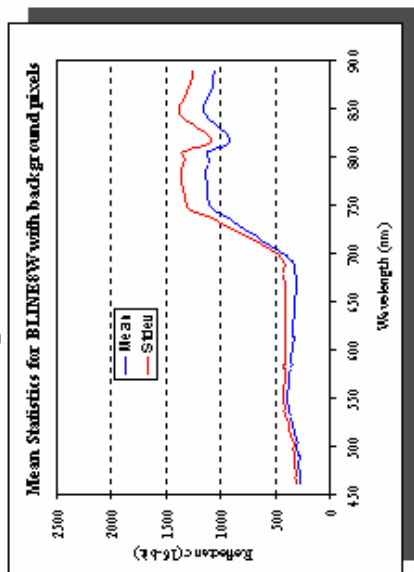
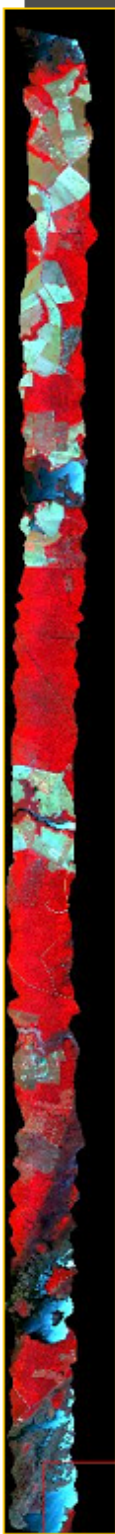


Figure 6. Flightlines BLINE7E and BLINE8W and their associated mean reflectance spectra including the background pixels

Table 3. Minimum and maximum reflectance values for flightlines BLINE7E and BLINE8W excluding the background (i.e., zero) pixels. Note negative minimums for band 1 of 7E and bands1 & 37 of 8W.

AISA	Wavelength	BLINE7E				BLINE8W			
		Band	(nm)	Min	Max	Mean	Stdev	Min	Max
1	461	-41	11436	553.7	177.3	-34	3616	545.8	166.9
2	469	219	11514	567.1	193.2	216	14406	556.0	182.1
3	474	235	11290	567.6	202.0	225	10631	555.0	190.1
4	480	234	11043	580.3	217.9	239	4675	566.6	205.1
5	492	246	9163	576.9	231.7	185	4643	561.3	217.9
6	498	246	8651	597.2	245.9	251	4937	581.3	230.0
7	505	240	7839	586.6	244.6	253	4829	569.1	229.4
8	511	244	7302	625.0	257.5	261	5129	607.3	240.9
9	526	263	6302	699.3	251.4	267	5201	676.0	237.4
10	532	256	5919	736.4	252.3	258	5328	712.1	240.2
11	539	250	5850	765.6	257.2	257	5405	738.8	244.8
12	552	256	5628	788.5	264.7	263	5423	759.5	252.6
13	560	252	5711	781.1	273.0	251	5372	749.5	258.4
14	568	249	5511	763.7	289.5	248	5491	727.8	268.4
15	581	247	4849	742.8	323.5	239	5702	706.8	295.2
16	586	235	4781	721.3	323.4	242	5739	685.5	291.6
17	602	225	4914	712.9	340.9	231	5719	675.6	308.1
18	614	222	4987	704.7	361.3	232	5890	665.2	323.2
19	640	203	5555	678.3	380.7	221	5875	642.5	339.7
20	652	196	6095	665.1	394.7	209	5889	630.3	350.6
21	664	192	5806	664.2	419.6	202	5987	618.5	369.1
22	671	191	5543	657.9	430.1	206	6118	613.1	376.1
23	680	193	5258	682.5	449.6	202	6259	634.3	390.1
24	692	195	5126	716.8	406.3	200	5720	669.3	353.6
25	702	211	5261	956.5	373.4	217	5887	906.9	343.4
26	711	217	5502	1213.8	374.9	220	6009	1159.3	384.0
27	739	195	5691	1948.5	720.7	169	5858	1896.8	840.5
28	744	209	5933	2142.5	825.5	177	6143	2084.9	959.9
29	751	206	6362	2225.6	890.1	179	6166	2178.0	1035.9
30	782	210	9161	2298.8	933.5	120	6054	2247.8	1081.1
31	793	208	10389	2262.4	912.0	169	5949	2212.3	1055.5
32	798	198	10779	2253.2	905.0	153	5941	2200.3	1045.9
33	805	170	11605	2279.7	910.9	105	5954	2220.1	1050.3
34	817	84	12859	1847.9	726.8	118	4739	1800.2	838.3
35	842	153	14629	2322.0	928.7	155	5885	2239.1	1059.5
36	852	129	16844	2344.2	935.7	156	5922	2272.4	1072.5
37	872	110	20458	2234.1	887.1	-31	5617	2138.4	1002.6
38	891	64	19244	2171.9	841.7	19	5516	2093.0	958.3

BLINE7E



BLINE8W

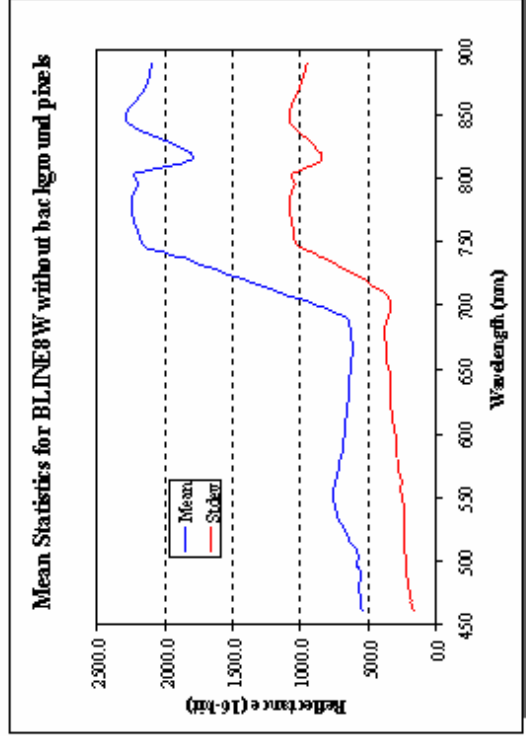
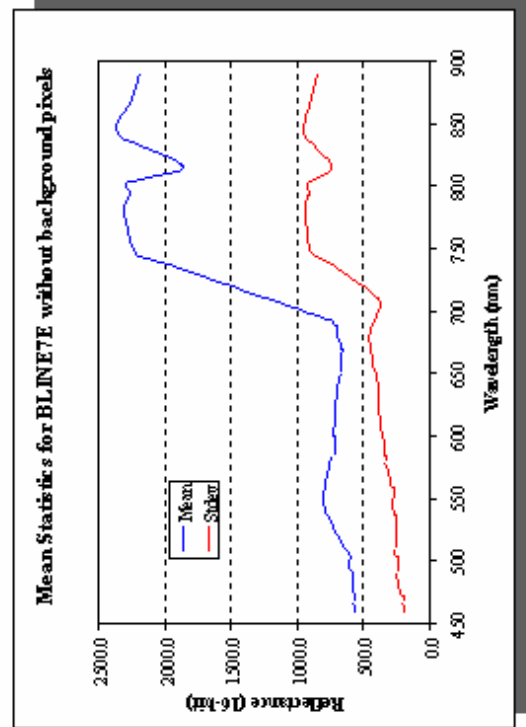
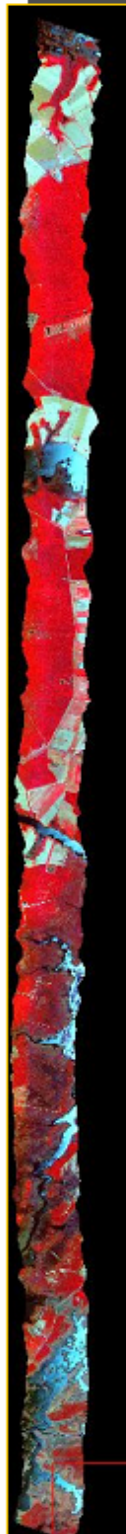


Figure 7. Flightlines BLINE7E and BLINE8W and their associated mean reflectance spectra without the background pixels

associated mean reflectance spectra without the background pixels. The means and standard deviations have shifted considerably. The negative numbers remain, suggesting that these pixels may be a problem.

Reflectance-calibrated imagery is normally plotted using “percent (%)” as the unit of measure for each pixel. Therefore, pixel values would theoretically have a range of 1 to 100%, assuming that a value of 0% (or DN = 0) would be reserved for any background pixels. Commercial image processing software generally does not store and process digital imagery, either reflectance-calibrated and non-calibrated, using DN’s scaled from 1 to 100. The most common digital data formats include:

- binary data where each pixel has a DN of either 1 or 0,
- 8-bit integer data with a DN range of 256 (2^8),
- 16-bit integer data with a DN range of 65,536 (2^{16}), and
- floating-point data where DN’s are stored as real numbers (positive or negative).

Furthermore, 8-bit and 16-bit data can be stored as signed or unsigned. Signed DN’s include a negative or positive sign with each integer value. Unsigned DN’s include only positive integers. Calibrated image data should be unsigned; negative DN’s should not exist since the theoretical minimum reflectance integer value is positive one (+1). As stated above, the AISA sensor acquires 12-bit data, resulting in a radiometric range of 4096 (2^{12}). Therefore, to conform to image processing software file formats, the calibrated AISA images should be stored in an unsigned (i.e., no negative numbers), 16-bit format with a minimum reflectance DN of 1 and a maximum DN of 4096. While this may not appear to be an acceptable scale for percent reflectance, the 1 to 100% scale has simply been re-scaled to 1 to 4096. For example, a reflectance value of 10% has a 12-bit integer value of 410 (or 409.6 rounded to the nearest whole number). A 70% reflectance measure is assigned a DN of 2867. Background pixels should maintain a DN of 0.

The AISA imagery does not follow these assumptions of the theoretical range associated with 12-bit data. Table 3 clearly shows that the maxima for each of the 38 bands in both flightlines exceed 4096. The graphs in Figure 8 show that the frequencies of pixels in the upper tails of the histograms are very small. It was assumed that this radiometric anomaly results from the reflectance calibration routine applied to the raw 12-bit irradiance images. Without better documentation from the vendor, this assumption cannot be confirmed. The negative DN’s presented a bigger problem. Several flightlines (not shown) had reflectance minima in one or more bands approaching $-32,000$. A complete assessment each of the 38 bands within all flightlines revealed channels 1, 2, and 38 had the most frequent occurrence of negative DN’s. This radiometric problem should be expected from the channels near the extremes of the range of the sensor CCD. That is, at the upper and lower limits of the CCD, the detector likely has the greatest signal-to-noise ratios and the lowest relative output (or responsivity). The number of pixels with negative values ranged from only a few to nearly 10,000. While the larger frequency appears alarming, 10,000 pixels represent less than 0.5 % of the total pixels within each image. Finally, the negative pixels were nearly always assigned to the first

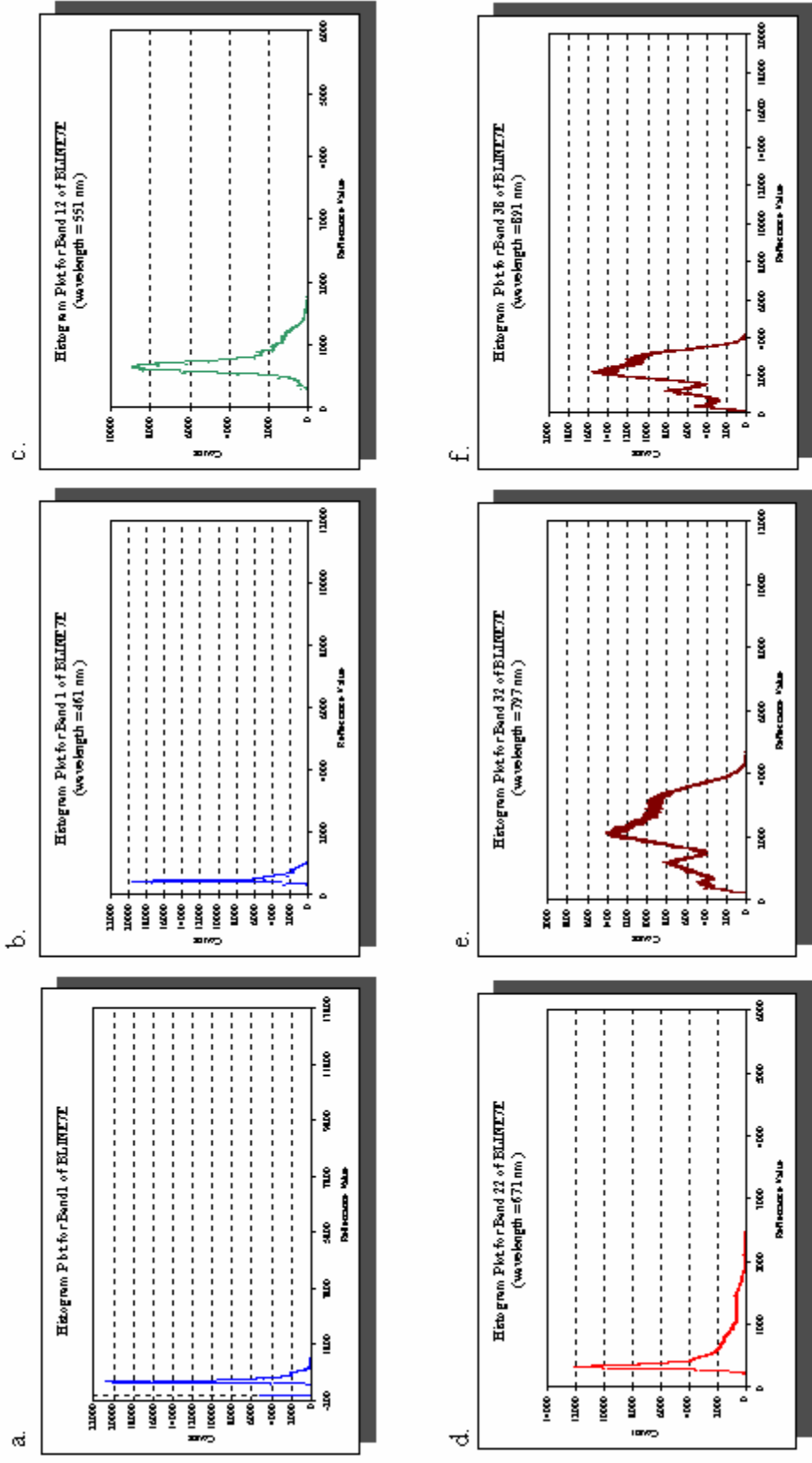


Figure 8. Examples of histograms for 6 of 38 AISA bands.

and last pixels in the cross-track direction. These are the outside pixels along the northern and southern edge of each flightline.

Several methods were employed to deal with the negative DN's. If all the anomalous pixels were indeed located at the edge of the flightline, they were simply assigned a value of zero becoming background pixels. In this case, all 38 bands lost these edge pixels to maintain the proper file size of the actual image data. If one or more of the negative pixels within an individual band were located in the interior of the image data, they were renumbered to a value of 1. This time consuming step in the post-processing the AISA data had very little impact on the overall radiometric quality of the imagery. However, it was thought to be critical in preparing the images for mosaicking. No other manual adjustments to the image histograms were employed.

3.2.2.2 Specular Reflectance or Water Glint

The saturated, or washed-out, water pixels are a normal phenomenon in both digital and analogue images. The AISA images are no exception. The saturation is a result of the specular reflectance properties of water. Specular reflectance occurs when nearly all of the incoming illumination (in this case, sunlight) is reflected from a non-diffuse, or smooth, surface (such as calm water) directly onto the optical focal plane. In other words, the water acts like a mirror, with the reflected sunlight saturating these pixels. Figures 4b & 5b clearly depict these saturated water pixels. Also note that the glare decreases in intensity from south to north across the image. The glinted pixels diminish towards the north side of the flightline because the mirror (i.e., the water) reflects the sunlight at an angle that passes below the far end of the detector. Any subsequent radiometric manipulations to try to improve the quality of the vegetated pixels would likely be negatively impacted by the presence of the glaring water pixels. Therefore, a masking procedure was implemented to remove all the pixels containing standing water.

Several techniques were considered for removing the water pixels. Both supervised and unsupervised classification routines, applied to each flightline independently were investigated, but were determined to require too much time and employed subjective delineation of land cover classes. Digitizing the water areas was also considered, but again would have required too much effort. The land/water mask for each flightpath was eventually created using the Normalized Difference Vegetation Index (NDVI). This simple mathematical expression uses the ratio of the difference between the reflectance DN's of a near infrared band and a red band as compared to their sum.

$$NDVI = \frac{NIR - Red}{NIR + Red} = \frac{AISA(30) - AISA(22)}{AISA(30) + AISA(22)}$$

where: AISA(30) = band 30 (782 nm), and
 AISA(22) = band 22 (671 nm).

The output floating point formatted image has a histogram range of -1 to $+1$. Pixel values below 0 are generally associated with non-vegetated, or only sparsely vegetated, surfaces. Such pixels include man-made features (e.g., roads, roofs), bare earth, and water. As the NDVI values increase, so does the amount of vegetative cover within each pixel to a theoretical maximum value of 1. Figure 9 shows the resulting NDVI image BLINE7E, as well as the original (i.e., floating point) histogram and the histogram after rescaling to an unsigned, 8-bit radiometric resolution.

To create the land/water mask, the NDVI 8-bit file was segmented into two new images, one with vegetated pixels and one with water pixels. The split was determined by examining the distribution of the NDVI histogram. Ranges of pixel values in the NDVI image associated with the major land cover classes, including water, land, and transition areas were determined through visual interpretation. Then a precise breakpoint coinciding with the separation of land pixels from water pixels was identified. In the case of BLINE7E, an acceptable break was found at $DN=145$ (Figure 9). Finally, the NDVI image was split into two distinct binary masks. The first mask represented water pixels ($DN_{NDVI} \leq 145$) and the second represented land pixels ($DN_{NDVI} > 145$). The land mask was applied to the full hyperspectral image such that only a subset of the original file remained depicting only those pixels supporting vegetation. The accuracy of this step was not quantified. However, a visual inspection was employed to determine if water pixels remained in the output “land-only” file. The output image was also inspected to determine if too many land pixels had been removed. If the land-only image was not acceptable, a new interpretation of the NDVI histogram was performed and a new breakpoint was selected. Across all flightlines, the breakpoints fell between 135 and 165. Figure 10 shows the vegetated pixels segmented from flightlines BLINE7E and BLINE8W. A plot of the mean DN’s for all 38 bands is also provided in Figure 10. All subsequent processing, including image classification, was performed on the vegetation-only images. Table 4 lists the means and standard deviations for all 38 bands for flightlines BLINE7E and BLINE8W after removal of both background pixels and water pixels.

3.2.2.3 Reduction in Data Dimensionality

An interpretation of the mean per band reflectance values, shown in Figure 10, suggests problems with data in the near infrared region of the spectrum. Specifically, the pronounced dip in the curve at band 34 (817 nm) is not normal, indicating a significant radiometric problem. Inspection of the raw (i.e., non-calibrated) irradiance image data showed the same anomalous dip in the band 34. A more extensive comparison of AISA vegetation spectral signatures to vegetation signatures contained with spectral libraries maintained at TEC revealed that bands 33 through 38 generally did not provide quality reflectance data. This analysis was not quantitative, but was based on extensive experience with analyzing vegetation signatures from more mature hyperspectral imaging systems (e.g., AVIRIS, HYDICE) and from ground-based vegetation signatures collected

BLINE7E NVDI Image

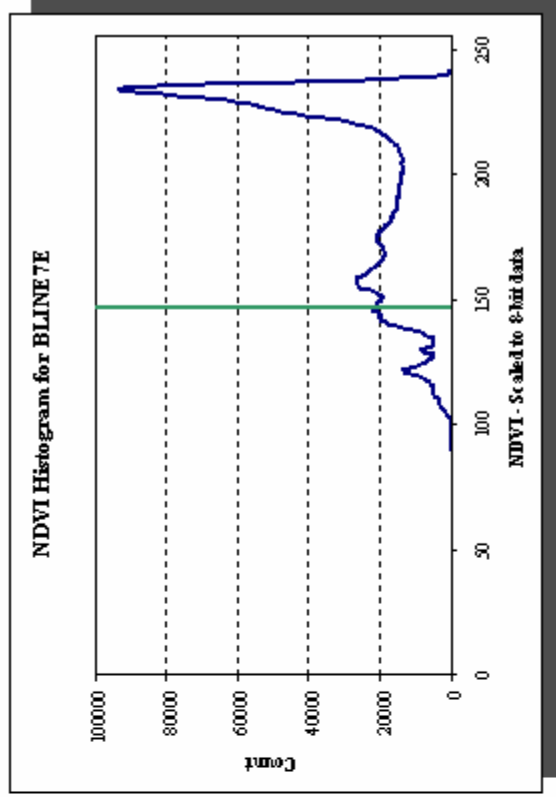
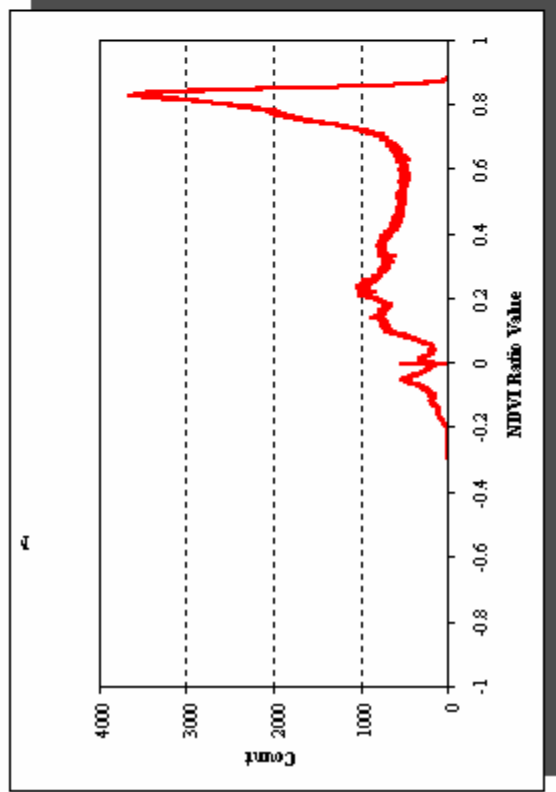
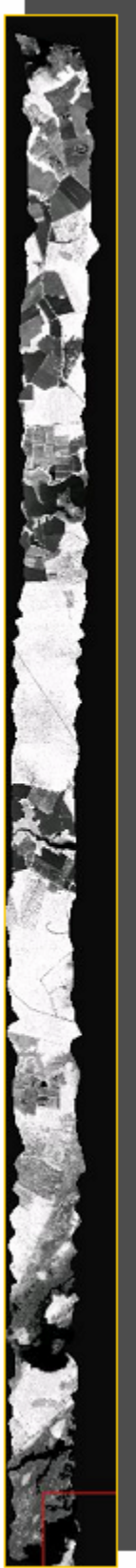


Figure 9. Example of NDVI image. Graphs of floating point NDVI values and NDVI values after scaling to 8-bit data.

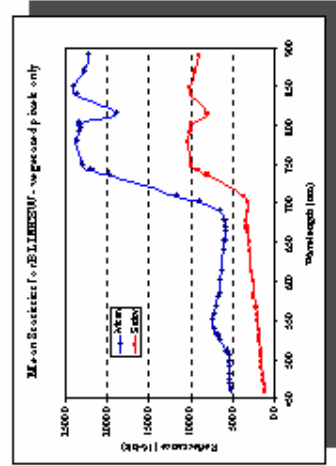
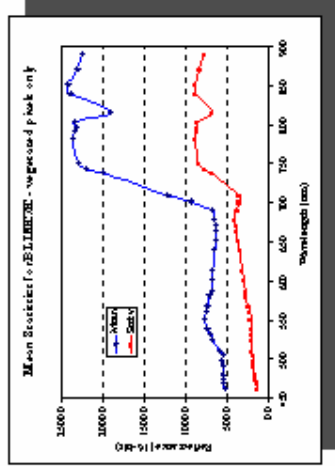
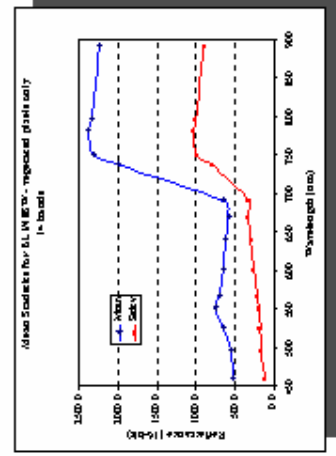
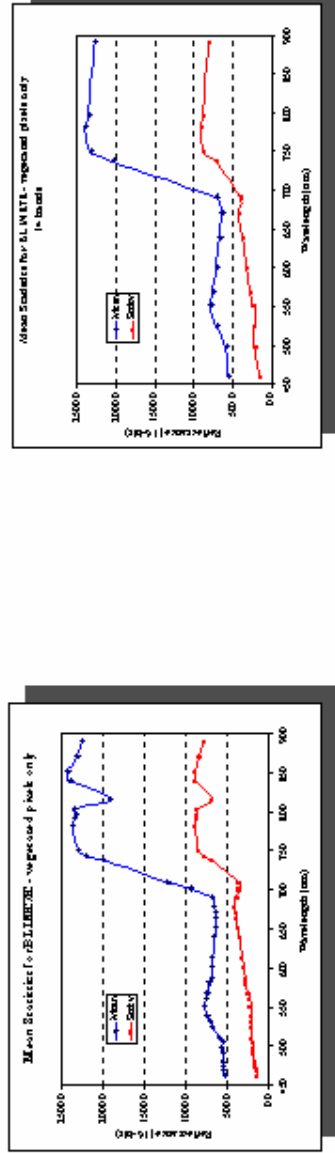
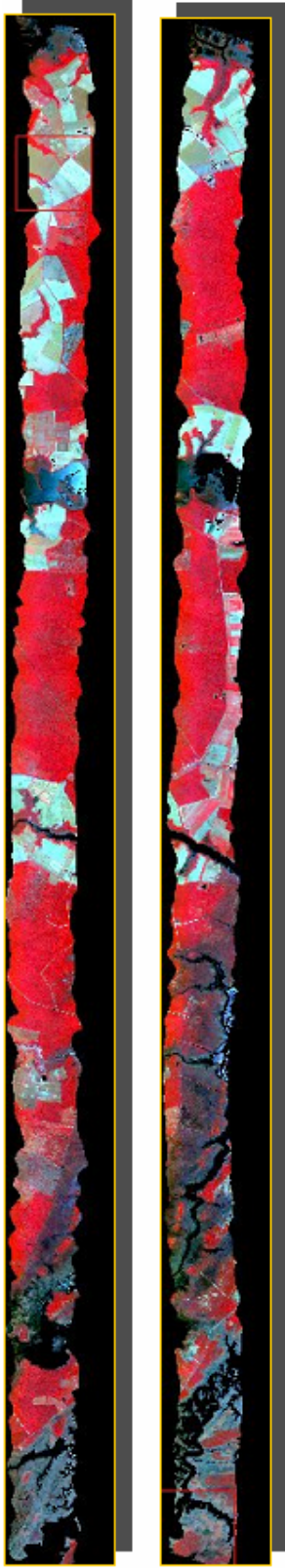


Figure 10. Flightlines BLINE7E and BLINE8W and their associated mean reflectance spectra after (1) removal of water pixels and (2) reduction in data dimensionality.

Table 4. Minimum and maximum reflectance values for flightlines BLINE7E and BLINE8W excluding the background (i.e., zero) pixels and the water pixels.

AISA	Wavelength	BLINE7E				BLINE8W			
		Band	(nm)	Min	Max	Mean	Stdev	Min	Max
1	461	-41	11436	535.6	136.5	-34	2853	521.9	107.0
2	469	219	11514	546.9	147.8	216	14406	529.1	115.3
3	474	237	11290	546.4	154.8	225	10631	526.6	120.6
4	480	234	11043	557.4	167.8	239	3300	535.7	131.2
5	492	246	9163	553.0	180.5	254	3337	528.8	142.5
6	498	246	8651	572.0	193.9	251	3504	547.2	152.9
7	505	240	7839	562.2	193.5	253	3335	535.9	154.2
8	511	244	7302	599.9	205.8	264	3559	573.5	164.2
9	526	263	6283	677.6	202.5	275	3548	648.0	167.1
10	532	256	5919	716.0	204.6	277	3588	686.3	172.7
11	539	250	5832	746.0	210.9	272	3600	714.3	179.8
12	552	256	5628	769.9	220.4	271	3568	736.4	191.0
13	560	252	5711	762.1	229.2	271	3580	725.4	197.1
14	568	249	5502	743.0	245.9	260	3644	700.9	206.0
15	581	247	4849	718.9	279.8	254	3866	674.8	230.3
16	586	235	4778	697.7	282.5	242	3797	653.9	230.2
17	602	225	4914	689.6	301.9	237	3948	643.8	248.4
18	614	222	4987	680.4	323.9	232	4034	631.9	264.9
19	640	203	5555	654.4	347.0	221	4192	608.6	286.5
20	652	196	6091	640.3	362.2	215	4289	594.9	297.9
21	664	192	5798	638.4	387.2	206	4522	581.8	315.9
22	671	191	5543	631.6	398.2	206	4628	576.1	323.4
23	680	193	5258	655.7	418.3	204	4914	596.9	337.9
24	692	195	5122	697.0	381.9	202	4577	641.8	311.5
25	702	211	5261	949.4	352.2	236	4830	899.3	307.7
26	711	217	5502	1220.8	352.3	247	5079	1175.2	350.5
27	739	202	5683	2004.4	685.9	193	5236	1997.4	795.0
28	744	214	5933	2207.0	787.8	249	5548	2200.5	911.0
29	751	215	6362	2295.5	851.6	249	5766	2303.5	985.8
30	782	219	9161	2374.6	891.1	258	6054	2381.9	1027.1
31	793	220	10389	2337.1	869.7	214	5949	2344.2	1001.7
32	798	225	10779	2327.8	862.4	247	5941	2331.4	992.1
33	805	170	11605	2355.2	867.2	245	5954	2352.5	995.2
34	817	84	12859	1909.4	690.2	201	4739	1907.7	792.0
35	842	171	14629	2403.2	878.2	197	5885	2379.5	994.4
36	852	129	16844	2426.8	883.3	192	5922	2415.8	1004.9
37	872	110	20458	2313.6	834.8	170	5617	2273.6	937.0
38	891	64	19244	2249.5	788.4	19	5516	2225.7	890.3

using hand-held spectroradiometers. The decision was made to potentially drop these bands from the images. Evaluation of the remaining 32 bands suggested that many could likely be dropped without any significant impact to image classification accuracy. Again, this was a qualitative evaluation based on research team experience. Therefore, of the original 38 bands, a total of 14 were retained. These 14 bands included:

- 1 (461 nm)
- 6 (498 nm)
- 9 (526 nm)
- 12 (522 nm)
- 14 (568 nm)
- 17 (602 nm)
- 19 (640 nm)
- 22 (671 nm)
- 24 (692 nm)
- 27 (739 nm)
- 29 (751 nm)
- 30 (793 nm)
- 32 (798 nm)
- 38 (891 nm)

As stated above, signal-to-noise ratios for bands 1 and 38 severely diminished the quality of these bands. However, band 1 is the only channel close to the center of the blue region of the spectrum (~ 450 nm) and was kept. Similarly, band 38, while of relatively poor quality, was kept to at least provide a signature end point well into the near infrared region. Figure 10 depicts a plot of the average DN's for BLINE7E and BLINE8W after this reduction in data dimensionality.

An additional benefit of reducing the dimensionality of the data was a significant decrease in the file size. For example, the full 38 band flightline BLINE7E is ~ 380 megabytes. After removal of 24 bands the file size is reduced to ~ 140 megabytes. By working with smaller files, subsequent image processing steps required much less CPU time.

3.2.2.4 Cross-Track Illumination Correction

Test mosaics created using the 14-band, vegetation-only images still had pronounced seams where adjacent flightlines overlapped. The mosaics showed that the south edge of each flightline was consistently darker than the north edge of the overlapping flightline within forested areas. An inverse shift in brighter to darker pixels was observed in the water and marsh vegetation pixels, with brighter pixels at the lower edge of the flightlines. This significant departure in the supposedly calibrated data was attributed to cross-track illumination irregularities, which can be caused by any number of factors, including:

- within sensor (i.e., system) radiometric distortions,

- flawed reflectance calibration, and
- bi-directional reflectance influences.

Regardless of the cause, the illumination anomaly within all of the images represented a significant problem in creating usable mosaics. The ENVI imaging processing software offers a cross-track illumination correction. The routine calculates the overall row (east-to-west) average DN's within an image and then fits a polynomial to the averages, for each band, to potentially correct (or flatten) the reflectance data in the cross-track direction (south-to-north). If applied properly, the darker southern edge of each image should brighten, while the pixels at the northern edge should darken slightly. This correction routine was applied to each flightline after removal of the water pixels. The correction algorithm ignores the background pixels (i.e., DN = 0) when calculating the across-track averages and when applying the polynomial functions.

3.2.2.5 Histogram Equalization

As a final step in preparing adjacent images for mosaicking an attempt was made to equalize the histograms of two overlapping flightlines. This technique uses a simple mathematical formula to match the general shape of the mean DN curves between two image files. Figure 10 displays the mean and standard deviation DN curves for the 14-band images BLINE7E and BLINE8W. These curves were calculated using only the overlap regions of the two adjacent flightlines. The formula employed to match one histogram to the other is:

$$DN_{out} = \left[\left(\frac{DN_{in} - \mu DN_t}{\sigma DN_t} \right) * \sigma DN_r \right] + \mu DN_r$$

Where:

DN_{out} = output pixel value

DN_{in} = input pixel value

μDN_t = mean pixel value of transform image

σDN_t = standard deviation of transform image

σDN_r = standard deviation of reference image

μDN_r = mean pixel value of reference image

Flightline BLINE7E was transformed to the reference image BLINE8W. Within the image processing software, the equation is applied to the 14-band input image (BLINE7E) using matrix algebra. The four mean and standard deviation terms are one-dimensional arrays (or vectors). The output image is an adjusted 14-band image. Figure 11 depicts the output mosaic, as both a true-color and false-color file. While the equalization calculation worked nearly perfectly, as is displayed by the second mean/standard deviation graph, the correction still left a noticeable seam between adjacent flightlines.

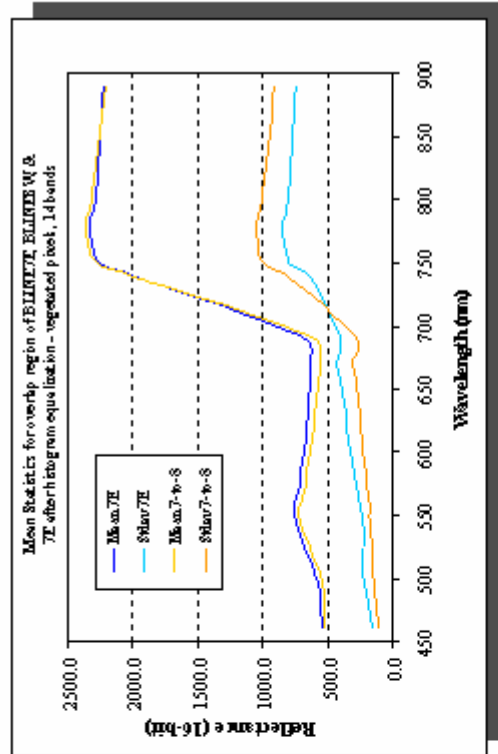
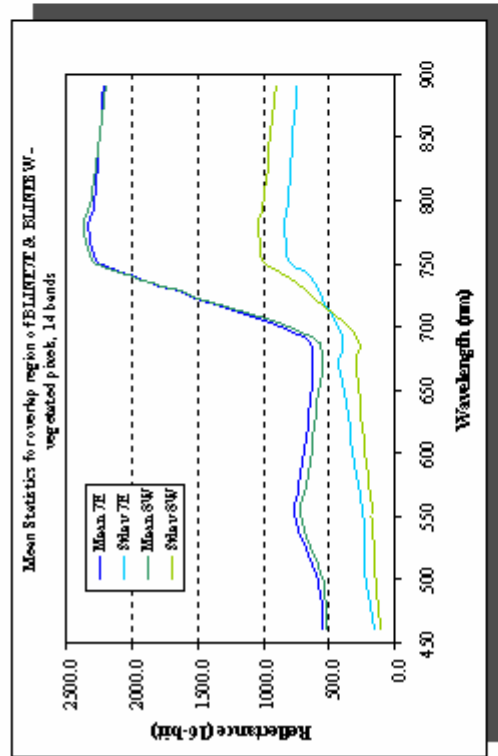
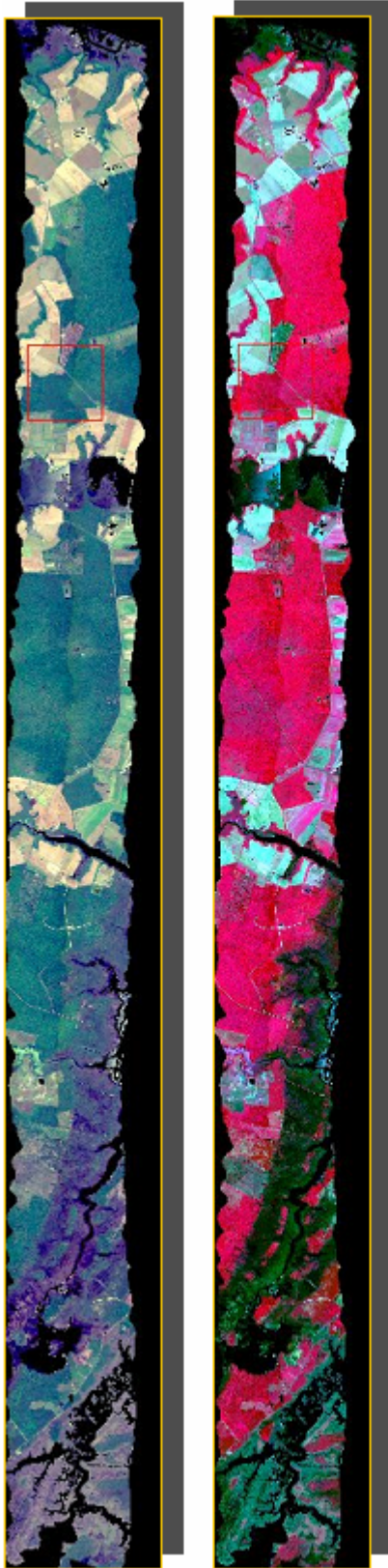


Figure 11. Histogram equalization results between BLINE7E and BLINE8W.

The technique was more successful between some pairs of flightlines and less successful between other pairs. Figure 12 displays the final output mosaic of flightlines BLINE7E through BLINE20E. Several seams are clearly visible. The most prominent is the seam between flightline 10E and 11E. Repeated attempts to improve the significant radiometric distortion between these two flightlines were equally unsuccessful.

3.2.3 Mosaicking

At the onset of this project, it was assumed that this would be the only post-processing step that would be required to prepare the AISA images for vegetation classification. However, as described in detail above, an array of additional post-processing techniques were applied to each AISA flightline to try to improve radiometric anomalies and distortions. The quality of the resulting mosaics, in terms of consistent reflectance values between and among the individual images, remained marginal. Flightlines BW1E1, BW2E, BW3E, BW4W, and BW5W, all acquired on 30 June 2000, produced the highest quality mosaic (Figure 13). During repeated attempts to remove seams between overlapping flightlines and to equalize the reflectance values, the best result for the final mosaic included the water pixels. The relatively small percentage of water pixels within these flightlines meant that the specular reflectance (i.e., glint or glare) problem had little affect on the quality of this mosaic. Seams are still visible and the histogram equalization procedure was moderately successful.

Flightlines BW6E1 and BW6E1A, also acquired on 30 June 2000, presented significant problems. None of the post-processing algorithms were successful in matching the histograms of these two flightlines to the BW1-thru-5 mosaic. Figure 14 displays the brightness shifts between the mosaic and the two additional files. Figure 14 also reveals a large holiday (or gap) near the center of, what should be, the center of a complete flightline 6E. This holiday was filled with the image file BLK1W, acquired on 12 October 2000. A visual interpretation of this early fall image clearly showed radically different vegetative reflective properties. Given the date of the ancillary acquisition, physiological changes associated with the change in season had altered the spectral properties of nearly all surface materials within the marsh. Therefore, flightline BLK1W was not used in this analysis, leaving a large holiday in the northern half of the mosaic.

3.3 Field Data Collection

Four brief field data collects, in support of this image classification effort, were completed during the Fall of 2001 and Summer of 2002. The specific dates were: 26 September, 11 October, 17 October 2001, and 7 August 2002. USFWS staff at the Refuge provided the 2001 data, while TEC staff collected a small set of additional field sites 2002. Table 5 shows the combined field data. Plot coordinates, were collected using Garmin hand-held GPS receivers, are in the UTM projection (zone 18s, units = meters) with datum WGS84. These coordinates were not differentially corrected. Therefore, the average coordinate accuracy is assumed to be between 5 and 10 meters. As shown in Figure 15, sample sites WP001 through WP023 fell within the 30 June (i.e., northern) mosaic. Site WP024, WP025, and WP026, as well as the 07 August 2002

a



b

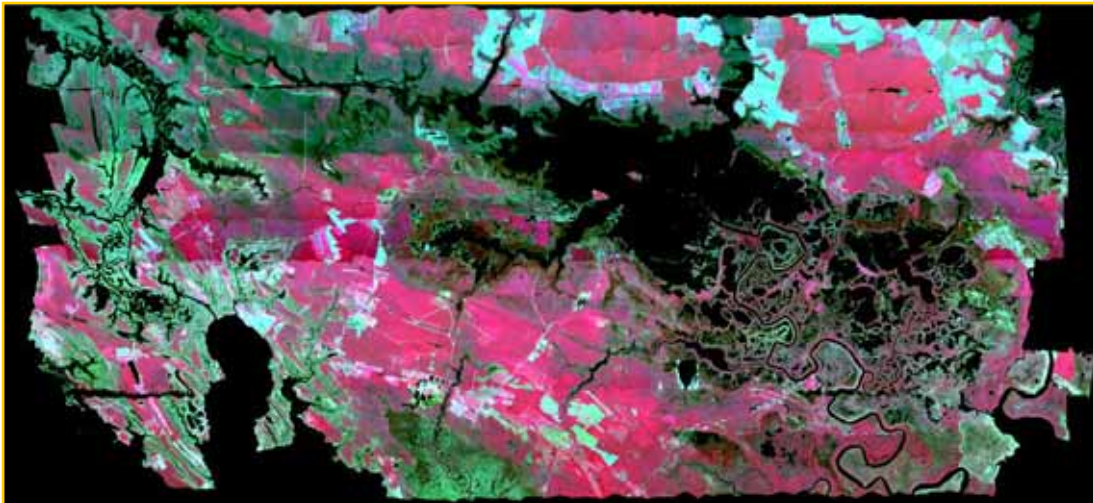


Figure 12. Southern Mosaic – flightlines BLINE7E through BLINE20E. (a) true color composite, and (b) false color composite.



a.



b.

Figure 13. Final mosaic for flightlines 1 through 5 acquired on 30 June 2000. (a) true color composite, and (b) false color composite.



a.



b.

Figure 14. Final mosaic for flightlines 1 through 6 acquired on 30 June 2000. (a) true color composite, and (b) false color composite.

Table 5. Location and description of field plots: Fall 2001 and Summer 2002.

Date	Plot ID	Vegetation Description	Easting	Northing
26-Sep-01	WP1	S. patens w/ juncus in background	390055	4259763
26-Sep-01	WP2	intersection of juncus, 3-square, patens	390077	4259750
26-Sep-01	WP3	intersection of patens, typha, 3-square	390145	4259738
26-Sep-01	WP4	typha angustifolia	390179	4259766
26-Sep-01	WP5	phragmites	390138	4259805
26-Sep-01	WP6	3-square/distichlis	390083	4259833
26-Sep-01	WP7	juncus	390064	4259911
26-Sep-01	WP8	Iva frutescens bounded by S. patens (10m from canal)	390039	4259871
26-Sep-01	WP9	alterniflora/distichlis/patens	389922	4259394
26-Sep-01	WP10a	intersection of patens, 3-square, juncus	390607	4258647
26-Sep-01	WP10b	same photo as 'a' but from other side	390607	4258647
26-Sep-01	WP11	3-square/patens	390978	4257961
26-Sep-01	WP12	3-square	390937	4257951
26-Sep-01	WP13	small juncus patch in middle of 3-square	390893	4257974
26-Sep-01	WP14	intersection of 3-square and distichlis	390848	4257915
26-Sep-01	WP15	distichlis	390853	4257885
26-Sep-01	WP16	phragmites	390860	4257852
26-Sep-01	WP17	intersection of 3-square, distichlis, phragmites	390883	4257854
11-Oct-01	WP18a	upper Corsey Creek looking west from White Marsh Road	393937	4259850
11-Oct-01	WP18b	upper Corsey Creek looking east from White Marsh Road	393937	4259850
11-Oct-01	WP19a	(looking north) Walter's millet, Chufa, Pluchea, Eleocharis, Myrica, redmaple, sweetgum	392925	4260539
11-Oct-01	WP19b	(looking south); flowering Bidens laevis in foreground	392925	4260539
11-Oct-01	WP20	upland site; loblolly pine saplings in field of Andropogon	392520	4260403
11-Oct-01	WP21	forest edge; loblolly pine, willow oak, white oak, red maple	392422	4259866
11-Oct-01	WP22a	(looking north) S. patens with some Myrica/Cyperus	392454	4259841
11-Oct-01	WP22b	(looking south)	392454	4259841
11-Oct-01	WP23a	(looking north) S. Patens	392322	4259190
11-Oct-01	WP23b	(looking south)	392322	4259190
11-Oct-01	WP23c	looking east towards Phragmites along forest edge on other side of creek	392322	4259190
17-Oct-01	WP24	3-square adjacent to Shorters Wharf Road	407858	4252836
17-Oct-01	WP25	<i>Spartina cynosuroides</i> , down-river from Shorters Wharf Bridge. GPS point is in center of <i>S. cynosuroides</i> patch.	406871	4248792
17-Oct-01	WP26	Reference, dead center of Shorters Wharf Bridge	406777	4248741
07-Aug-02	01	Patens beneath pine forest	399310	4256050
07-Aug-02	02	Mixed salt community	399170	4256082
07-Aug-02	03	Pine forest, thinned, 10 to 12'	397030	4256315
07-Aug-02	04	Cattail mixed with Eleocharis	399148	4256258
07-Aug-02	05	Patens marsh	392304	4259152
07-Aug-02	06	Freshwater marsh on Corsey Creek	393936	4259849
07-Aug-02	07	Three-square mixed with Patens, Distichlis	407898	4252605
07-Aug-02	08	Phragmites mixed with three-square	407923	4252613
07-Aug-02	09	Alterniflora	406724	4549409
07-Aug-02	10	Dense Patens	407464	4251205
07-Aug-02	11	Dense shrubs	407130	4250922
07-Aug-02	12	Pine forest with Phragmites and shrub understory	407111	4251043
07-Aug-02	13	Dense shrubs with a few pines	407288	4250492

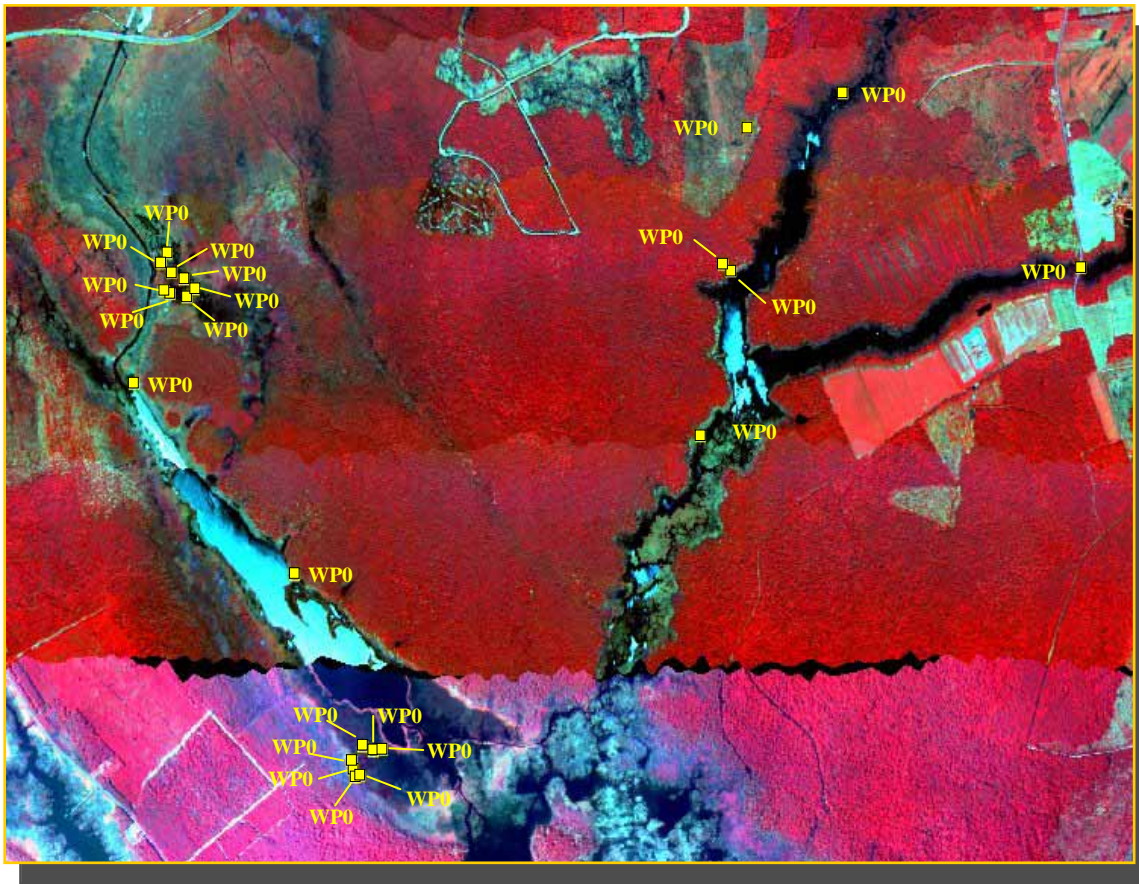


Figure 15. Location of training sites within western part of northern mosaic.

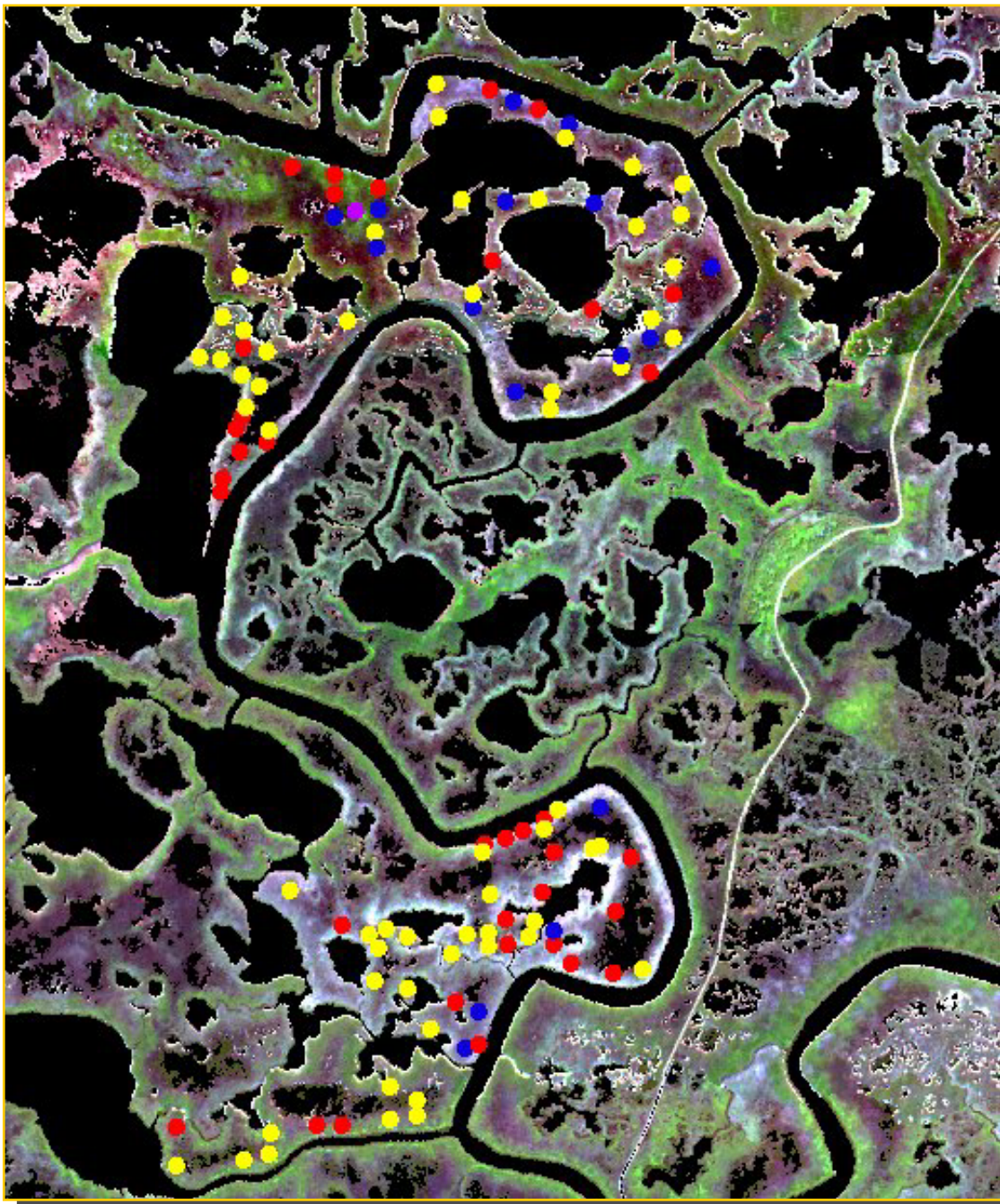
sample sites, were located in the 7 June (i.e., southern) mosaic, adjacent to Shorters Warf Road.

The Refuge provided additional field data, collected during the summer of 2000. These data were reported as percent vegetative cover, by species, within 1m² quadrats. The plots were divided into five areas (2 through 6) throughout the southeast portion of the Blackwater Refuge and the northeast portion of the Fishing Bay Wildlife Management Area. Areas 2 and 3 were located just west of Shorters Warf Road. Areas 4, 5, and 6 were to the east, in the Fishing Bay Area, and were not located within the southern ASAI mosaic. The 240 quadrats within areas 2 and 3 supported non-woody vegetation. The dominant species included: *Scirpus olneyi* (Threesquare bulrush), *Spartina alterniflora* (Smooth cordgrass), and *Spartina patens* (Salt hay). *Pluchea purpurascens* (Saltmarsh fleabane), *Spartina cynosuroides* (Big cordgrass) and *Distichilis spicata* (Salt grass) were minor components within the sampled sites. Litter, mud, and/or water occupied non-vegetated areas within the plots. Only those plots with at least 50% cover by any of the three dominant species were used for spectral signature extraction. Given that the radiometric variation between some flightlines in the southern mosaic approached 20%, it was assumed that subtle spectral variations associated with mixed species compositions in many plots would be lost in the between-flightline noise. Therefore a total of 111 quadrats were determined to be suitable for signature extraction. Figure 16 displays the locations of these sample sites and indicates the dominant species present. Table 6 lists these plots. The accuracy of the geographic coordinates for these data is unknown.

The Refuge also provided a forest type map, in the form of an ArcView shapefile (Figure 17). The database was exported and deciphered, with a total of seven forest cover types identified, including: cutover stands, loblolly pine dominated, loblolly pine-oak mixed, loblolly pine-hardwood mixed, mixed hardwood, morbid/declining stands, and stands with scattered overstories. The shapefile polygons were displayed as overlays on the mosaics and suitable locations within individual stands were selected for training data extraction. A total of 28 training sites were delineated.

3.4 Signature Extraction

The ENVI software routines for building training data sets to perform discriminant analyses, including a variety of supervised classification algorithms, extract reflectance value statistics using user defined polygons. These polygons, called Regions of Interest (ROI's), can be of any size. The objective of extracting DN's from a multi- or hyperspectral digital image is to define the n-dimensional statistical space unique to individual, or groups, of separable surface elements. Because training data sets must build multivariate statistics, including the mean, the standard deviation, and the accompanying covariance matrix, for each individual land cover class, ROI's generally encompass more than one single pixel. Furthermore, multiple roi's must be used, potentially throughout the entire image space, to account for spatial variability within the scene.



- DISP – *Distichilis spicata*
- SPPA - *Spartina patens*
- SPAL - *Spartina alterniflora*
- SCOL - *Scirpus olneyi*

Figure 16. Location of training sites adjacent to Shorters Warf Road.

Table 6. Location and description of 1 m² quadrats.

Original REC NUM	Plot ID	UTM		Dominant Species	Percent Cover by Species and Non-Veg								
		Eastings	Northing		Disp	Lit	Mud	Plpu	Scol	Spal	Spcy	Sppa	Watr
31	2BT1-1	406085	4251781	Scol	0	0	10	0	68	0	0	22	0
26	2AT7-4	405780	4251973	Scol	5	0	0	0	75	0	0	5	15
81	2CT7-3	406184	4252121	Scol	0	0	15	0	61	24	0	0	0
72	2CT4-3	406465	4252114	Scol	0	10	14	0	58	18	0	0	0
46	2BT6-3	406553	4251632	Scol	0	10	15	0	71	4	0	0	0
239	3DT9-2	406104	4249548	Scol	10	0	25	0	65	0	0	0	0
36	2BT3-2	406219	4251517	Scol	0	18	12	0	59	0	0	11	0
235	3DT8-1	406058	4249433	Scol	0	10	20	0	55	15	0	0	0
49	2BT7-3	406646	4251685	Scol	0	12	21	0	67	0	0	0	0
15	2AT5-3	405646	4252074	Scol	0	0	0	0	60	0	0	5	35
59	2BT10-2	406840	4251910	Scol	4	7	28	0	61	0	0	0	0
73	2CT5-1	406387	4252363	Scol	0	15	20	0	61	0	0	4	0
24	2AT7-2	405782	4252094	Scol	0	0	40	0	50	0	0	10	0
168	3BT6-3	406337	4249806	Scol	0	18	23	0	55	4	0	0	0
79	2CT7-1	406212	4252436	Scol	0	0	42	0	54	4	0	0	0
200	3CT7-2	406484	4250198	Scol	0	0	47	0	53	0	0	0	0
25	2AT7-3	405772	4252024	Spal	0	0	0	0	0	80	0	10	10
109	2DT6-3	405405	4251531	Spal	0	0	0	0	0	80	0	10	10
132	3AT5-1	405438	4249098	Spal	25	0	10	0	0	50	0	15	0
234	3DT7-1	405947	4249495	Spal	0	0	10	3	0	87	0	0	0
87	2CT9-2	406049	4252127	Spal	0	0	1	0	8	81	0	0	0
50	2BT7-4	406651	4251745	Spal	0	0	12	0	14	54	2	18	0
103	2DT5-6	405366	4251466	Spal	0	0	15	0	0	85	0	0	0
104	2DT5-7	405354	4251570	Spal	0	0	0	0	2	73	0	10	15
106	2DT5-9	405354	4251710	Spal	0	0	0	0	0	85	0	0	15
129	3AT4-1	405358	4249080	Spal	15	0	15	0	0	50	0	20	0
164	3BT5-2	406258	4249788	Spal	0	0	17	0	0	83	0	0	0
32	2BT1-2	406080	4251824	Spal	0	0	18	0	0	82	0	0	0
39	2BT4-2	406332	4251517	Spal	12	0	18	0	0	70	0	0	0
183	3CT1-3	406137	4249924	Spal	3	0	18	0	7	72	0	0	0
224	3DT4-4	405754	4249797	Spal	0	18	0	0	0	64	0	18	0
2	2AT1-2	405345	4251884	Spal	0	0	0	0	5	75	0	0	20
38	2BT4-1	406328	4251463	Spal	0	8	12	0	0	80	0	0	0
90	2CT10-3	405970	4252389	Spal	0	8	12	0	16	64	0	0	0
97	2DT4-6	405290	4251753	Spal	0	0	0	0	10	55	0	15	20
121	3AT1-1	405141	4249064	Spal	0	0	20	0	0	80	0	0	0
229	3DT6-3	405877	4249791	Spal	0	0	20	0	0	80	0	0	0
52	2BT8-2	406715	4251688	Spal	0	0	21	0	17	62	0	0	0
45	2BT6-2	406553	4251594	Spal	0	0	22	0	15	63	0	0	0
149	3AT11-1	405906	4249221	Spal	0	0	22	0	0	78	0	0	0
151	3BT1-1	406016	4249731	Spal	0	0	22	0	0	73	0	5	0

Original REC NUM	Plot ID	UTM		Dominant Species	Percent Cover by Species and Non-Veg								
		Eastings	Northing		Disp	Lit	Mud	Plpu	Scol	Spal	Spcy	Sppa	Watr
158	3BT3-2	406130	4249803	Spal	0	0	23	0	12	65	0	0	0
223	3DT4-3	405784	4249754	Spal	0	8	15	0	0	77	0	0	0
68	2CT3-2	406592	4252231	Spal	0	0	24	0	17	59	0	0	0
182	3CT1-2	406114	4250055	Spal	0	0	24	0	3	73	0	0	0
96	2DT4-5	405282	4251621	Spal	0	0	0	0	0	75	0	0	25
108	2DT6-2	405437	4251394	Spal	0	0	0	0	5	60	0	10	25
127	3AT3-1	394074	4253427	Spal	0	0	25	0	0	60	0	15	0
134	3AT5-3	405441	4249165	Spal	0	0	25	0	0	75	0	0	0
62	2CT1-2	406751	4252173	Spal	0	0	27	0	15	56	0	2	0
78	2CT6-3	406289	4252124	Spal	0	0	27	0	22	51	0	0	0
54	2BT8-4	406715	4251913	Spal	3	0	28	0	0	69	0	0	0
146	3AT10-1	405823	4249209	Spal	0	0	28	0	0	72	0	0	0
157	3BT3-1	406135	4249758	Spal	0	0	28	0	7	65	0	0	0
110	2DT6-4	405432	4251645	Spal	0	0	0	0	10	60	0	0	30
63	2CT1-3	406745	4252075	Spal	0	10	21	3	4	62	0	0	0
148	3AT10-3	405823	4249312	Spal	0	0	32	0	13	55	0	0	0
179	3BT10-2	406622	4249683	Spal	0	0	32	0	0	68	0	0	0
201	3CT7-3	406484	4250075	Spal	0	0	32	0	3	65	0	0	0
74	2CT5-2	406376	4252323	Spal	0	21	12	0	14	53	0	0	0
91	2DT3-1	405216	4251624	Spal	0	0	0	0	2	65	0	0	33
155	3BT2-2	406064	4249795	Spal	2	0	33	0	3	62	0	0	0
228	3DT5-4	405806	4249812	Spal	8	0	34	0	4	54	0	0	0
69	2CT3-3	406601	4252038	Spal	0	5	31	0	3	61	0	0	0
150	3AT11-2	405907	4249269	Spal	0	0	38	0	0	62	0	0	0
191	3CT4-2	406306	4250130	Spal	0	0	38	0	2	60	0	0	0
231	3DT6-1	405876	4249626	Spal	0	0	38	0	0	62	0	0	0
88	2CT10-1	405968	4252489	Spal	0	25	15	0	8	52	0	0	0
120	2DT10-2	405684	4251741	Spal	0	0	0	0	0	60	0	0	40
193	3CT5-1	406352	4250189	Spal	0	28	12	0	6	54	0	0	0
212	3DT1-2	405502	4249937	Spal	0	0	40	0	5	55	0	0	0
222	3DT4-2	405771	4249650	Spal	0	0	40	0	0	60	0	0	0
198	3CT6-3	406460	4250067	Spal	0	15	28	0	0	57	0	0	0
165	3BT5-3	406280	4249835	Spal	0	0	48	0	0	52	0	0	0
107	2DT6-1	405428	4251355	Sppa	0	0	0	0	0	25	0	75	0
192	3CT4-3	406301	4249927	Sppa	0	0	0	0	0	32	0	68	0
195	3CT5-3	406338	4250058	Sppa	0	0	0	0	0	12	0	88	0
177	3BT9-3	406532	4249871	Sppa	23	0	5	0	0	8	0	64	0
181	3CT1-1	406120	4250082	Sppa	0	5	0	0	7	1	0	87	0
237	3DT8-3	406030	4249584	Sppa	0	0	8	0	0	30	3	59	0
6	2AT3-1	405508	4252231	Sppa	15	0	0	0	10	0	0	65	10
13	2AT5-1	405645	4252206	Sppa	15	0	0	0	25	0	0	50	10
100	2DT5-3	405344	4251328	Sppa	0	0	0	0	10	15	0	65	10
101	2DT5-4	405331	4251398	Sppa	0	0	0	0	3	15	0	72	10

Original REC NUM	Plot ID	UTM		Dominant Species	Percent Cover by Species and Non-Veg								
		Easting	Northing		Disp	Lit	Mud	Plpu	Scol	Spal	Spcy	Sppa	Watr
207	3CT9-3	406581	4250041	Sppa	0	10	0	0	0	18	0	72	0
83	2CT8-1	406141	4252472	Sppa	0	0	12	0	28	0	3	57	0
14	2AT5-2	405642	4252141	Sppa	10	0	0	0	25	0	0	50	15
43	2BT5-3	406460	4251780	Sppa	0	0	15	0	12	18	0	55	0
94	2DT4-3	405287	4251242	Sppa	0	0	15	0	10	25	0	50	0
140	3AT8-1	405667	4249193	Sppa	0	0	15	0	0	25	0	60	0
137	3AT7-1	405591	4249190	Sppa	0	0	18	0	0	28	0	54	0
167	3BT6-2	406340	4249766	Sppa	0	0	18	0	0	8	0	74	0
219	3DT3-3	405668	4249827	Sppa	0	19	0	0	0	23	4	54	0
102	2DT5-5	405353	4251435	Sppa	0	0	20	0	0	25	0	55	0
123	3AT1-3	405144	4249185	Sppa	0	0	20	0	0	15	0	65	0
238	3DT9-1	406099	4249445	Sppa	0	20	0	0	0	20	0	60	0
171	3BT7-1	406397	4249704	Sppa	0	12	10	0	0	22	0	56	0
184	3CT2-1	406188	4250099	Sppa	0	0	22	0	0	18	0	60	0
190	3CT4-1	406307	4250163	Sppa	5	0	22	0	3	0	0	70	0
162	3BT4-3	406189	4249842	Sppa	1	0	23	0	0	18	0	58	0
93	2DT4-2	405283	4251198	Sppa	0	0	25	0	0	0	0	75	0
105	2DT5-8	405355	4251658	Sppa	0	0	0	0	0	10	0	65	25
175	3BT9-1	406526	4249675	Sppa	0	25	0	0	0	7	0	68	0
76	2CT6-1	406289	4252416	Sppa	0	27	0	0	15	5	0	53	0
85	2CT8-3	406142	4251928	Sppa	0	10	17	0	0	12	0	61	0
187	3CT3-1	406244	4250123	Sppa	0	0	27	0	0	1	0	72	0
161	3BT4-2	406191	4249765	Sppa	0	0	0	0	0	22	0	50	28
47	2BT7-1	406644	4251575	Sppa	0	0	29	0	10	5	0	56	0
53	2BT8-3	406717	4251830	Sppa	0	18	16	0	12	0	0	54	0
23	2AT7-1	405781	4252160	Sppa	5	0	0	0	10	0	0	50	35

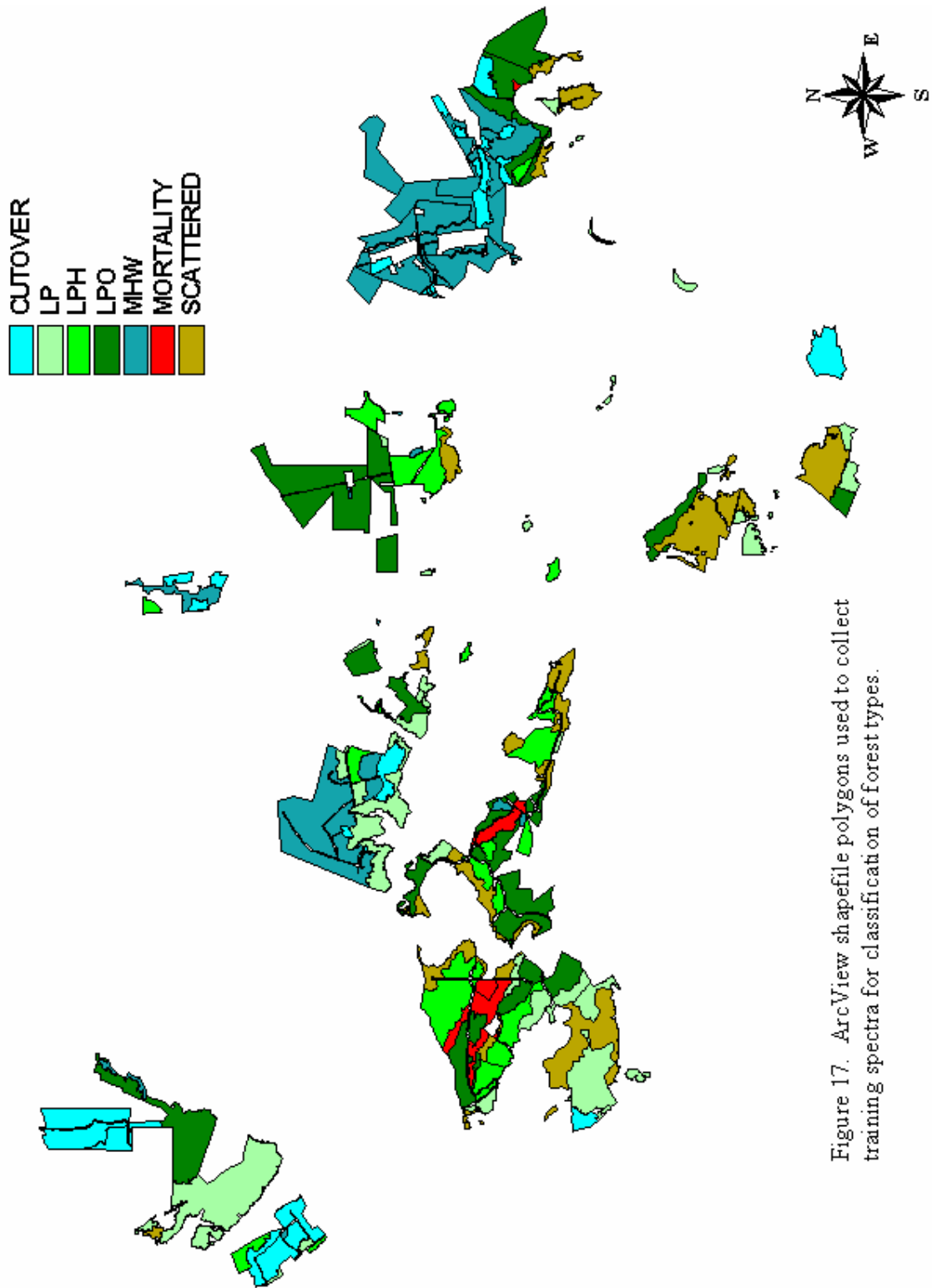


Figure 17. ArcView shapefile polygons used to collect training spectra for classification of forest types.

3.4.1 30 June Mosaic

ROI's were delineated within the northern mosaic over the vegetation sample sites visited during the fall of 2001. The signatures (i.e., spectral curves) for these sites were stored as a spectral library to be used for supervised classification. Supplementary training sites were identified using the forest type map and using supplemental on-site observations collected in February 2002.

3.4.2 7 June Mosaic

Similarly, a spectral library was constructed for the southern mosaic using the georeferenced field data sets, including the 1 m² quadrats and the forest type map. A few additional sites were identified in February 2002.

3.5 Image Subsetting

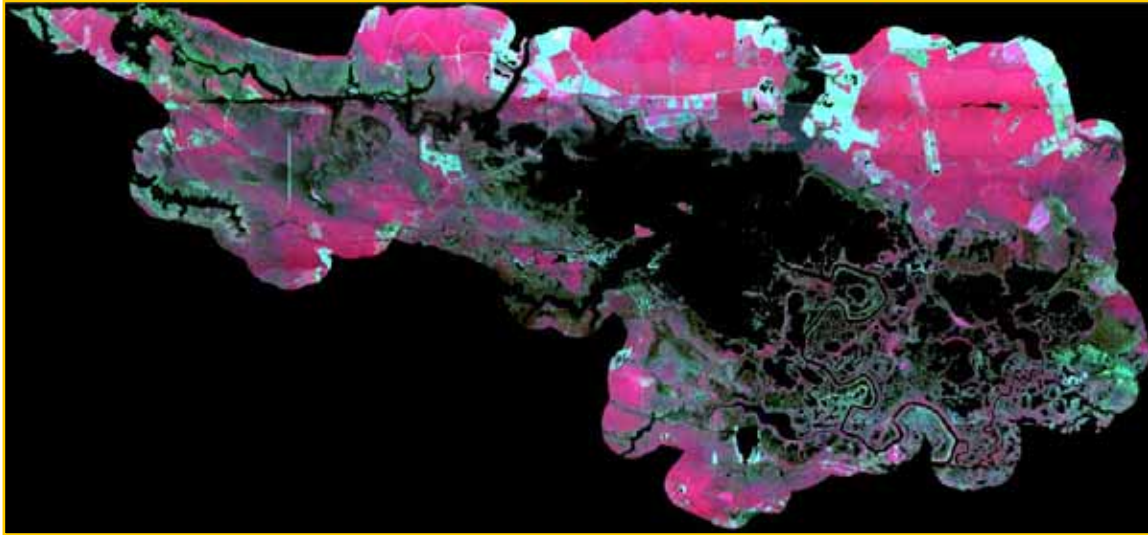
During several preliminary image classifications and signature analyses, performed on sets of adjacent flightlines as the larger mosaics were constructed, a number of land cover classes were identified as potentially problematic. Specifically, the agricultural fields within and adjacent to the Refuge maintain spectral properties very similar to several of the marsh vegetation associations of interest. Attempts to assign unique signatures to the croplands, particularly in the larger southern mosaic, proved unsuccessful. Attempts to mask (i.e., turn off) the agricultural pixels resulted in the loss of a significant number of marsh vegetation pixels. Therefore, the Refuge boundary, plus a 500 meter buffer zone, was used to subset (or clip) the full southern mosaic (Figure 18). This step removed the majority of the agricultural lands. The northern mosaic was not clipped, with the entire set of six flightlines classified into vegetation classes including 5 agricultural classes.

3.6 Signature Separability Analyses

Before applying the newly created spectral signatures as training data to the 14-band images, the signatures were evaluated for separability. Signature separability is a standard tool in commercial image processing software packages. A variety of algorithms are generally available. ENVI offers two: Jeffries-Matusita and Transformed Divergence. Both use the n-dimensional mean vectors and covariance matrices of the training statistics to measure the magnitude of the difference, or separability, of the mean vectors. The Transformed Divergence statistics were used for these data. The algorithm calculates a separability statistic for all pair-wise combinations of signatures.

Tables 7 and 8 list the names and descriptions of the final signatures used for classification for the southern (7 June) and the northern (30 June) mosaics, respectively. A meticulous and iterative evaluation of the class statistics generated for each individual training site identified these mean signatures as the most representative of the spectral properties within the northern and southern mosaics. During this evaluation the separability analysis was repeated many times. The output of each iteration identified the

a



b

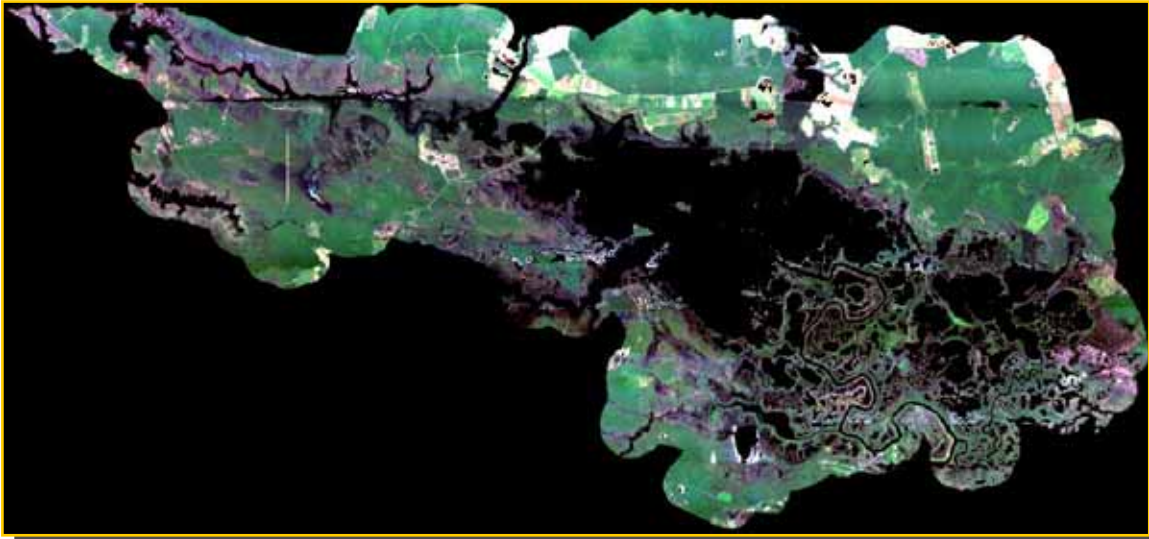


Figure 18. Southern Mosaic – flightlines BLINE7E through BLINE20E. (a) false color composite, and (b) true false color composite.

Table 7. Description of training classes for southern mosaic.

CLASS NAME	DESCRIPTION
J1	Juncus – low density
J2	Juncus – high density
J3	Juncus/Panicum mix
Scol1	Scirpus – medium density, water
Scol2	Scirpus – medium density, mud, litter
Scol3	Scirpus – medium density, mixed, mud, litter
Scol4	Scirpus – low density, mud
Spal1	<i>S. alterniflora</i> – variable density, mixed, mud, litter
Spal2	<i>S. alterniflora</i> – high to medium density, water, mud, litter
Spal3	<i>S. alterniflora</i> – high density, water
Sppa3	<i>S. patens</i> – medium density, mixed, litter
Sppa5	<i>S. patens</i> – medium density, mixed, mud, litter
Sppa2	<i>S. patens</i> – medium density, mixed
Sppa4	<i>S. patens</i> – low density, water
Sppa6	<i>S. patens</i> – high density, mixed
Sppa1	<i>S. patens</i> – medium density, mixed, mud
Sppa7	<i>S. patens</i> – medium density, mud
P/Sppa	Pine with <i>S. patens</i> beneath
Sppa8	<i>S. patens</i> – medium, density mixed
PY	Pine young
Cattail	<i>Typha</i> spp. mixed
Sppa/Scol	<i>S. patens</i> /Scirpus mix
Phrag/Scol	Phragmites mixed with Scirpus
Sppa9	<i>S. patens</i> – medium density, mixed
Sppa/Shrubs	<i>S. patens</i> with shrubs
Phrag/Shrubs	Phragmites with shrubs
P/Phrag-Shrubs	Pine with understory of Phragmites and shrubs
P/Shrubs	Pine with shrubs
Mort	Morbid and declining forests
MHW-high	Mixed hardwood forests, high density
MHW-low	Mixed hardwood forests, low density
P	Pine
PH2	Pine hardwood mix
PH1	Pine hardwood mix
PH4	Pine hardwood mix
PH3	Pine hardwood mix
Cut	Cutover forest

Table 8. Description of training classes for northern mosaic.

Class Name	Description
Pine Mixed	Coniferous dominated mixed forest
Hardwood	Deciduous dominated forest
Juncus/Scirpus1	Juncus / 3-square dominated marsh
Patens/Distichlis1	Dense cover marsh grasses – Patens / Distichlis
Patens/Scirpus	Less dense, more open grasses –Patens / 3-square
Juncus/Scirpus2	Lower density Juncus / 3-square in standing water
Water1	Water, canals, ponds and pools
Roads/Dark Soils	Roads and some dark soils
Cutover	Cut-over areas – light vegetation and exposed soil
Water2	Water in creeks
Shrubs/Grasses	High density light- green grasses and shrubs
Pine	Coniferous forest (Pinus)
Patens/Distichlis2	Medium density marsh grass – Patens / Distichlis
Ag1	Ag fields1 – fallow –damp- no green veg - stubble
Ag2	Ag fields2 – fallow – light veg cover
Ag3	Ag fields3 – fallow – dry surface – light veg
Ag4	Ag fields4 – medium density cover – veg 1
Ag5	Ag fields5 – medium density cover – veg 2
Ag6	Ag fields6 – dense cover – mature green crop

statistically indistinct training sites. Non-separable classes were either dropped from the data set if they were determined to be outliers, or merged with other training sites. The results of the last transformed divergence tests suggested that all of the pair-wise comparisons were at least moderately separable. However, because this analysis was based on an extremely small sample size (i.e., total number of pixels in each training class relative to the total number of pixels in the mosaics), it was expected that an inspection of the final class map would reveal some overlap between relative similar vegetation classes. Figures 19a and 19b display the spectral curves of the 37 class signatures used for the southern mosaic. Note the overlap of many of the signatures, particularly in the marsh grass communities.

3.6 Image Classification

3.6.1 Spectral Angle Mapper

The images were classified using the Spectral Angle Mapper (SAM) routine within ENVI. This function assigns each individual pixel to a class based on the calculated angle, measured as the arc distance, between that pixel's DN values (using all 14-bands) and each of the mean vectors of the training signatures. The maximum spectral angle is user-defined within the routine and is given in units of radians, not degrees. For the first run of the SAM algorithm in the southern mosaic, a spectral angle of 0.08 radians (~ 4.58 degrees) was chosen. The 14-row, 1-column vector for the first pixel in the image (i.e., the unknown spectrum) and the 14-row, 1-column mean vector for a single reference spectrum are used as inputs into the following equation.

$$\alpha = \cos^{-1} \left\{ \frac{\sum_{i=1}^{nb} t_i r_i}{\left(\sum_{i=1}^{nb} t_i^2 \right)^{1/2} \left(\sum_{i=1}^{nb} r_i^2 \right)^{1/2}} \right\}$$

where: α = spectral angle
 t_i = spectral vector of unclassified pixel
 r_i = mean spectral vector of training (reference) signature
 nb = number of bands

The spectral angle is then calculated 37 times for each image pixel (t_i) since there are 37 r_i reference signatures or classes. The pixel is then assigned to the class where the spectral angle is the smallest. If all 37 angular estimates are greater than the maximum specified angle (i.e., 0.08 radians or 4.58 degrees), the pixel is assigned to an "unclassified" group.

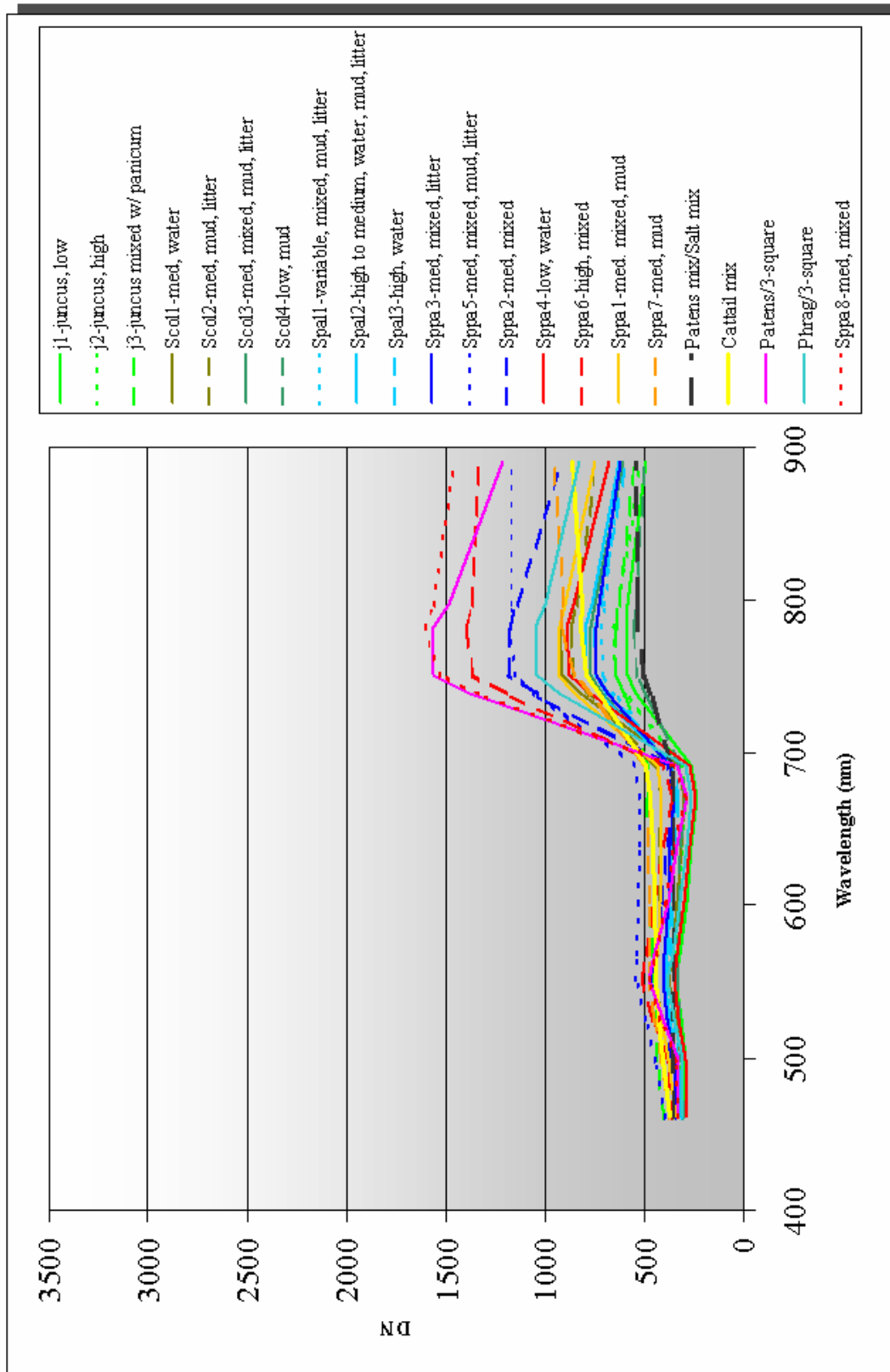


Figure 19a. Spectral plots of low reflectance signatures used to classify the southern mosaic.

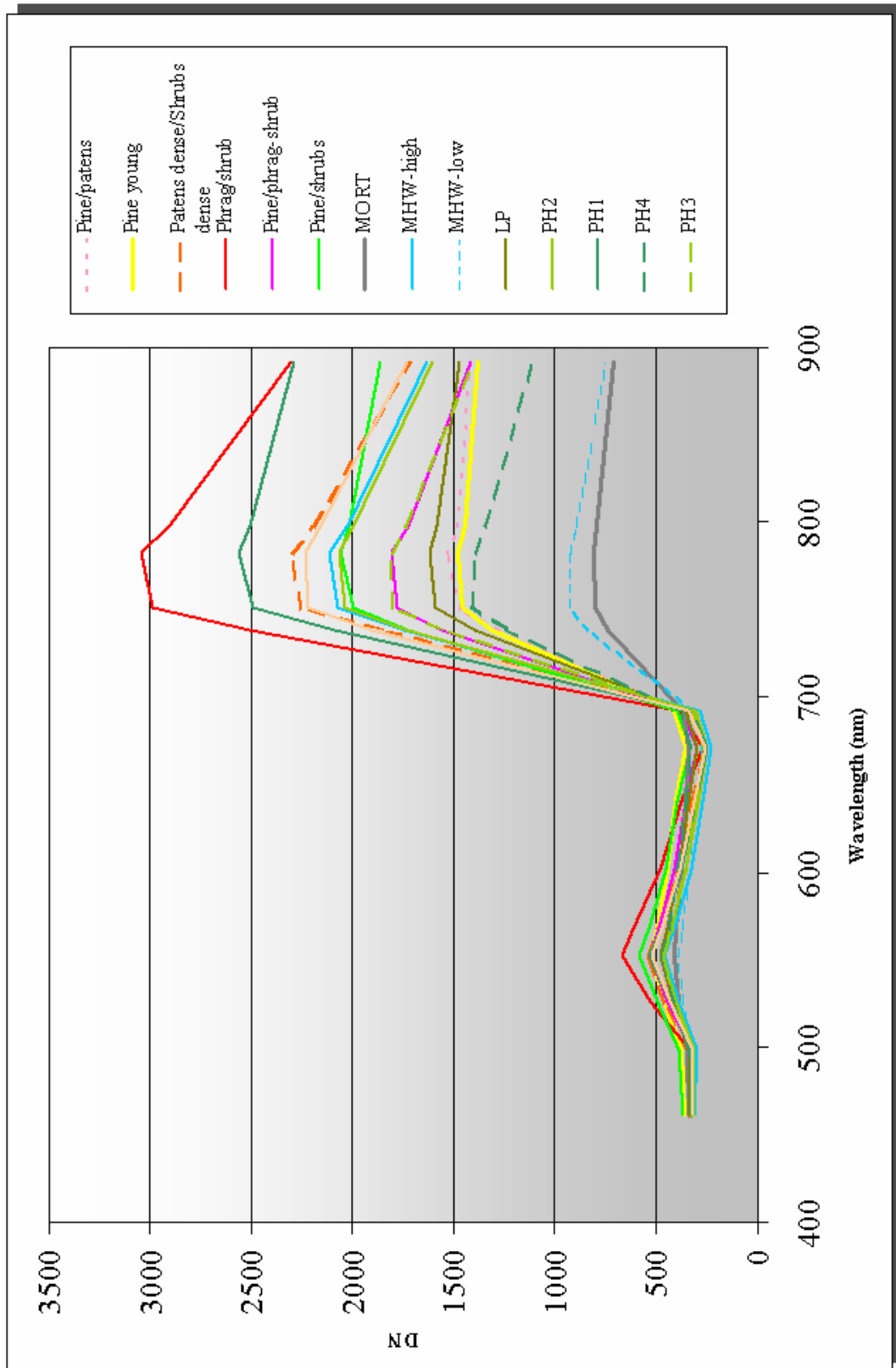


Figure 19b. Spectral plots of high reflectance signatures used to classify the southern mosaic.

The results of the initial classification using the SAM algorithm showed some confusion among the vegetation classes. Also, some pixels (approximately 10% in both mosaics) were not classified. Additional SAM runs using larger spectral angles (0.09 – 0.12) successfully increased the number of pixels that were classified. However, the confusion among classes was also increased. Therefore, the results from the 0.08 spectral angle were retained for the final class maps.

3.6.2 *Maximum-Likelihood Classifier*

A maximum-likelihood classifier was then applied to the unclassified image pixels. This algorithm uses the class-conditional probability density functions to calculate the likelihood that a given pixel, with its unique spectral vector (i.e., variable t_i from the SAM equation), belongs to each of the reference classes (i.e., variable r_j). Every pixel is then assigned to the class with the maximum probability of membership. This classification technique is used extensively with both multispectral and hyperspectral imagery.

4.0 RESULTS

The results of the SAM classification and the maximum likelihood classification were combined to create the complete vegetation class maps. An evaluation of the 37 classes associated with the southern mosaic indicated significant confusion within and between the vegetation types, particularly within the marsh communities. Therefore, a number of classes were combined, based on the spectral and spatial characteristics of the class signatures in the completed thematic map. A simple GIS operation was used to recode (or renumber) classes that were spectrally similar. The resulting vegetation map depicted 26 vegetation classes. The northern mosaic maintained 19 vegetation classes.

4.1 **Minimum Mapping Unit Filter**

A minimum mapping unit (mmu) filtering routine was also applied to the full thematic resolution class maps. This filtering algorithm first delineates all of the raster polygons throughout the thematic image. A raster polygon is defined as a group of adjacent (i.e., connected) pixels with the same thematic class value. The adjacency criterion defines the polygon using pixels joined along the four flat edges of the square and those pixels joined only at the corners. For example, the full resolution class map for the southern mosaic had 1,541,906 raster polygons ranging in size from a single pixel to over 100,000 pixels. Both accuracy assessment and vector conversion of the thematic map is greatly hampered by so many polygons. The second step is to define a mmu. For this project, a minimum mapping unit of 25 pixels (225 m²) was selected. At nine m² per pixel, 25 pixels cover only 0.0225 hectares (0.0556 acres). The next step is to delete all raster polygons that are less than 25 pixels. This operation is synonymous with applying a polygon sieve to the thematic image, where all raster polygons below the mmu threshold size are “dropped.” The final step in the technique is to iteratively apply a majority filter to the sieved image. This majority filter, usually a 3x3 pixel matrix, uses a neighborhood operation to reassign sieved pixels to a larger polygon. As the center pixel passes over each dropped pixel, the

class values for the eight surrounding pixels in the matrix are tallied. The center pixel is then assigned the same class value as the majority of the pixels in the matrix. The filter then moves to the next sieved pixel and repeats the operation. The filter is passed over the image many times until all pixels within the deleted polygons are reassigned a new class value. The operation ignores any background pixels that were already present in the full resolution thematic map.

The threshold of 25 pixels was assumed to be adequate for retaining the majority of the thematic information throughout the study site, while removing a significant amount of thematic speckle (or noise) and reducing the number of raster polygons to 32,710. Figure 20 shows the 30 June (southern mosaic) class map after application of the minimum mapping unit filter. Figure 21 shows the 7 June (northern mosaic) class map after filtering and subsetting with a 500-meter buffer around the Refuge boundary. Table 9 lists the area cover by each of the vegetation classes in southern mosaic. Table 10 lists the coverage for each vegetation class in the northern mosaic.

4.2 Accuracy Assessment

Quantitative thematic accuracy assessment is critical in determining the quality of the vegetation classification. Typically, independent field data is used to calculate thematic accuracy. Due to budgetary and time constraints associated with this effort, no ancillary field points were available. Instead, thematic accuracy was determined using the training data field sites. Use of the training sites in this manner is commonly performed only as a preliminary step in assessing classification accuracy.

The training sites used for classification were initially associated with very detailed vegetative parameters, including species composition, species density and background material. However, because of the relative lack of geometric accuracy in locating the one m² quadrats on the imagery combined with the marginal spectral separability of all of the class spectra, the final southern mosaic class map was recoded to only nine vegetation classes. These classes are: *Juncus*, *Scirpus*, *S. alterniflora*, *S. patens*, *Typha* spp., *Phragmites*, Mixed Pine/Hardwood Forest, Pine, and Declining Forest. The northern mosaic was recoded to 10 classes, including: Pine Forest, Hardwood Forest, Mixed Forest, Shrubs, *Patens* Marsh, *Juncus* Marsh, Cutover, Roads/Soils, Water, and Agriculture. The geo-registered training sites for each of the mosaics were similarly aggregated to the same classes.

Image processing software generally offers accuracy assessment routines. In this case, ERDAS Imagine was used to overlay a single point, generally the center pixel of the training area, onto the renamed class maps. The thematic class from the image was then compared to the true class for that point. For both class maps the overall thematic

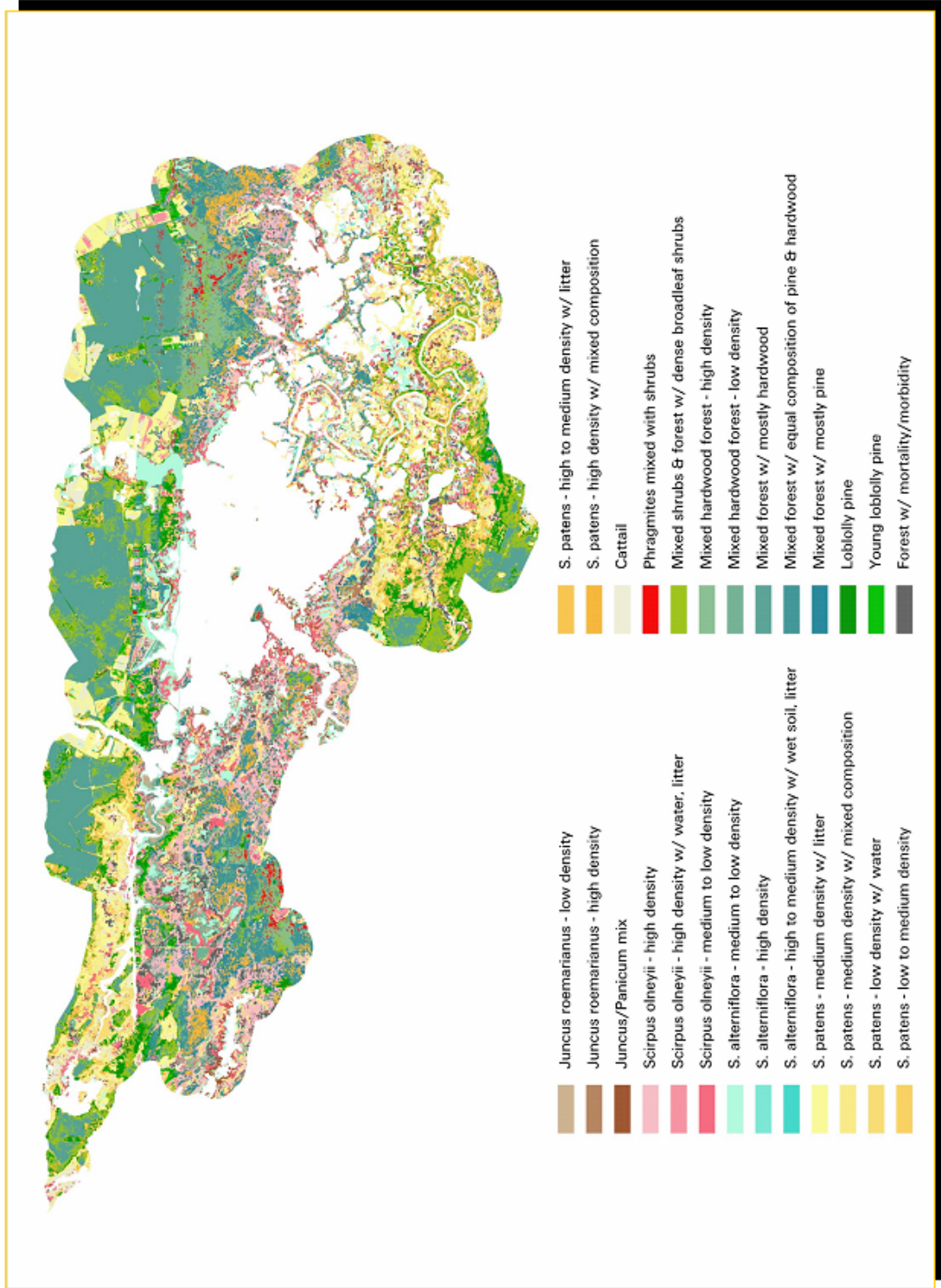


Figure 20. Final vegetation class map for southern mosaic (7 June 2000).



Figure 21. Final vegetation class map for northern mosaic (30 June 2000).

Table 9. Class names and areas of final 26 classes in southern mosaic.

Vegetation Class	Area (ha)	% of Total
Juncus roemarianus - low density	73.1	0.7
Juncus roemarianus - high density	105.7	1.0
Juncus/Panicum mix	167.0	1.6
Scirpus olneyii - high density	887.0	8.2
Scirpus olneyii - high density w/ water, litter	119.7	1.1
Scirpus olneyii - medium to low density	489.7	4.5
S. alterniflora - medium to low density	633.9	5.9
S. alterniflora - high density	21.8	0.2
S. alterniflora - high to medium density w/ wet soil, litter	0.7	0.0
S. patens - medium density w/ litter	1187.3	11.0
S. patens - medium density w/ mixed composition	338.5	3.1
S. patens - low density w/ water	209.2	1.9
S. patens - low to medium density	12.4	0.1
S. patens - high to medium density w/ litter	644.8	6.0
S. patens - high density w/ mixed composition	418.8	3.9
Typhus spp.	246.2	2.3
Phragmites mixed with shrubs	62.6	0.6
Mixed shrubs & forest w/ dense broadleaf shrubs	809.0	7.5
Mixed hardwood forest - high density	375.1	3.5
Mixed hardwood forest - low density	250.2	2.3
Mixed forest w/ mostly hardwood	1635.2	15.2
Mixed forest w/ equal composition of pine & hardwood	695.9	6.5
Mixed forest w/ mostly pine	376.1	3.5
Loblolly pine	500.6	4.7
Young loblolly pine	134.0	1.2
Forest w/ mortality/morbidity	368.7	3.4

Table 10. Class names and areas of final 19 classes in northern mosaic.

Vegetation Class	Area (ha)	% of Total
Coniferous dominated mixed forest	381.9	15.9
Deciduous dominated forest	327.5	13.7
Juncus / 3-square dominated marsh	56.4	2.4
Dense cover marsh grasses – Patens / Distichlis	202.7	8.5
Less dense, more open grasses –Patens / 3-square	101.4	4.2
Lower density Juncus / 3-square in standing water	30.7	1.3
Water, canals, ponds and pools	2.5	0.1
Roads and some dark soils	4.0	0.2
Cut-over areas – light vegetation and exposed soil	18.3	0.8
Water in creeks	9.3	0.4
High density light- green grasses and shrubs	210.8	8.8
Coniferous forest (Pinus)	733.4	30.6
Medium density marsh grass – Patens / Distichlis	137.3	5.7
Ag fields1 – fallow –damp- no green veg - stubble	37.2	1.6
Ag fields2 – fallow – light veg cover	97.5	4.1
Ag fields3 – fallow – dry surface – light veg	34.2	1.4
Ag fields4 – medium density cover – veg 1	3.8	0.2
Ag fields5 – medium density cover – veg 2	0.4	0.0
Ag fields6 – dense cover – mature green crop	5.6	0.2

accuracy was approximately 60%. This relatively low overall accuracy suggests only a marginally useful vegetation classification.

5.0 CONCLUSIONS

The objective of this image processing research effort was to create an accurate thematic map depicting detailed vegetation classes throughout the Blackwater Wildlife Refuge. A preliminary evaluation of the AISA hyperspectral imagery suggested that association level classification would be feasible, considering the high spatial resolution (3 meters) and the excellent geo-registration of the 20 flightlines needed to cover the Refuge. However, as the individual flightlines were assembled to form a complete mosaic, serious radiometric problems were discovered. Much of the research effort was spent trying to remove a significant cross-track illumination anomaly and attempting to match, or balance, the histograms of adjacent, overlapping flightlines to remove the visible seams. The final mosaic was of acceptable quality for image classification, but retained some radiometric distortions, including several significant seams and a number of holidays (i.e., holes in the mosaic).

The iterative spectral analyses employed to generate training signatures for classification showed that stands of wetland plants, especially different reeds, rushes, and vertical habit grasses were spectrally inseparable. This observation is not unexpected. Past research where spectral signatures of vegetation were collected using ground-based spectroradiometers, under natural illumination, concluded that reflectance properties of unique vegetation types are not dependent on species, but rather on the plant phenology and the types of background materials. Within the AISA imagery, a variety of factors influence the spectral characteristics of the selected ROI's, including: above-ground biomass, plant distribution within the sensor field of view, crown and foliar structure, within-/between-plant shadowing, and the background soil properties. With such a wide range of interacting physical parameters, many ROI signatures were not separable within one standard deviation of their means. For example, deciduous tree crowns were spectrally similar to dense grass cover or dense broad-leafed crops, and dead/dying forests were spectrally confused with wetland grasses or reeds that support necrotic stems and leaves. This inseparability produced a vegetation classification with a relatively low overall accuracy.

The high spatial resolution acquired by the AISA sensor for this project would suggest the potential for classifying the wetland vegetation classes with a greater level of detail and accuracy. The marginal quality of the final map suggests that smaller pixels do not necessarily result in a better classification. The highly variable spectral response of adjacent pixels within the homogenous marsh grass communities illustrates this dilemma found in all high spatial resolution digital imagery. Homogeneity with respect to species composition may not mean homogeneity with respect to biomass distribution and foliar density. For example, *S. patens* can exist as uniform mats composed of both live and dead stems, as well as widely spaced clumps. Both densities of *S. patens* would be classified as salt meadow hay from ground surveys. However, the spectral response of a pixel within

the high-density *S. patens* is significantly different from a pixel within the low-density *S. patens*. The spectral mixture of the low-density *S. patens* is easily confused with low-density stands of the other marsh grass species.

The best solution to classify spectrally similar species is to collect large numbers of ground truth plots, stratified primarily by composition and density. Additional variables needed for stratification to ensure a representative sample may include background materials namely soils and water quality (i.e., clarity). From a practical standpoint, a comprehensive vegetation inventory over a small study area, perhaps no greater than few hundred acres, could supply the stratified sample needed for a quality image classification. However, for an area as large as the Refuge, such a sample is relatively impractical to provide enough useful ground truth data for a useable thematic map from high-resolution imagery. A more practical approach may be to divide the Refuge into a set of smaller areas, or tiles, concentrating ground truth data collection within project specific management or study sites.

6.0 RECOMMENDATIONS

The implementation of high resolution airborne digital remotely sensed imagery, both multispectral and hyperspectral, is advancing with the enhancements to both the sensor systems and the computer hardware/software needed for data processing. The obstacles encountered in this applied research effort significantly affected the final product, in terms of both the accuracy of the thematic map and the time required to complete the project. As these technologies improve it will be important for Corps personnel to understand the basic principles of how the imagery are collected, how the imagery are post-processed, and how the final map product is created. An example Performance Based Statement of Work is provided in Appendix A as a guide to developing a sound aerial mapping contract.

The costs associated with this project started with a reasonable sum for image acquisition. The vendor, 3Di, LLC captured and post-processed over 9 gigabytes of hyperspectral images, covering ~ 30,000 acres of Refuge property, for only \$20,000. However, as described above, a significant amount of additional post-processing was required to create a marginally useful mosaic. The total additional cost for developing this mosaic and producing the final class map was in excess of \$100,000. The contractor should be responsible for these tasks and should be able to provide a detailed, and understandable, description of all acquisition and post-processing techniques and algorithms as part of the required metadata documentation.

A comprehensive set of ground truth sample sites would likely have cost another \$25,000 to \$50,000. When compared with traditional aerial photography, the digital imagery is initially cheaper to acquire and process. Furthermore, the digital imagery will likely have a much quicker delivery timeframe as compared to analogue photography. However, the questionable accuracy of the thematic map suggests that for projects where very detailed vegetation classification is required (i.e., species alliances or associations), large scale

true-color or false-color photography, combined with intensive field data collection, may be the most cost effective alternative. Digital aerial mapping camera technologies are also maturing rapidly and may represent an alternative to hardcopy photography. While not specifically designed or suited for computer-aided classification, very high-resolution digital photos can provide an excellent source of interpretable images with very good geometry (i.e., spatial accuracy) and with a very rapid turn-around time.

Future attempts to develop a useable base map for an area as large as the Blackwater Wildlife Refuge should employ either medium or high-resolution multispectral satellite imagery. Medium resolution sensors include the latest SPOT and Landsat systems. These sensors provide 10- to 30-meter pixels, respectively. SPOT and Landsat also provide 5- and 15-meter panchromatic (i.e., black & white) imagery, respectively. The process of combining the higher resolution panchromatic pixels with the larger multispectral pixels is called pan-sharpening. The result is a multispectral image with the higher (i.e., small pixel size) panchromatic spatial resolution. Costs for pan-sharpened medium resolution imagery covering the Refuge will be in the \$10,000 to \$20,000 range. This price includes radiometric post-processing to remove internal sensor distortions and anomalies, and geometric registration equivalent to national map accuracy standards for 1:24000 USGS topographic quadrangles. These satellite data sources should provide an adequate source to delineate vegetation to the subgroup or formation level as defined by the National Vegetation Classification Standard.

Current high-resolution satellite sensors are IKONOS and QuickBird. IKONOS acquires four-meter multispectral pixels and one-meter panchromatic pixels. QuickBird collects 2.8-meter multispectral pixels and 0.7-meter panchromatic pixels. Both sources maintain price ranges from \$30,000 to \$40,000 to cover an area as large as the Refuge. As with the medium resolution image, these high-resolution sources are provided with radiometric and geometric post-processing already completed.

Detailed information concerning the acquisition of both archival (i.e., existing) and new remotely sensed imagery is available from:

Alana Hubbard
US Army Topographic Engineering Center
ATTN: CEERD-TO-I
7701 Telegraph Road
Bldg. 2592
Alexandria, Virginia 22315
Phone: 703-428-6717 ext. 2485
Email: Alana.J.Hubbard@erdc.usace.army.mil

7.0 DATA

The data created by this project includes hyperspectral images, multispectral images (i.e., spectral subsets of the hyperspectral data), raster vegetation class maps, and vector vegetation class maps. Specific file names and descriptions are presented below. All

images are delivered in the ERDAS *Imagine* format, which includes the *.img file containing the image data and the accompanying *.rrd file holding the pyramid file format for faster viewing. The *.e00 files are Arc Interchange coverages. Two *.csv files list the class names for each thematic vegetation map; these files are formatted for import into an ArcMap relate file.

1thru5_14band.img – Hyperspectral mosaic of flightlines 1 through 5 (north mosaic); see page 29 for the description of the 14 bands.

1thru5_4band.img – Multispectral mosaic of flightlines 1 through 5; bands are labeled as: 1 = AISA band 1 (461 nm -> blue), 2 = AISA band 12 (522 nm -> green), 3 = AISA band 22 (671 nm -> red), and 4 = AISA band 32 (798 nm -> near infrared).

1thru6_14band.img - Hyperspectral mosaic of flightlines 1 through 6 (north mosaic).

1thru6_4band.img - Multispectral mosaic of flightlines 1 through 5; same band configuration as 1thru5-4band.img (above).

1thru6_Vegclasses.img – Raster thematic map with 19 vegetation classes for the north mosaic (minimum mapping unit = 25 pixels).

North_veg.e00 – Arc Interchange vector file of north mosaic.

North_names.csv – Comma delimited ascii file with class number (from raster and vector vegetation maps) and class names north mosaic.

7thru20_14band_east.img – Hyperspectral image of the eastern half of the mosaic of flightlines 7 through 20 (south mosaic).

7thru20_14band_west.img – Hyperspectral image of the western half of the mosaic of flightlines 7 through 20 (south mosaic).

7thru20_4band.img - Multispectral mosaic of flightlines 7 through 20.

7thru20_14band_buffer_east.img – Hyperspectral image of the eastern half of the buffered mosaic of flightlines 7 through 20 (south mosaic).

7thru20_14band_buffer_west.img – Hyperspectral image of the western half of the buffered mosaic of flightlines 7 through 20 (south mosaic).

7thru20_4band_buffer.img - Multispectral image of the buffered mosaic of flightlines 7 through 20.

7thru20_Vegclasses.img - Raster thematic map with 26 vegetation classes for the south mosaic (minimum mapping unit = 25 pixels).

South_veg.e00 – Arc Interchange vector file of south mosaic.

South_names.csv – Comma delimited ascii file with class number (from raster and vector vegetation maps) and class names for south mosaic.

Due to the overall volume of the images and vector products, the data are not provided with this document. The complete set of digital images can be obtained from:

Michael V. Campbell
US Army Topographic Engineering Center
7701 Telegraph Road, Bldg. 2592
Alexandria, Virginia 22315
Phone: 703-428-6538 ext. 2204
Fax: 703-428-6425
Email: Michael.V.Campbell@erdc.usace.army.mil

OVERALL CONCLUSIONS AND RECCOMENDATIONS

Each of the four study sites demonstrated the potential utilization of high spatial resolution digital remotely sensed imagery for a specific application. Successes and shortcomings were presented for each application. The following broad recommendations provide guidance in the effective and efficient application of high-resolution imagery.

- The total size of the project site(s), measured as the total study area (acres or hectares), will be one of the primary factors in determining the type of high-resolution imagery to acquire. For areas less than 50 km², airborne imagery may provide the most cost effective image source. For areas of interest approaching 100 km², high-resolution satellite data will be the cheapest solution.
- When contracting the acquisition of airborne digital imagery, either multispectral or hyperspectral, ensure that the contractor provides accurate and comprehensive metadata describing the precise acquisition parameters, as well as the tools and techniques used to radiometrically and geometrically post-process the images. Generally, expect higher image post-processing costs for hyperspectral imagery versus multispectral imagery. If the contractor is to develop a map product, require an exhaustive report that documents all ground truth data collection procedures and image processing routines, including a statistically valid accuracy assessment.
- Ensure that an adequate volume of reliable ground truth data is collected and analyzed to meet the objective(s) of the mapping component of the overall project. Roughly plan on equal dollar amounts for image acquisition and ground truth data collections costs. Image post-processing, image classification, accuracy assessment, and report generation costs will be determined by the overall size of the project site.

APPENDIX A

Examples of:

1. **PERFORMANCE WORK STATEMENT For ACQUISITION OF HIGH RESOLUTION AIRBORNE DIGITAL MULTISPECTRAL AND HYPERSPECTRAL IMAGERY, and**
2. **QUALITY ASSURANCE SURVEILLANCE PLAN For Contract ACQUISITION OF HIGH RESOLUTION AIRBORNE DIGITAL MULTISPECTRAL AND HYPERSPECTRAL IMAGERY**

**PERFORMANCE WORK STATEMENT
For**

**ACQUISITION OF HIGH RESOLUTION AIRBORNE DIGITAL
MULTISPECTRAL AND HYPERSPECTRAL IMAGERY**

Topographic, Imagery and Geospatial Research Division
Topographic Engineering Center
Engineer Research and Development Center
U.S. Army Corps of Engineers

1.0 Introduction

The Performance Work Statement (PWS) defines all technical specifications for the acquisition and delivery of digital airborne multispectral and hyperspectral imagery to the Topographic Engineering Center (TEC), of the U.S. Army Corps of Engineers, Engineer Research and Development Center. The detailed specifications presented below address the unique technical elements applicable to acquiring airborne digital images.

2.0 Background

TEC conducts both basic and applied geospatial research utilizing a variety of remotely sensed data sources. Many research initiatives require very high spatial resolution imagery (e.g., ≤ 1 meter). Therefore, TEC solicits and contracts data acquisition services from qualified aerial mapping companies. This PWS describes the unique characteristics that qualify an aerial mapping company to acquire remotely sensed imagery meeting TEC's research requirements.

3.0 Scope

This PWS defines the basic tasks required to acquire high quality digital airborne imagery. Its objective is to list the steps that the Contractor must follow to successfully meet TEC's data quality requirements. The Contractor must communicate with TEC during all phases of the project. The Contractor will be responsible for capturing remotely sensed data and for delivering the data to TEC. Unless otherwise specified, the Contractor will not be responsible for advance digital processing of the imagery. In this context, the word "advanced" defines, but is not limited to, the following image processing techniques or algorithms:

- Correction of radiometric distortions,
- Correction of geometric displacements and distortions,
- Creation of image mosaics, and
- Image classification and/or feature extraction.

These, and any similar, image post-processing tasks will be considered new work.

The required products from the aerial mapping efforts will include the complete set of raw digital imagery and a brief, but detailed, metadata/post mission evaluation report.

4.0 Applicable Directives

There are no specific technical directives that govern the acquisition of digital aerial imagery. However, the Contractor is encouraged to be aware of the Code of Ethics of the American Society for Photogrammetry and Remote Sensing (published by the American Society for Photogrammetry & Remote Sensing, 5410 Grosvenor Lane, Suite 210, Bethesda, Maryland 20814-2160).

5.0 Performance Requirements

The detailed Performance Requirements, listed below, define each stage of the image acquisition process. The Requirements include both mission and data parameters that are applicable to both multispectral and hyperspectral data sets. However, in some instances, the Requirements are unique to either multispectral (frame grabber systems) or hyperspectral (pushbroom or whiskbroom systems) scanners.

- 5.1 Flight Plan Development. The contractor shall develop a flight mission plan based on specific information provided by TEC. The site-specific information to be provided by TEC will include:
- The geographic coordinates defining the study area,
 - The spatial, spectral and radiometric resolutions required, and
 - The temporal window within which the imagery must be acquired.
 - The required frame-to-frame overlap (units = %) and flightline-to-flightline sidelap (units = %).
- 5.1.1 *Flight Plan.* The contractor shall develop the mission-specific flight plan using the information provided by TEC (listed above). The mission-specific parameters required in the flight plan will include, but not be limited to:
- A list of polygon coordinates defining the study site; when possible the polygon defining the study site should be rectangular.
 - A list of individual straight-line coordinates defining the starting and stopping points of each flight line.
 - A statement, including calculations if necessary, confirming that the distance between flightlines will provide the required percent sidelap.
 - A statement, including calculations if necessary, confirming that the required percent overlap will be provided considering both the nominal aircraft airspeed and the nominal aircraft altitude above-ground-level (agl).

- A statement confirming that the required spectral and radiometric resolution(s), as defined by TEC, will be met.
- A proposed flight schedule for meeting the temporal requirements as defined by TEC.
- A cost estimate for completing image acquisition. The cost estimate will provide estimated costs for all components of the data capture and the data delivery tasks.

5.1.2 *Flight Plan Review.* The contractor shall provide the completed flight plan, including the cost estimate, to TEC for review and approval.

5.1.3 *Flight Plan Approval.* Upon approval of the flight plan, the contractor will be notified. The contractor shall prepare for data acquisition.

5.1.4 *Flight Plan Modifications.* In the event that modifications to the flight plan are required to satisfy altered project objectives, TEC will notify the contractor and a modified flight plan, to include altered cost estimates (if required), will be created, reviewed, and approved.

5.2 Flight Plan Implementation

5.2.1 *Image Acquisition.* The contractor will implement the approved flight plan and complete all image acquisition to the best of their abilities. The contractor shall be responsible for meeting image quality standards as defined below:

- All images will be in focus with a vertical (i.e., nadir) nominal view angle.
- All images will be acquired using instrument gain and integration settings to both maximize the dynamic range of the digital numbers and minimize pixel saturation.
- All images will be free on “excessive” levels of radiometric distortion, including: water surface induced specular reflectance (glare or glint), significant radial field-darkening, and extremely bright “hot-spots.”
- The required frame-to-frame percent overlap will be met.
- The required adjacent flightline-to-flightline percent sidelap will be met.
- All images will as free from clouds and cloud-shadows as possible.

5.2.2 *Communication.* The contractor will maintain communication with the TEC POC before, during, and after image acquisition. Specifically, the contractor will notify TEC:

- of weather delays resulting in standby time,
- at the start of image acquisition, and
- if unforeseen circumstances (e.g., continuing poor weather conditions, equipment/aircraft problems) are likely to result in flight plan modifications.

5.3 Data Delivery

- 5.3.1 *Raw Imagery*. The contractor will deliver the raw digital imagery to TEC as soon as possible after the flight mission is completed. The data will be transfer to TEC in the most efficient format (e.g., CDROM, Zip disk, hard drive), based on the volume of imagery.
- 5.3.2 *Metadata*. The Contractor will produce a brief, but detailed, acquisition report, including:
- Nominal aircraft parameters – altitude, heading, airspeed, general flying conditions.
 - A description of atmospheric conditions during the data acquisition.
 - Imaging system parameters (e.g., integration time, gain settings).
 - Number of flightlines per study area.
 - Number of frames per flightline.
 - File naming conventions for all output images and GPS files.

The report will be complete and easily comprehensible.

- 5.4 Post Flight Mission Evaluation. The contractor shall critique the completed mission and provide TEC with any suggestions that will improve the efficiency of data collection and/or reduce costs of subsequent image acquisitions. The critique can be communicated in the simplest format (e.g., brief memo, telephone conference).

6.0 Deliverables

Upon the completion of each image acquisition mission, the contractor will deliver the following products in accordance with the Performance Requirements listed above.

- 6.1 Raw Imagery. The contractor will deliver the raw digital imagery to TEC as soon as possible after the flight mission is completed. The data will be transfer to TEC in the most efficient format (e.g., CDROM, Zip disk, hard drive), based on the volume of imagery.
- 6.2 Acquisition/Metadata Report. The contractor shall provide TEC with a detailed acquisition report, including:
- Nominal aircraft parameters – altitude, heading, airspeed, general flying conditions.

- A description of atmospheric conditions during the data acquisition.
- Imaging system parameters (e.g., integration time, gain settings).
- Number of flightlines per study area.
- Number of frames per flightline.
- File naming conventions for all output images and GPS files.

QUALITY ASSURANCE SURVEILLANCE PLAN

For Contract

ACQUISITION OF HIGH RESOLUTION AIRBORNE DIGITAL MULTISPECTRAL AND HYPERSPECTRAL IMAGERY

I Objective

This plan provides a quality surveillance strategy applicable to the acquisition and delivery of digital airborne multispectral and hyperspectral imagery to the Topographic Engineering Center (TEC), of the U.S. Army Corps of Engineers, Engineer Research and Development Center. The performance indicators and evaluation methods presented below address the unique technical elements applicable to acquiring airborne digital images. The primary intent of this plan is to provide the basis for a contract performance evaluation by either the Contracting Officer's Representative (COR) or any other technical point of contact (POC) at TEC.

II Performance Indicators (Measures)

Quality level. The COR and POC will determine whether the contractor has completed the four major tasks as defined, in detail, in Section 5.0 Performance Requirements of the Performance Work Statement (PWS). Specifically, these four tasks are:

- 5.1 Flight Mission Development**
- 5.2 Flight Plan Implementation**
- 5.3 Data Delivery**
- 5.4 Post Flight Mission Evaluation**

The COR and POC will determine whether the contractor has delivered the imagery and the metadata consistent with the quality standards detailed in PWS paragraphs 5.2.1. and 5.3.2.

Frequencies. The COR or POC will evaluate the quality of the aerial mission and the delivered product(s) on a per mission basis.

III Evaluation Methods

The COR and POC will initiate and perform evaluations based on the indicators in paragraph II of this plan. The POC will ultimately be responsible for assessing the overall quality and acceptability of the imagery and metadata. The POC will visually evaluate the quality of the delivered images. The POC will also read and confirm the completeness and clarity of the metadata document.

The POC will forward the completed performance evaluation to the COR.